CORROSION BEHAVIOUR OF WC-VC-Co HARDMETAL IN VARIOUS ACIDIC AND CHLORIDE CONTAINING MEDIA

David Sasu Konadu

A dissertation submitted to the Faculty of Engineering and the Built Environment, University of the Witwatersrand, in fulfillment of the requirements for the degree of masters of Science in Engineering

Johannesburg, 2009

DECLARATION

I declare that this dissertation is my own unaided work. It is being submitted to the Degree of Master of Science in Engineering to the University of the Witwatersrand, Johannesburg. It has not been submitted before for any degree or examination to any university.

_____

(Signature of Candidate)

_____ day of _____ 2009

ABSTRACT

Cemented carbides have been used for milling and cutting, as a result of their high hardness and toughness, but their poor resistance to chemically aggressive environments calls for some modifications to improve their corrosion resistance. VC with a grain size of less than 2 µm was added, which improved the hardness and toughness compared to the straight grade. In this work, the corrosion behaviour and surface films of WC-VC-Co hardmetals were investigated in acids and neutral chloride salts as VC content was increased, while keeping the binder content constant. Characterisation of the microstructure and composition of the alloys, before and after corrosion, were done with scanning electron microscopy (SEM), X-ray diffraction (XRD) and Raman spectroscopy. The electrochemical techniques used for the investigation were: open circuit potential (OCP), potentiodynamic anodic polarisation and chronoamperometry. Increasing VC content improved corrosion resistance in HCl solution, but little change was experienced in H_2SO_4 according to corrosion rate values. The surface film formed on all the test specimens in HCl was $WO_3.H_2O$. In H_2SO_4, all the specimens formed $WO_3.xH_2O$ and at high VC content, $VOSO_4.H_2O$. Increasing VC content makes the OCP in H_2SO_4 more negative than in the base alloy. The OCP in HCl only becomes more negative at very high VC additions. An increase in VC content did not affect the variation of current during chronoamperometric tests in the acidic media. Different tungsten oxides formed as passive films in NaCl. Corrosion resistance decreased with increasing VC content for the WC-VC-Co alloys in NaCl. In synthetic mine water (SMW), all specimens showed continuous anodic dissolution as there was minimal influence of increasing VC additions. There was no trend in the variation of the OCP values as the VC content varied and increasing VC content resulted in an increase in the value of current density during chronoamperometry in the neutral salts. The lack of effect on the corrosion resistance is attributed to the fact that VC does

not possess passivation characteristics. In the neutral salts, there was formation of a green V^{2+} solid compound, accompanied by oxygen reduction.

DEDICATION

This dissertation is dedicated to my wonderful wife, **Mrs Cynthia Konadu**, for her patience whilst I was studying.

ACKNOWLEDGEMENTS

I give thanks to the Most High God for His love, protection, wisdom and understanding. I humbly express my deepest appreciation to the following persons for their immense contributions towards the completion of my study.

Professor J. Herman Potgieter, whom God used for me to undertake this study at WITS University. Prof, I am highly indebted to you.

Professor Sanja Potgieter-Vermaak for your supervision of the work especially, the Raman experiments. I am grateful to her for the patience when the going was tough, her encouragement, motherly advice, mentoring me to be a good researcher and financial support.

Dr. C. N. Machio for being more than a brother to me, even though you left WITS for the CSIR. You never stopped following my progress and stayed with me till I completed this project. God richly reward you for all that you did for me.

Mr. Josias Van der Merwe, for your guidance and supervision, brotherly kindness and seeing to all the SEM work.

Mr. Bruce Mothebedi, Doctor Mbensi and **Mr. Aubrey Xoseka** for all the assistance you gave me and provision of laboratory materials for the success of this project.

Mr. Rudolph Erasmus, Miss Beauty Nthabiseng and **Prince Vongani** for the help you gave me in doing the Raman experiments.

I will not forget the corrosion group for their immense sharing of ideas for every step of the way. To **Dr. Peter Olubambi**, **Zvanaka Msindo, Mrs. Victoria Adams** and **Nompumelelo Thanjekwayo**, I appreciate you all.

My parents; **Mr. and Mrs. Konadu**, brothers and sisters, and all friends in the department, for your prayers and moral support, not forgetting **Dr Anthony Andrews** whose help also brought me to WITS.

Finally, I want to thank Centre of Excellence in Strong Materials and National Research Foundation for your financial assistance in funding my studies in South Africa.

TABLE OF CONTENTS

LIST OF FIGURES

LIST OF TABLES

LIST OF SYMBOLS AND ABBREVIATIONS

A …….. area, cm^2

Ag/AgCl …….. silver – silver chloride

ASTM …….. American Society for Testing and Materials

c ……concentration, mol cm^{-3}

CE …… counter electrode

Co …… cobalt

$Co(OH)_2$ …….. cobalt hydroxide

CO_2 …… carbon dioxide

CoO …… cobalt oxide

$CoSO_4$ …… cobalt sulphate

Cr_3C_2 …….. chromium carbide

D …… diffusion coefficient, cm^2s^{-1}

e^- …… an electron

E_B …… anodic breakdown potential, V

E_{corr} …… corrosion potential, V

EDS, EDX, EDXS… energy dispersive X-ray spectroscopy

EELS …….. electron energy loss spectra

EIS …….. electrochemical impedance spectroscopy

F …….. Faraday's constant

fcc ……... face centered cubic

Fe …… iron

FT-IR …….. Fourier transform infrared

GPES …… General Purpose Electrochemical System

H^+ …… hydrogen ion

H_2 …… hydrogen gas

H_2O …… water

H_2SO_4 …… sulphuric acid

HCl …….. hydrochloric acid

hcp …….. hexagonal close packed

i …… current at over voltage

i_{corr} …….. corrosion current density, A/cm^2

i_{crit} …….. critical current density, A/cm^2

i_{pass} …… passivation current density, A/cm^2

i_{pp} …… primary passivation current, A/cm^2

ICP-MS ……..... inductively coupled plasma - mass spectroscopy

ICP-OES ……. inductively coupled plasma – optical emission spectroscopy

log …….... logarithm

LSV …… linear sweep voltammetry

m …… metal

m^{n+} …… metal ion

n …….. number of electrons

Na_2SO_4 …….. sodium sulphate

NaCl …….. sodium chloride

Ni …… nickel

Ni-Cr …….. nickel - chromium

Ni-Cr-Mo…… nickel - chromium - molybdenum

O_2 …… oxygen gas

OCP …….. open circuit potential

pH …….. $-\log_{10}[H^+]$

R_p …….. polarisation resistance

SEM …….. scanning electron microscopy

SKPFM ……... scanning Kelvin probe force microscopy

SMW …… synthetic mine water

SSE …….. silver/silver chloride electrode

TaC …….. tantalum carbide

TEM …… transmission electron microscopy

TiC …… titanium carbide

VC …… vanadium carbide

VO^{2+} …….. vanadium oxide ion

$VOSO_4.H_2O$ ……. vanadyl sulphate

W …….. tungsten

WC…….. tungsten carbide

WC-Co …….... tungsten carbide – cobalt

WC-Co-Cr_3C_2 …….. .tungsten carbide – cobalt – chromium carbide

WC-Co-Cr_3C_2-VC..... tungsten carbide – cobalt - chromium carbide – vanadium carbide

WC-Co-Ni-Cr_3C_2 …. tungsten carbide – cobalt – nickel - chromium carbide

WC-Fe …….. . tungsten carbide – iron

WC-Ni …….. tungsten carbide – nickel

WC-Ni-Cr …….... tungsten carbide – nickel – chromium

WC-Ni-Cr-Co ……..... tungsten carbide – nickel – chromium – cobalt

WC-Ni-Cr-Mo …….. tungsten carbide – nickel – chromium – molybdenum

W-Co-Ni …….. tungsten – cobalt – nickel

W-Co-Ni-Fe …….. tungsten – cobalt – nickel – iron

WC-VC …….. tungsten carbide – vanadium carbide

WC-VC-Co……tungsten carbide – vanadium carbide – cobalt

WO_3 …….... tungsten oxide

$WO_3.H_2O$ ……..... hydrated tungsten oxide

wt% …….. weight percent

XPS …….. X-ray photoelectron spectroscopy

XRD …….... X-ray diffraction

β …….. Tafel constant

ε …….. over potential

(W,V)C …….. (tungsten, vanadium) double carbide

(W,V,Co)C …….. (tungsten, vanadium, cobalt) carbide

CHAPTER ONE

1 INTRODUCTION

1.1 Background

Tungsten carbides or cemented carbides are composite hardmetals consisting of a hard phase, tungsten carbide (WC), and a metal binder, and are known for their high hardness and working toughness. WC gives the alloys the necessary strength and hardness, whereas the binder contributes to the toughness of the alloys. Cobalt (Co) is the most commonly used metal binder. Other carbides get added to the WC–Co for various purposes. For example, vanadium carbide (VC) can be added to the binder to restrict local WC crystal grain growth (da Silva *et al.,* 2001; Adorjan *et al.*, 2006).

The combination of high hardness and good working toughness mentioned above has resulted in the application of WC–Co hardmetals in many engineering fields. Their major usage is as cutting tools, for example, turning, facing and milling operations; glass cutting; swaging dies, drawing dies, and other metal-deformation applications, such as cold heading and Send-zimir mill rolls; and tools for mining operations such as oil wells, coal mining, and tunnel boring (Yih & Wang, 1979).

Most of the above mentioned applications are performed in chemically aggressive environments, which make the tungsten carbides susceptible to corrosion. Corrosion resistance is therefore an important property in the industrial use, since corrosion degrades the hardmetal and thus shortens its service life (Engqvist *et al*., 2000).

1.2 Motivation

There is a considerable amount of research on the corrosion of cemented carbides, which, however, has largely been limited to comparisons of corrosion rates in different solutions and the effects of change of binder and addition of third hard phases on the corrosion behaviour of WC – Co (Tomlinson and Linzell, 1988, Wentzel and Allen, 1995, Mori *et al.*, 2001, Human *et al*., 1991). Further, there have only been a few studies aimed at understanding the processes involved and these have all made use of electrochemical measurements (Hochstrasser-Kurz *et al*., 2007, Bozzini *et al*., 2003 {a}).

Sebeya (2006) investigated two sets of WC-Co alloys, one with a 10% Co binder content and the other with a 30% Co binder content. In the one case 10% VC has been added, and in the other 67% VC. The purpose was to establish what changes take place in the Co binder phase, and how it affected the corrosion of the alloy. It seemed that increasing VC content stabilized fcc Co, increasing the ratio of fcc to hcp Co, and that this had a beneficial effect on corrosion resistance.

Broccardo (2003) investigated the effect of varying Co contents in a WC-10%VC-Co series of alloys on their corrosion behaviour, and concluded that the increasing Co content lead to an increase in the corrosion resistance. However, the effect of varying VC contents in a WC-Co alloy in different media, has not received any attention so far. The aim of this study was therefore to investigate this in more detail. Also, since most previous studies concentrated on electrochemical measurements only, this study will attempt to combine the electrochemical investigations with spectroscopy observations from Raman spectroscopy measurements and spectra.

1.3 Hypothesis

It is postulated that an increasing amount of VC added to the WC-Co with a constant binder content will increase the corrosion resistance of the overall alloy.

1.4 Aim

The aim of this project is to develop a better understanding of the corrosion mechanisms in WC – based hardmetal in sulphuric acid, hydrochloric acid, sodium chloride, and synthetic mine water solutions using potentiodynamic and Raman Spectroscopy studies. These studies will identify the surface film(s) formed on WC-VC-Co test materials during anodic polarisation. The electrolytes give an adequate approximation of the industrial environments in which WC-Co hardmetals normally operate.

1.5 Layout of dissertation

This chapter, Chapter One, has introduced the material that will be used in this study and described the motivation of this study. Chapter Two, Literature Review, will review the available literature on the corrosion of WC – based materials. The experimental procedures that will be used to achieve the aim of this study will be outlined in Chapter Three. Chapter Four will present the results of the characterization of the materials before and after corrosion, and the corrosion behaviour of the test materials in all the test solutions, i.e., hydrochloric acid, sulphuric acid, sodium chloride and synthetic mine water. Chapter Five will present the conclusions of the observations made in this study and recommendations for further work and/or on how industry can use the results of this study.

CHAPTER TWO

2 LITERATURE REVIEW

2.1 Introduction

This is a brief description of corrosion and its measurement, and the analytical methods that will be employed in the project work. The literature work done on WC-hardmetals and the addition of other phases are also reported in this chapter.

2.2 Vanadium carbide in WC-Co hardmetal

VC was used during World War II in Germany as a hardmetal but its use was discontinued due to difficulties in manufacturing processes. The problems encountered were unacceptable porosity and excessive brittleness of the VC particles (Luyckx, 1994 {b}). WC-VC-Co alloys with particle sizes greater than or equal to 10 µm have higher hardness, abrasion and erosion resistance, but lower toughness than WC-Co hardmetal of equal cobalt content (Luyckx, 1994 {a}). Reducing the VC particle size to less than 2µm resulted in WC-VC-Co hardmetal of higher toughness than WC-Co (Luyckx *et al.*, 1996). It was concluded that the addition of VC improved the mechanical properties of WC-Co hardmetal. VC is the best grain growth inhibitor compared to the other carbides that would usually be added to WC-Co for WC grain refinement (Hashe *et al*., 2008; Luyckx *et al.*, 1996; Fang *et al*., 2005).

Hashe *et al*. (2008) investigated the effect of nitrogen on the grain growth inhibition of large additions of VC in WC-Co. Results from vacuum sintering revealed that the hardness, the toughness, and the grain size were not significantly different as compared to sintering in nitrogen atmosphere. Though the average grain size was found to be the same, the spread was found to be smaller, indicating a substantial reduction of the grain size. The

spread of the grain size during vacuum sintering was 2.6, which reduced to 0.75 during nitrogen sintering.

The densification rate of WC-Co nanocyrstalline powders decreased dramatically when 1 %wt VC was added. It also revealed a much finer grain size and maintained a primary equi-axial shape of the grains as compared to the un-doped WC-Co hardmetal. The faceted grain structure of the doped hardmetal was observed around 1300 ℃, whilst the un-doped material changed from equi-axial shape to faceted platelet shape during heat-up from 800 ℃ to 1200 ℃. This proved that VC inhibited grain growth and slowed densification at low solid-state and liquid phase sintering temperatures. VC was found to change the surface and interface energies of WC grains and also the driving force for the grains to change from equi-axial to faceted shape (Fang *et al*., 2005).

Lay *et al*. (2002) reported on the location of VC in VC-doped WC-Co. Energy dispersive X-ray spectroscopy (EDXS) showed that all the space between two WC crystals was filled with a vanadium-rich phase. A small tungsten signal of about 10 at.% was present in the VC, which was in agreement with the solubility limit of tungsten in VC. Smaller vanadium-rich phases were also observed by transmission electron microscopy (TEM) in corners between WC grains in conjunction with the Co binder. No vanadium was detected in the Co binder, though about 2-3% was found in the liquid at the sintering temperature. Between WC crystals, VC occupied a small triangular part of the space whereas Co occupied the rest. Along the interfaces, electron energy loss spectra (EELS) images showed a third vanadium-rich phase as a small vanadium signal. This was observed along the faceted interface between WC and Co which indicated vanadium segregation and extended on several atomic planes.

Terada and Suzuki (1997) concluded that the effect of up to 5 wt% VC on structure and properties of coarse grained WC-10%Co was to produce a more uniform grain size as the % VC was increased. This was due to the inhibiting effect of VC on grain growth of WC.

2.3 Corrosion

Corrosion is the destructive result of a chemical reaction between a metal or metal alloy and its environment. The metals are converted into chemical compounds that are similar or even identical to the minerals from which the metals were extracted. “Thus corrosion has been called extractive metallurgy in reverse” (Denny, 1996; Fontana & Greene, 1982). There are two types of corrosion: low and high temperature corrosion (Denny, 1996). This study will concentrate on low temperature corrosion, also called electrochemical corrosion.

2.4 Electrochemical reactions

When a metal is immersed in a corrosive medium, called the electrolyte, electrochemical reactions characteristic of the metal-solution interface occur at the surface of the metal, causing the metal to change its oxidation state, i. e., corrode. Consider a metal M immersed in a corrosive medium containing H^+ ions. The metal reacts with the solution forming a metal ion M^{n+}, where n is the number of electrons according to the equation (2.1):

$$M \rightarrow M^{n+} + ne^- \qquad (2.1)$$

The free electrons liberated by the metal react with the hydrogen ions or oxygen present in the solution to yield either hydrogen gas or hydroxide ions as follows:

$$2nH^+ + 2ne^- \rightarrow nH_2 \quad (2.2)$$

$$O_2 + 2nH_2O + 2ne^- \rightarrow 4nOH^- \quad (2.3)$$

Equation (2.1) is an oxidation reaction in which the metal valency increases from 0 to +n and is also termed the anodic reaction, while equations (2.2) and (2.3) are reduction reactions since the oxidation state of hydrogen or oxygen decreases and are also called the cathodic reactions. In this way, the metal dissolves by liberating electrons into the bulk of the metal which migrate to the adjoining surface, where they react with H^+ ions or oxygen to liberate hydrogen or hydroxide ions. As oxidation or reduction reaction takes place, a flow of electrons from the metal gives rise to current (Denny, 1996).

When the metal is in contact with the corrosive medium and is not connected to any instrument, as it will be in service, the metal assumes a potential termed the corrosion potential, E_{corr}. At E_{corr}, the metal has both anodic and cathodic currents present on its surface and these are exactly equal in magnitude and so there is no nett current to be measured. The potential at the metal surface becomes more negative when electrons are made available to equations (2.2) or (2.3). Excess electrons with their negative charges accumulate at the metal/solution interface since the reaction is not fast enough to use all the available electrons. This is termed cathodic polarisation. It is possible to draw away the electrons generated by equation (2.1) more than they are made available: the deficiency of electrons is termed anodic polarisation (Denny, 1996).

2.5 Corrosion measurements

2.5.1 Potentiodynamic polarisation

Potentiodynamic polarisation is the characterisation of a metal specimen by its current-potential relationship. Potentials are imposed, other than the corrosion potential, E_{corr}, at the metal-solution interface by scanning slowly in the positive direction which brings about corrosion. Polarisation characteristics are measured by plotting the current response as a function of the applied potential. When the logarithm of the current function is plotted against the potential on a semi-log graph, it is termed a potentiodynamic polarisation plot. The shape of the curve shows the corrosion behaviour of the specimen in the electrolyte. The passivation behaviour i. e. whether a protective oxide forms or not or no oxide, can also be determined from this curve, but one cannot identify the passive films formed (Denny, 1996).

2.5.2 Tafel Plots

Corrosion current, i_{corr}, is measured by this technique so as to calculate corrosion rate. A Tafel plot is generated by beginning to scan at E_{corr} and continuing to a negative value of E_{corr}, for cathodic Tafel plot and for anodic Tafel plot, the scanning is done positive of E_{corr}. The potential is plotted against the resulting current on a logarithmic scale as shown in Figure 2.1.

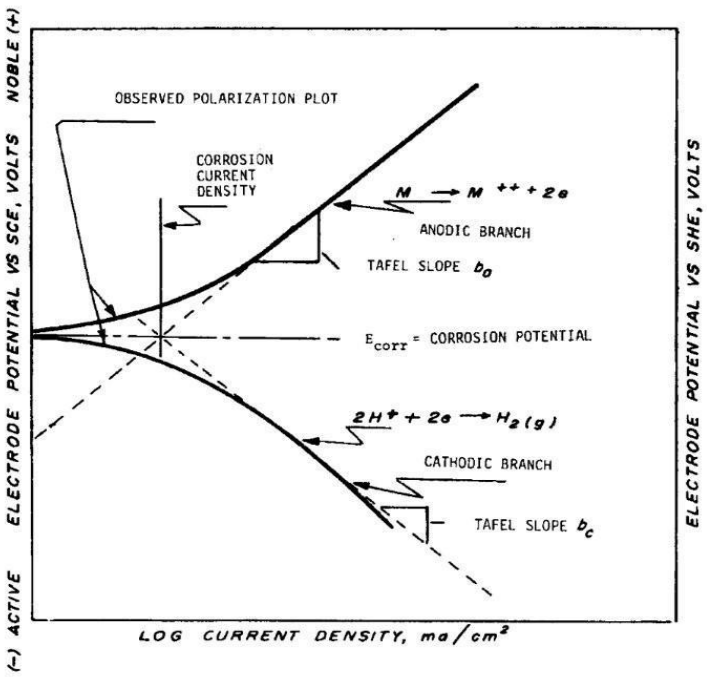

Figure 2.1 Hypothetical cathodic and anodic polarisation diagram (ASTM G3-1999)

By extrapolating the linear portion of the curve from the Tafel plot, the corrosion current is obtained as seen from Fig 2.1. The Tafel equation is given by

$$\varepsilon = \beta \log\left(\frac{i}{i_{corr}}\right) \tag{2.4}$$

Where

ε = overvoltage, the difference between corrosion potential and the potential of the specimen

β = Tafel constant

i = current at overvoltage.

Expanding Equation 2.4 gives

$$\varepsilon = \beta \log i - \beta \log i_{corr}$$

This equation is of the form y = mx + c, so plotting ε against log*i* is a straight line with slope β and intercept – $\beta \log i_{corr}$. The corrosion current, i_{corr}, is determined from the graph, and is directly proportional to corrosion rate (Denny, 1996; Fontana & Greene, 1982).

2.5.3 Chronoamperometric measurements

The current response as a function of time is called chronoamperometry. This response is obtained by applying a potential which can cause electrochemical reactions to occur on a metal surface. The response monitors the conversion of elements into ions and the rate at which the ions diffuse out through the metal carbide. A plot of current against the reciprocal of the square root of time should be linear because current decays with time, as indicated by Cottrell's diffusion control equation, reproduced here as Equation 2.5:

$$i = nFACD^{1/2}\pi^{1/2}t^{-1/2} \qquad (2.5)$$

where :n = number of electrons transferred/molecule

F = Faraday's constant

A = electrode area (cm^2)

D = diffusion coefficient (cm^2s^{-1}) and

C = concentration (mol cm^{-3})

From the plot, the slope is calculated and any one of the parameters n, A, D, and C can be determined provided any three of them are known (Wang, 2006).

2.6 Raman spectroscopy

Raman spectroscopy uses the scattering of monochromatic (single frequency) radiation that is incident on a sample to give information about the

sample's molecular structure. It uses a shift in wavelength of inelastically scattered radiation to provide information about the chemical composition and structure of the molecule (Colthup *et al*., 1975).

2.7 Tungsten carbide microstructure

2.7.1 WC-Co

A typical microstructure of sintered WC-Co shows bright prismatic grains of WC and dark Co areas between WC grains. (Makhele, 2001; Hochstrasser-Kurz *et al*., 2007). During sintering, WC dissolves in Co: the dissolution can be significant, as high as 26 wt.%, but only a small amount of Co, i. e. 0.8 wt.%, dissolves in the WC (Hochstrasser-Kurz *et al*., 2007). Human & Exner (1996) reported that for conventionally sintered hardmetals, the level of dissolved tungsten in the binder varied and there was a tungsten depleted zone at the phase boundaries. An average tungsten content of 3.2 at.% (9.4 wt%) was found in the interior of the binder regions. Generally however, the solubility of WC in Co is governed by a solubility constant involving WC and C: [WC][C] = constant (Exner, 1979). The solubility of WC and its distribution thereof in Co is bound to affect the corrosion behaviour of the material.

2.7.2 WC-VC-Co

Scanning electron microscopy (SEM) images of WC-VC grades show bright WC grains and a darker contrasted (V,W)C phase (Huang *et al*., 2007; Broccardo, 2003; Machio, 2005). For WC-VC-Co hardmetal, there is difficulty in distinguishing between the VC and the binder phase due to the closeness of their average atomic numbers (Broccardo, 2003). Sebeya (2006) in backscattered electron SEM mode found a light phase of Co, (V,W,Co)C as a gray phase and pores of a dark phase. The VC changes to the double carbide (V,W)C because WC dissolves in VC (Exner, 1979).

Hashe *et al.* (2008) also investigated the microstructure of WC-VC-Co by back scattered SEM, and it was revealed that there was a light region of WC grains, cubic carbonitride [(W,V)(C,N)] grayish region grains and a dark region of binder phase. There were two types of cubic carbonitride grains which were of a high vanadium content in the composition i. e. $(W_{0.21}$ $V_{0.79})$(C,N) and $(W_{0.30}$ $V_{0.70})$(C,N) as determined by SEM – EDS analysis. TEM – EDS measurements revealed a binder phase of 98 at.% cobalt, 1.5 at.% tungsten and traces of vanadium. This was an indication of nitrogen decreasing the solubility of vanadium in the binder phase during sintering.

Energy dispersive X-ray (EDX) analysis has shown that the solubility of vanadium in the cobalt binder is low. According to the V/Co ratio this was 0.02. Moreover, VC segregates as a thin layer between WC grains in addition to precipitation in pockets. On the surfaces of WC grains were depositions of less than 1 nm thick layer of VC. This layer acted as a liner and separated the Co binder from WC grains (Sutthiruangwong *et al*., 2005).

2.8 Corrosion of tungsten carbide

2.8.1 Corrosion behavior of WC – Co

It is generally accepted that the corrosion resistance of WC–Co hardmetals in acidic and neutral electrolytes is controlled by the corrosion resistance of the binder. This is because the oxidation potential of WC is nobler than that of Co (Ghandehari, 1980). As a result, in an electrolyte, a galvanic coupling forces the anodic part of the overall corrosion reaction to proceed on the Co phase. The Co dissolution gets enhanced due to the unfavourable surface area ratio of anodic sites compared to cathodic sites. In parallel, the cathodic reaction, i.e. the reduction of oxygen or hydrogen, takes place on the WC phase, which in principle is protected against electrochemical dissolution in neutral and acidic solutions (Hochstrasser-Kurz *et al*., 2007).

Recent corrosion studies have shown beyond doubt that the binder phase does control the corrosion behaviour of WC–Co materials. Hochstrasser-Kurz *et al*. (2007) studied WC–Co, Co and WC corrosion in aqueous solutions of different pH – values at open circuit corrosion potentials using electrochemical impedance spectroscopy (EIS) measurements and observed that the spectrum of pure Co was similar to the spectrum of WC-Co hardmetal while that of pure WC was different. This showed that the corrosion behaviour of the composite was being dominated by that of the Co phase.

The same authors (Hochstrasser-Kurz *et al*., 2007), analysed the electrolyte solutions after immersion tests by inductively coupled plasma-mass spectroscopy (ICP-MS) and found that the time dependant Co dissolution from the WC–Co composite was more enhanced than the dissolution from pure Co samples. The accelerated dissolution of the Co from the WC–Co samples was accounted for by the galvanic coupling of Co and WC. A corresponding comparison of the WC dissolution from the composite and from the pure WC sample was made. It was shown that the uncoupled WC sample continuously dissolved, while the WC dissolution from the composite stopped shortly after it started, indicating the WC was cathodically protected by the dissolution of the Co.

In a more recent work by Hochstrasser-Kurz *et al*. (2008), using the scanning Kelvin probe force microscopy (SKPFM) technique (which measures local electrochemistry with submicrometer resolution), it was found that WC grains acted cathodically and Co binder as the anodic site. This was in agreement with macroscopic measurements. Measurements done directly on the real system showed a 200 – 250 mV potential difference microscopically between the two phases and proves galvanic coupling between the WC and Co phases in the hardmetal.

Online time resolved analysis of the dissolution of Co and W was studied for various pHs using ICP-MS. In alkaline media, W dissolution increased for the first five minutes, rose to a peak at about twelve minutes, then decreased and a second increase started at about twenty two minutes. The Co dissolution had a similar shape but was retarded in comparison to that of W. For pH 13, Co showed no dissolution at all and indicated good passivation behaviour in this pH domain. For pH 9, there was Co dissolution and it was due to the W dissolving to expose unpassivated Co phase (Hochstrasser-Kurz *et al*., 2008).

In slightly acidic and neutral solutions, a simultaneous dissolution of both WC and Co phases occurred as there was a decrease in the dissolution rate after an initial peak rise between five and fifteen minutes. This showed a chemical dissolution process taking place as against cathodic protection of WC electrochemically (Hochstrasser-Kurz *et al*., 2008).

2.8.2 Effect of binder on corrosion

It is expected that as the binder corrosion resistance is increased, the effect of galvanic coupling between WC and the binder is reduced and corrosion of both WC and binder can take place. For example, in sulphuric acid and nitric acid, significant corrosion of the WC grains occurs when coupled with Ni-Cr and Ni-Cr-Mo binders (Human *et al*., 1991).

Immersion tests in boiling 6 N hydrochloric acid have revealed that WC-Ni, WC-Ni-Cr, and WC-Ni-Cr-Mo hardmetals show little improvement in corrosion resistance over WC-Co. The corrosion current density for the Co binder was higher than the Ni-Cr-Mo binder which had the lowest critical current density and increased passivation at lower potentials (Human *et al*., 1991).

The corrosion behaviour of WC-Co, WC-Fe, and WC-Ni hardmetals was also studied in sulphuric acid. It was generally found that the corrosion resistance of WC-Ni was excellent, WC-Co was good, and WC-Fe was poor (Scholl *et al*., 1992).

The inclusion of iron (Fe) in tungsten-cobalt-nickel (W-Co-Ni) leads to a reduction in the overall solubility of tungsten in the binder phase. Consequently the binder in the W-Co-Ni-Fe hardmetal is susceptible to galvanic corrosion. For tungsten with copper as a binder, it was observed that the tungsten grains corroded and were transformed into spherical crystals (Ogundipe *et al*., 2006).

Magnetic saturation, which gives an indication of the amount of tungsten dissolved in the binder phase during sintering, has been used by Sutthiruangwong and Mori (2003) to determine the effect of dissolved W on the corrosion behaviour of Co. A low magnetic saturation implies a high W content in the binder. Polarisation of WC – 15%Co with a 100% magnetic saturation in 1 N H_2SO_4 solution yielded the highest primary passivation current (i_{pp}), whereas WC – 6%Co with 85% magnetic saturation ratio produced the lowest. Also, cemented carbides with a constant binder content and lowest magnetic saturation ratio exhibited the lowest i_{pp}. This occurred since a high W content in the binder led to high corrosion resistance. As the magnetic saturation is kept constant, i_{pp} decreased with decreasing Co content. The corrosion properties of cemented carbides are thus influenced by binder surface area.

Tomlinson and Linzell (1988) have reported that hardmetals with Ni and Ni-Co binders had a very limited passivation range compared with pure Ni in a 0.01 M H_2SO_4 + 0.99 M Na_2SO_4 solution. Further, the presence of chloride in the solution increased the dissolution rate.

Anodic polarisation curves for WC-Ni, WC-Ni-Cr, WC-Ni-Cr-Co, and WC-Co in silica water slurry have shown that a Ni-Cr-Co binder has the lowest passivation current density, followed by Ni-Cr, Ni, and Co binder in that order. The polarisation behaviour indicated that the Ni-Cr and Ni-Cr-Co binders were more corrosion resistant than the pure metal binders, i. e. Ni and Co. This was attributed to the inclusion of chromium in the alloy binders (Wentzel & Allen, 1995).

Bozzini *et al*. (2002) reported on the corrosion behaviour of WC-Co, WC-Co-Ni, and WC-Co-Ni-Cr_3C_2 in sodium chloride and sulphuric acid. The hardmetal with higher Ni content in the binder displayed the lowest critical density i_{crit}, lowest current density at a fixed anodic potential of -100 mV, i_{100}, the most noble anodic breakdown potential (E_B) and the highest linear polarisation resistance (R_p) in both media. The R_p was derived from the linear range of a linear sweep voltammetry (LSV) around the open circuit potential. E_B was taken at a plateau region at which a marked increase in current density was observed. The hardmetal with a lower Ni content in the binder and an addition of Cr_3C_2 showed intermediate electrochemical behaviour.

2.8.3 Effect of the electrolyte on the corrosion behavior of WC–Co

Potentiodynamic polarisation measurements on WC–Co, Co and WC have shown that pure Co dissolves in acidic and neutral solutions, while it passivates in alkaline solutions. In contrast, pure WC dissolves in alkaline solutions but not in acidic or lower pH solutions. The WC-Co composite polarisation curves in acidic and neutral solutions are identical to those taken from pure Co, again confirming the prominence of the binder in corrosion (Ghandehari, 1980; Hochstrasser-Kurz *et al*., 2007, 2008; Schnyder *et al*., 2004).

WC-Co carbides in hydrochloric acid solution exhibited a higher critical current density (i_{crit}) and minimum current density in the pseudopassive region than in H_2SO_4. This was the result of different anions which had an influence on corrosion properties of the cemented carbides by changing primary passivation (Sutthiruangwong & Mori, 2003).

Human and Exner (1996) found that the corrosion potential of WC-Co hardmetal shifted to a more negative value in synthetic mine water compared to sulphuric acid. The current density was found to increase with increasing polarisation and pseudopassivity was not as pronounced as was the case in sulphuric acid.

2.8.4 Effect of grain size on corrosion of WC – Co

There appears to be no consensus on the effect of grain size on the corrosion of cemented carbides. While Human & Exner (1997) found no measurable difference in the polarisation behaviour when the WC grain size was changed, Tomlinson and Ayerst (1989) reported that coarse grained hardmetal corrodes more than medium grain size hardmetal. This might have been due to the binder having less tungsten dissolved in it.

It would appear that different grains can display different degrees of oxidation as a result of inhomogeneities in current density distribution during anodic polarisation (Bozzini *et al*., 2003 {a}). However, this theory is not fully tested because an inconsistency in results has been obtained when WC – 6%wtCo is polarised in 2 N H_2SO_4: the corrosion rate did not increase or decrease with increasing WC grain size (Fernandes *et al*., 1992).

2.8.5 Anodic polarisation behaviour of WC – Co

The electrochemical behaviour of WC-Co in normal sulphuric acid is characterised by anodic dissolution with increasing polarisation. There is a tendency for the corrosion current density to decrease with increasing polarisation but the current remains high (around 50 mA/cm^2) in comparison to passive current densities (below 10 $\mu A/cm^2$). This electrochemical behaviour is termed pseudopassivity (Human & Exner, 1997).

The polarisation behaviour changes when the binder is changed from Co to Ni-Cr-Mo. In this case, anodic polarisation in synthetic mine water produces a drop in the critical current density from around 300 $\mu A.\ cm^{-2}$ to 1 $\mu A.\ cm^{-2}$ (Human & Exner, 1997).

In general, more corrosion resistant binders improve the corrosion resistance of cemented carbide hardmetals (Bozzini *et al*., 2002). Sutthiruangwong & Mori (2003) reported that between Co and WC, and in anodic polarisation tests in aerated 1 N H_2SO_4, WC has the lower corrosion current density and exhibits passivation unlike pure Co.

When WC – 9%Co material is polarised in aerated and deaerated HCl and H_2SO_4 solutions, the curves are almost identical except for the cathodic reaction. It was found that oxygen reduction resulted from aerated solutions whereas hydrogen evolution dominated in deaerated solutions (Sutthiruangwong & Mori, 2003).

2.8.6 WC–Co Corrosion products

The corrosion products formed when WC–Co corrodes appear to be dependent on the electrolyte. Bozzini *et al*. (2002) investigated the corrosion of WC-Co in H_2SO_4 and NaCl using an immersion test method. X-ray

diffractometer measurements for the hardmetal in H_2SO_4 showed the presence of $CoSO_4$, which is contrary to later findings by the same authors.

In 0.1 M sulphuric acid, two-phase structures of WO_3 and hydrated WO_3, i.e. $WO_3.xH_2O$ (with x = ½, 1, 2) have been reported (Bozzini *et al*., 2003 {a}, 2004). These products have been detected by X-ray diffraction and Raman spectroscopy studies. It has been postulated that the $WO_3.xH_2O$ species inhibits the corrosion of the binder phase, resulting in the passivation of the hardmetal.

Scholl *et al*. (1992) worked on WC–Co immersed in sulphuric acid and postulated that the corrosion product was made up of an inner layer of CoO and an outer layer of variable composition of $Co_{3-x}O_4$, depending on the passivation potential and pH values. They found that the corrosion product of a WC-Fe sample consisted of WO_3 and reaction products of the binder, i. e. iron oxides mixed with soluble salts of Fe^{2+} and Fe^{3+} cations.

Anodic polarisation of pure Co in 0.01 M H_2SO_4 + 0.99 M Na_2SO_4 showed a pink colour of Co^{2+} which appeared on the surface. This gradually disappeared as the surface was covered with a jet-black film (Tomlinson & Linzell, 1988).

An in-situ Fourier Transform Infrared (FT-IR) investigation of the corrosion products of WC-Co in 0.5 M Na_2SO_4 showed the formation of hydrated carbon dioxide (CO_2). This occurred for the potentials in the range + 1.0 to + 1.2 V vs Ag/AgCl. Time-dependent bands recorded showed the formation of $Co(OH)_2$ at the corrosion potential and at anodic polarisation potentials (Bozzini *et al*., 2003 {b}).

Hochstrasser-Kurz *et al*. (2008) used X-ray photoelectron spectroscopy (XPS) measurements to investigate polished and air exposed WC-Co hardmetal and found that $Co(OH)_2$ was the dominant constituent covering the Co phase. On the WC phase, a thin layer of WO_2 and WO_3 compounds were found. After one hour of exposure in borate buffer solution (pH 8.4), the XPS spectra gave an indication of a thickening $Co(OH)_2$ layer in parallel with selective W dissolution.

This study aims to further investigate some of the issues raised here by using Raman and X-ray diffractometry to determine the molecular composition(s) of compounds formed on corroded surfaces in various corrosive electrolytes.

2.8.7 WC – Co corrosion: Effect of other carbides

Electrochemical tests done on WC-Co, WC-Co-Cr_3C_2 and WC-Co-Cr_3C_2-VC in H_2SO_4 + Na_2SO_4 have shown that the passivation current density, i_{pass}, is substantially decreased by chromium whereas the presence of vanadium has, at best, only a marginal effect (Tomlinson & Ayerst, 1989). Sutthiruangwong *et al*. (2005), amongst others, have also confirmed the beneficial effect of Cr_3C_2 in WC-Co. Furthermore, they found that VC decreased the current density dramatically by about two orders of magnitude in the pseudopassive region. This was attributed to the VC segregating as a thin layer between the WC grains and thus separating the binder from the WC grains, as well as to the formation of VO^{2+} in the passivation range.

The positive effect of VC had also been reported earlier by Sutthiruangwong & Mori (2003). When a chronoamperometry measurement was run on WC-6% Co-0.5% VC in 1 N H_2SO_4, the current density measured at an active potential decreased steadily with time while at the pseudopassive potentials, there are oscillatory current responses. This was due to film formation in the

pseudopassive potential range which dropped the current density to a lower value because of the high resistivity of the passive film. Due to the instability of the film, the current increased again, leading to an oscillating current density response with time. The oscillatory current response might be due to pitting (Human & Exner, 1997; Ringas *et al*., 1990). Also vanadium, which is a grain growth inhibitor, formed a thin layer and was deposited on the basal planes of the WC grains. As Co dissolved, Co ions (Co^{2+}) had to diffuse out through the porous WC and this diffusion was slower than free diffusion.

Work in the WITS laboratory (Broccardo, 2003) has shown that the corrosion resistance of WC-VC-Co grades increases with increasing Co content when polarised in H_2SO_4. This corrosion behaviour was in agreement to the case with the straight WC-Co grades, since there was an increase in corrosion resistance when the Co content was increased.

Sebeya (2006) investigated the cause of the difference in the corrosion behaviour of WC-Co and WC-VC-Co hardmetals in 1 N H_2SO_4. The corrosion rate of WC-10Co and WC-67VC-10Co alloys were similar since there was no difference between the two hardmetals of low Co content (10 wt% Co). In comparison to the results obtained by Broccardo (2003), VC addition to the WC-Co alloy appeared to improve corrosion resistance with a high Co content. The fcc-Co/hcp-Co ratio was high at high Co content (30%) in the WC-VC-Co hardmetal which contributed to the improved corrosion resistance. At low Co content (10%), the fcc-Co/hcp-Co amounts as determined by Rietveld analysis were similar.

The addition of refractory metal carbides such as TiC and TaC in WC-Co appear to have mixed results. Mori *et al*. (2001) reported that small amounts appear to have no influence on corrosion resistance of WC-Co in acidic, neutral, and alkaline solutions. However, higher amounts of TiC and TaC

appear to decrease current density at potentials over – 200 mV by approximately one order of magnitude in both acidic and neutral solutions, but not in alkaline media. They postulated that the lower current density was due to the partial dissolution of TiC and TaC in the binder. It is probable though, that the higher amounts of TiC and TaC reduced the volume percent of Co present, hence making less Co available for corrosion. On the other hand, Tomlinson and Linzell (1988) reported that TiC and TaC as additions in the hardmetal had little effect on the polarisation behavior in a 0.01 M H_2SO_4 + 0.99 M Na_2SO_4 solution. Lower concentrations of carbon in the TiC and TaC hardmetal produced lower values of i_{crit} and i_{pass} and a significantly higher value of E_{corr}. This was as a result of a high concentration of W in the binder when the concentration of carbon in the binder was low and this produced a correspondingly higher degree of passivation.

The literature survey shows that there is not much corrosion work that has been done on WC-VC-Co hardmetals, even though their mechanical properties have been found to be superior to the straight WC-Co hardmetal. For example, there is no work in literature describing the effect of increasing VC concentrations on the corrosion process, or the nature of passive film formation during the corrosion process.

CHAPTER THREE

3 EXPERIMENTAL PROCEDURE

3.1 Introduction

Various experimental procedures have been employed to determine the effect of varying VC contents on the corrosion behaviour of the WC-VC-Co materials. The experimental procedures are described in detail below.

3.2 Experimental materials

Four samples of WC-Co with different VC contents were used for this project. Though the Co content is not exactly the same, the effect of the difference in content on corrosion behavior is deemed to be insignificant. Table 3.1 gives the percentage chemical composition of each sample.

Table 3.1 The material specification of WC-VC-Co

Material	%WC	%VC	%Co
1	90	0	10
2	89.6	0.4	10
3	78	10	12
4	62	27	11

3.3 Microstructure and composition

The samples were characterised before and after corrosion using scanning electron microscopy (SEM), X-ray diffraction (XRD), and Raman spectroscopy. The samples were polished to a 1 µm surface finish using diamond spray and diamond extender (lubricant) after grinding on a Struers, Aka-Piatto grinder with grades of 80, 120, 220, 600, and 1200.

3.3.1 Scanning electron microscope (SEM)

To identify the corrosion morphological of the alloys used, a JEOL 5800 scanning electron microscope was used at a voltage of 20 kV.

3.3.2 X-Ray Diffraction (XRD)

X-ray diffraction experiments were performed using a Phillips PW 1710 based powder diffractometer. A scan with a step size of 0.02° per minute was run from 10° to 80° 2 θ. Operating conditions were 40 kV and 20 mA, with a copper K-alpha tube as the anode. After each scan, the identification of peaks was done by using Expert HighScore® software.

3.3.3 Raman spectroscopy

A micro-Raman spectrometer (Senterra, Bruker Optics) coupled with a Peltier cooled CCD detector (576×288 pixels) and equipped with two lasers of 532 nm and 785 nm wavelengths was used. Samples were scanned over a range of 80 to 3200 cm^{-1} with a spectral resolution of about 2 cm^{-1}. A spatial resolution of up to 1 µm was achieved, depending on the set parameters. The number of acquisitions varied and signals were accumulated to improve the signal-to-noise ratio. Various power densities were used and delivered from 0.2 – 20 mW for the green laser and 1 – 100 mW for the near infrared laser. Spectral analysis was conducted using an in-house library and reports from literature were.

3.4 Electrochemical corrosion measurements

Samples were attached to insulating copper wires on one face with an aluminum conductive sticker tape and cold mounted, using epoxy resin and a

catalyst, in sample moulds. The samples were prepared as mentioned in Section 3.3 and cleaned in an ultrasonic bath with ethanol before immersion into the electrolyte.

An Autolab potentiostatic/galvanostatic instrument connected to a personal computer with General Purpose Electrochemical System (GPES) software was used for the electrochemical analysis. All tests were done at room temperature and the samples were scanned to obtain potentiodynamic anodic polarisation and chronoamperometry curves. A silver/silver chloride reference electrode (SSE) was connected to the cell via a Luggin probe capillary. A graphite rod was used as the counter electrode (CE). The tip of the probe was suspended approximately 2 mm from the working electrode. All the potentials reported were versus the SSE potentials.

After immersion of the samples, the open circuit potential (OCP) was measured for two hours. The potentiodynamic anodic polarisation scan followed the OCP. The scan rate and scan width were 2 mV/s and -600 mV to +1200 mV, respectively, for all the samples. The E_{corr}, i_{corr}, and the corrosion rate values were retrieved from the corrosion measurement data. Chronoamperometry measurements were done for at least eight hours with respect to the selected pseudopassivation potential to investigate the oxide film formed. All three scans were done one after the other in the order mentioned using the same solution so that the film formed could accumulate on the surface of the test specimen. After completion, the specimen was placed in a desiccator to dry before further analyses.

Reagent grade chemicals and distilled water were used for the preparation of the electrolytes and solutions were not deaerated. The electrolytes used were sulphuric acid (H_2SO_4), sodium chloride (NaCl), hydrochloric acid (HCl) and

synthetic mine water (SMW). The calculations of the amounts of chemicals used to prepare SMW are given in Appendix A.

3.5 ICP-OES analysis

A volume of 1 ml nitric acid (HNO_3) was used to digest the light green solid suspensions that evolved alongside the bubbles from the graphite rod during the chronoamperometry measurements of WC-0.4VC-10Co, WC-10VC-12Co and WC-27VC-11Co hardmetals in sodium chloride and synthetic mine water. After digestion, the solutions were analysed on a Genesis inductively coupled plasma-optical emission spectrometer (ICP-OES) to determine the amount of vanadium in solution. The wavelength used to measure the vanadium concentration was 292.464 nm, with an argon and crossflow nebulizer flowrate of 1 L/min. During the analysis, the plasma was viewed axially and the power of the ICP-OES was 1400 watts.

CHAPTER FOUR

4 RESULTS AND DISCUSSION

4.1 Introduction

The characteristics of the materials before corrosion are presented first, followed by the results of electrochemical corrosion investigations on the samples and the analysis of the corrosion products formed after the electrochemical experiments by X-ray diffraction and Raman spectroscopy. The reporting of the corrosion behaviour of the samples will start with hydrochloric acid, followed, respectively, by sulphuric acid, sodium chloride and synthetic mine water.

4.2 Characterisation of the materials before corrosion

4.2.1 X-ray diffraction (XRD)

Figures 4.1 to 4.4 show the XRD patterns of the samples before corrosion. Specimens WC-10Co and WC-0.4VC-10Co had similar patterns showing WC and Co. This is because the VC in WC-0.4VC-10Co (wt.%) was in quantities below the detection limit of the XRD. For the WC-10VC-12Co (wt.%) and WC-27VC-11Co (wt.%) , the VC was shown as (W,V)C and the intensity of the XRD peaks appeared to correspond with the amount of VC: the intensity was higher in the higher VC content alloy. The occurrence of (W,V)C was due to the dissolution of WC in VC (Exner, 1979). It has been shown by TEM studies that the (W,V)C is actually (V,W,Co)C (Sebeya, 2006). There was no eta phase in any of the specimens, implying that the sintering procedure for all the specimens was optimized. All the International Centre for Diffraction Data (ICDD) reference codes used to identify the XRD compounds in this study are given in Appendix C.

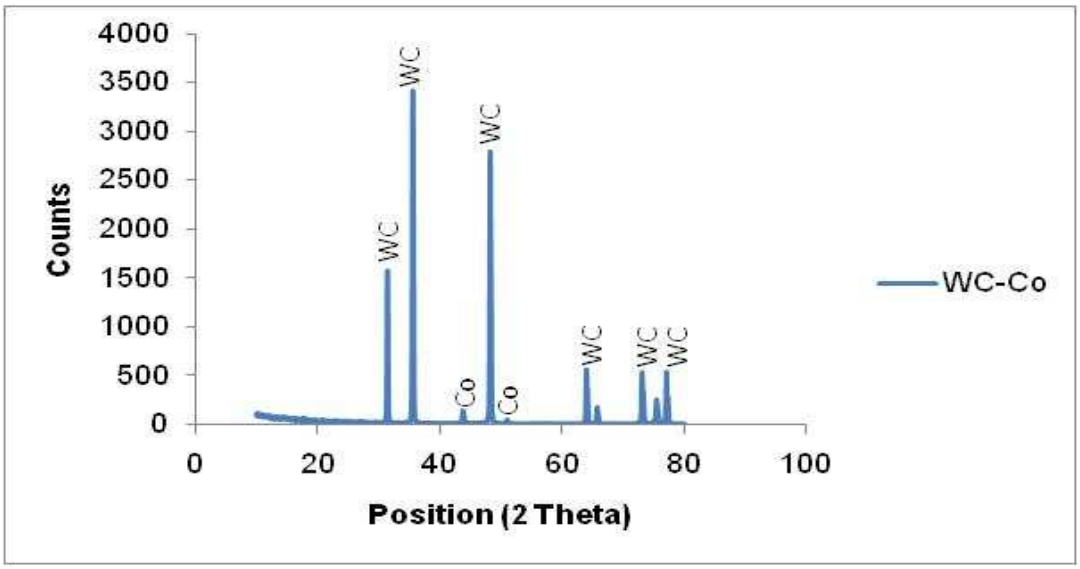

Figure 4.1. XRD pattern of the WC-10Co (wt.%) alloy showing WC and Co phases

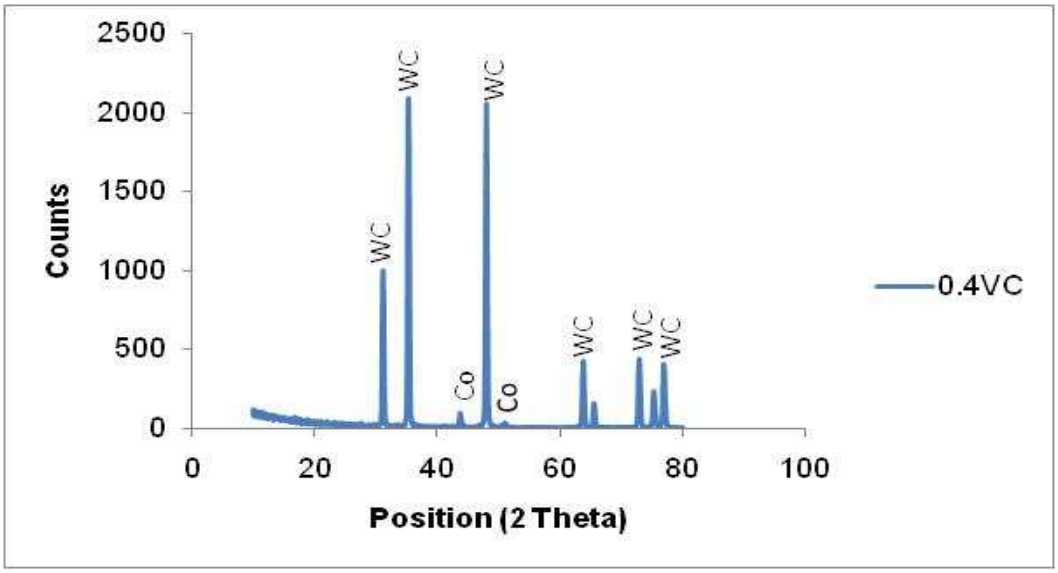

Figure 4.2. XRD pattern of the WC-0.4VC-10Co (wt.%) alloy showing WC and Co phases

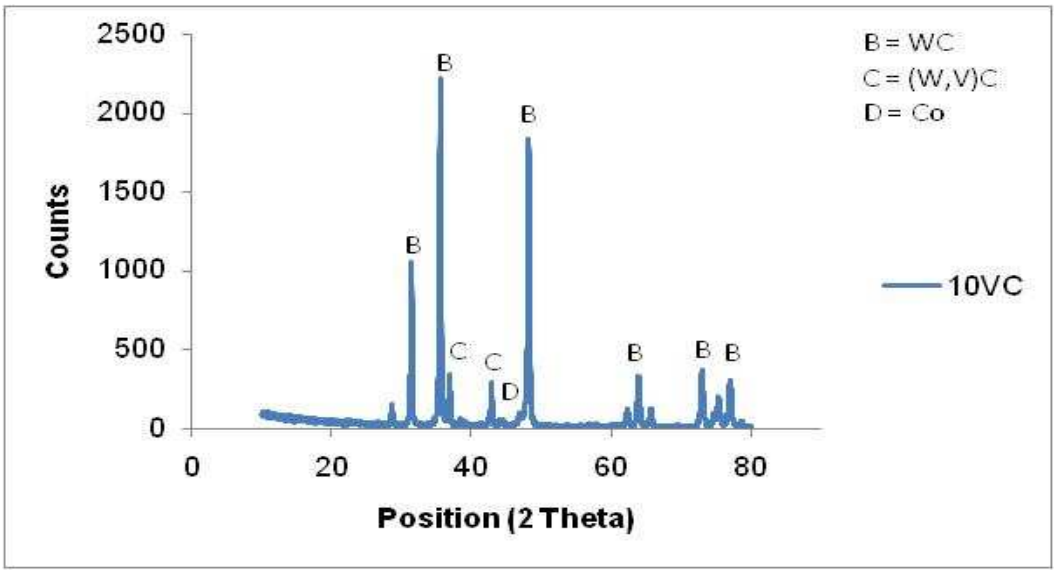

Figure 4.3. XRD pattern of WC-10VC-12Co (wt.%) alloy showing WC, (W,V)C, and Co phases. Not all the peaks were matched

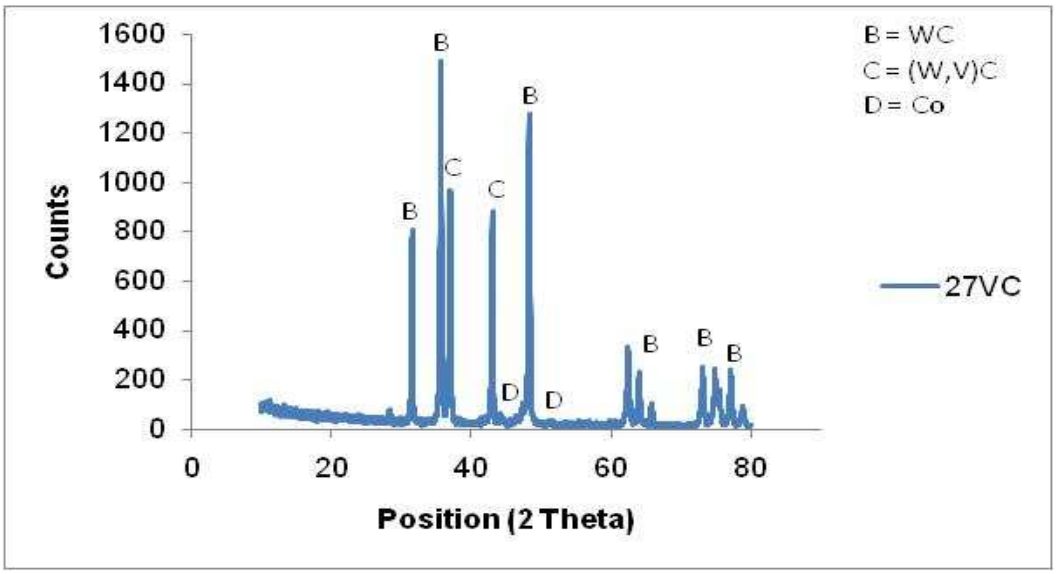

Figure 4.4. XRD pattern of WC-27VC-11Co (wt.%) alloy showing WC, (W,V)C, and Co phases. Not all the peaks were matched.

4.2.2 Scanning electron microscopy (SEM)

Figures 4.5 to 4.8 are the SEM microstructures of WC-10Co (wt.%), WC-0.4VC-10Co (wt.%), WC-10VC-12Co (wt.%), and WC-27VC-11Co (wt.%), respectively. There were two phases visible in the WC-10Co (wt.%) and WC-0.4VC-10Co (wt.%) alloys namely WC, being the light region and Co being the dark region. The vanadium carbide (VC) in the WC-0.4VC-10Co (wt.%) was not seen, because of its small quantity. The WC grain sizes are small in the WC-0.4VC-10Co (wt.%) compared to the straight grade WC-10Co (wt.%). This could have been caused by the VC acting as a grain growth inhibitor (Hashe *et al*., 2008; Luyckx *et al.*, 1996; Fang *et al*., 2005). In WC-10VC-12Co (wt.%) and WC-27VC-11Co (wt.%), there were three visible phases namely WC, the light region, a (W,V)C gray region as revealed by the XRD and a dark Co region.

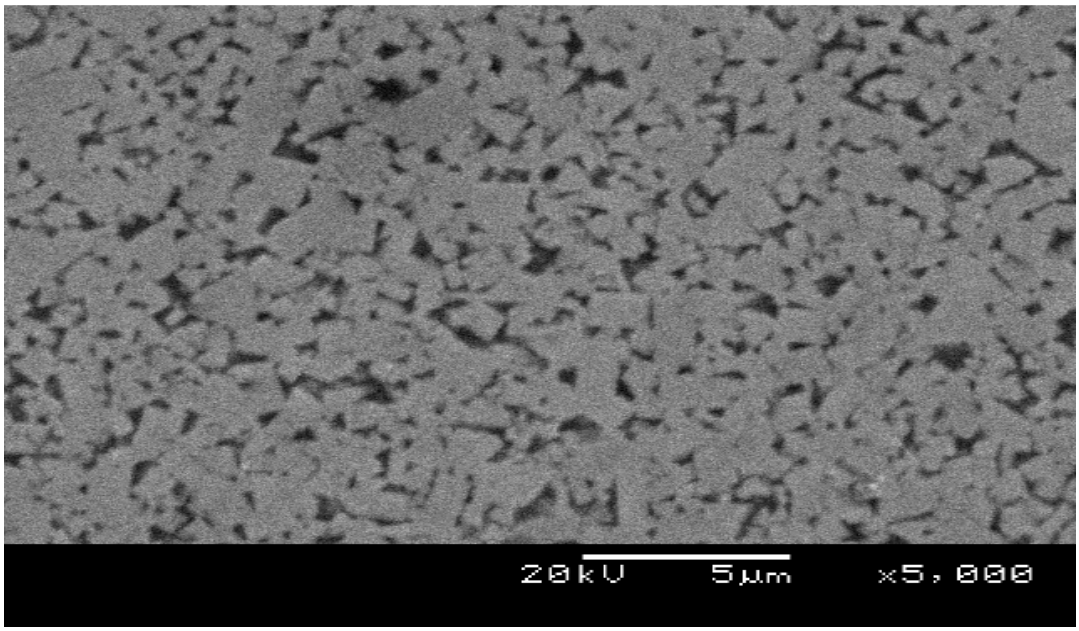

Figure 4.5. SEM image of WC-10Co (wt.%) before corrosion: the light particles are WC and the dark regions represent Co.

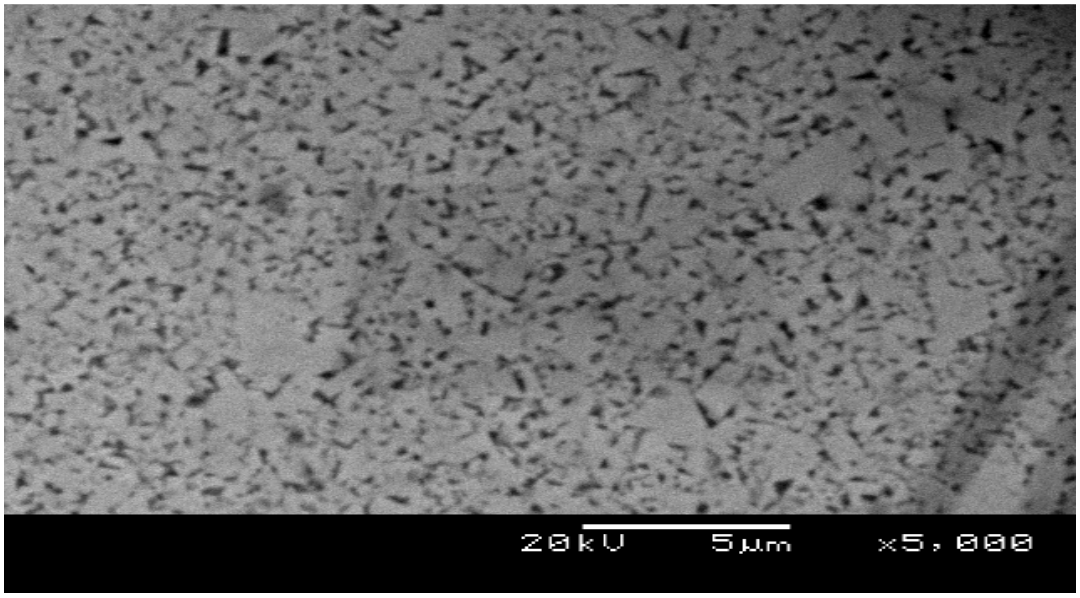

Figure 4.6. SEM image of WC-0.4VC-10Co (wt.%) before corrosion: the light particles are WC and the dark regions represent Co.

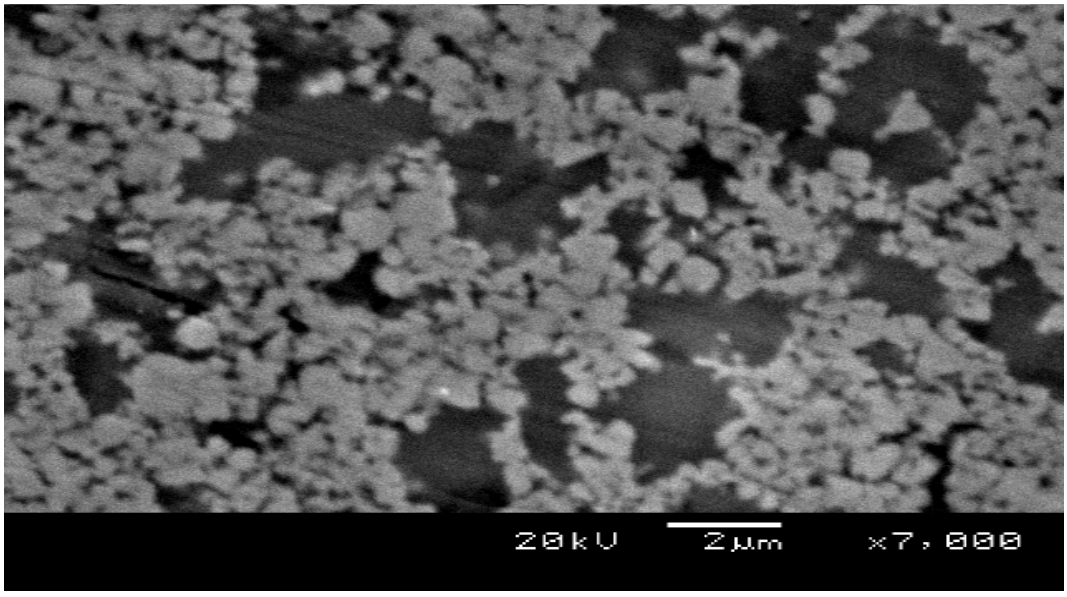

Figure 4.7. SEM image of WC-10VC-12Co (wt.%) before corrosion: the light regions are WC, gray regions (W,V)C and dark regions are Co areas.

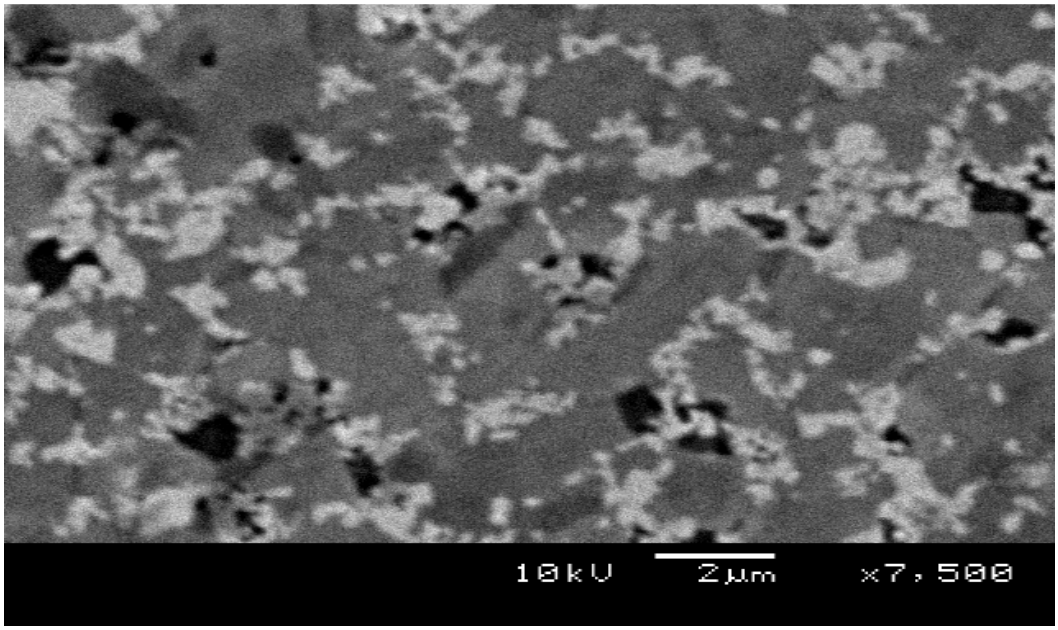

Figure 4.8. SEM image of WC-27VC-11Co (wt.%) before corrosion: light region is WC, gray region (W,V)C and a dark region Co.

4.2.3 Raman spectroscopy

The Raman spectra for all the hardmetals are presented in Figures 4.9 to 4.12. The WC-10Co exhibited four defined Raman peaks at 130, 684.5, 805 and 882 cm^{-1}. The 130 and 805 cm^{-1} are assignable to WC, while 684.5 cm^{-1} is assignable to Co. Similar peaks were observed in WC and Co powders (Appendix B). Two different spectra were found in WC-0.4VC-10Co (wt.%) and WC-27VC-11Co (wt.%). Except the peaks at 181.5, 416, 864 and 1136 cm^{-1} on the WC-27VC-11Co (wt.%), all the other peaks were almost the same as in the WC-10Co alloy. It is assumed that this difference could be due to the difference in amount of the VC and WC in the alloys. WC-10VC-12Co (wt.%) exhibited a lot of background noise and it was difficult to obtain a spectrum.

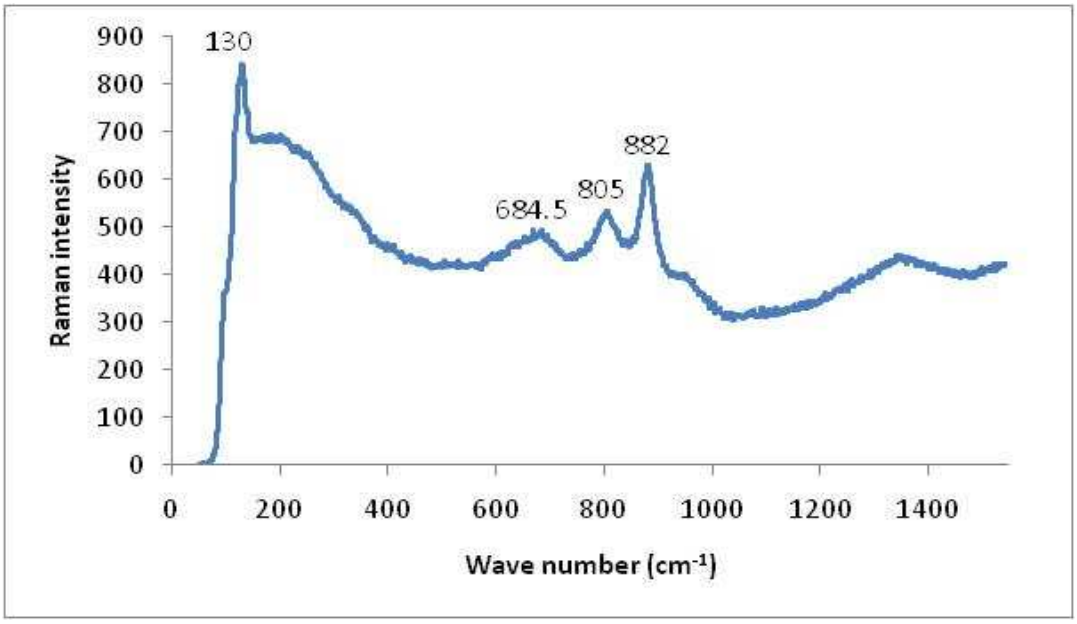

Figure 4.9. Raman spectrum of WC-10Co (wt.%) hardmetal before corrosion.

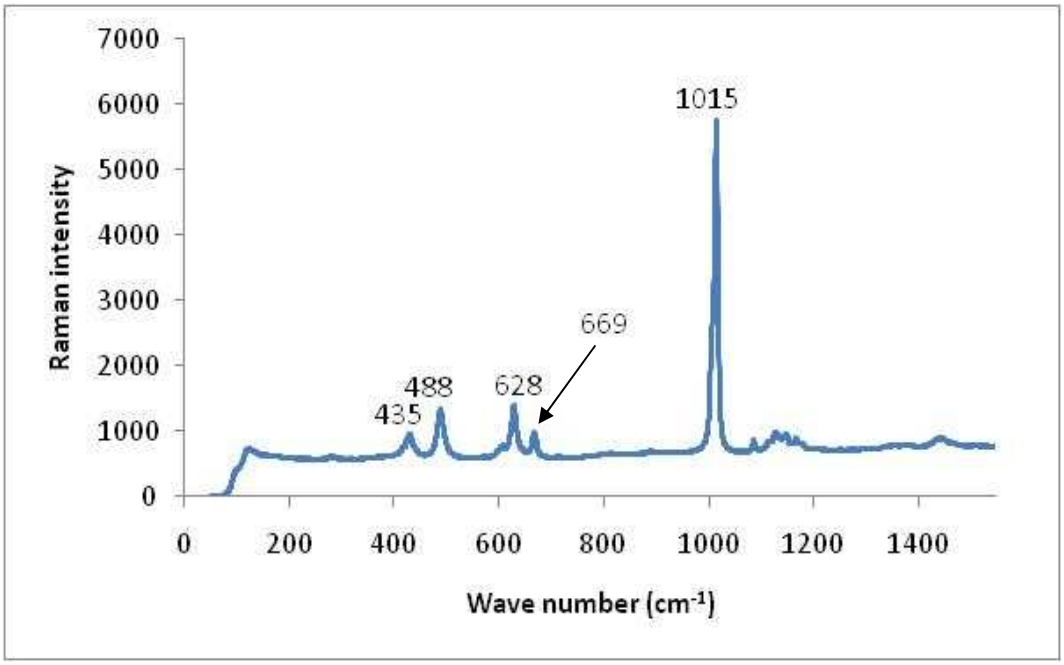

Figure 4.10. Raman spectrum of WC-0.4VC-10Co (wt.%) hardmetal before corrosion.

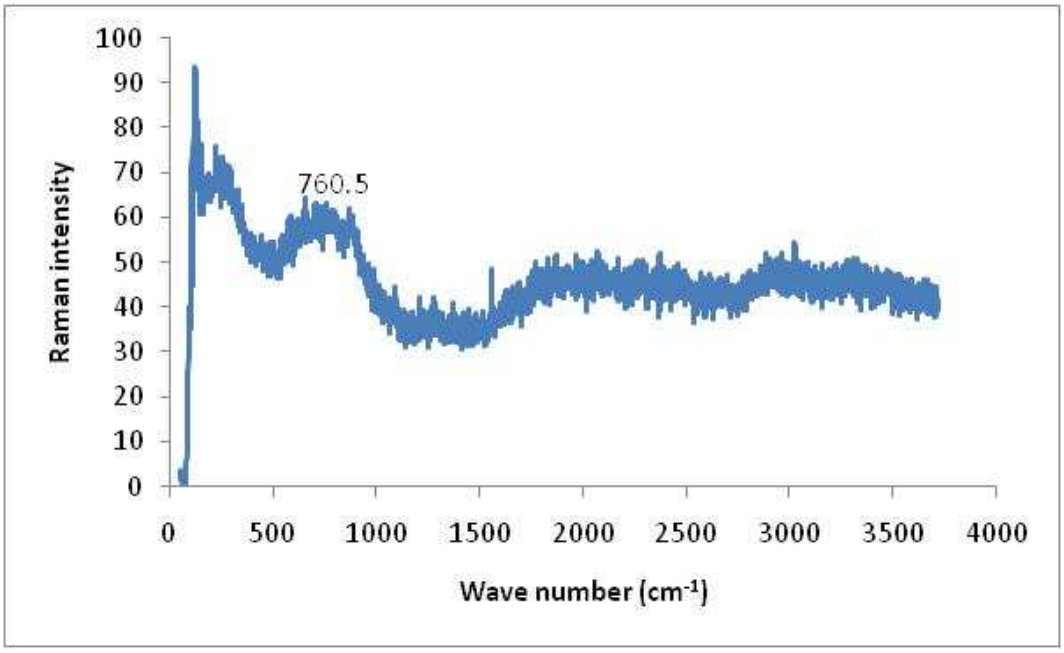

Figure 4.11. Raman spectrum of WC-10VC-12Co (wt.%) hardmetal before corrosion.

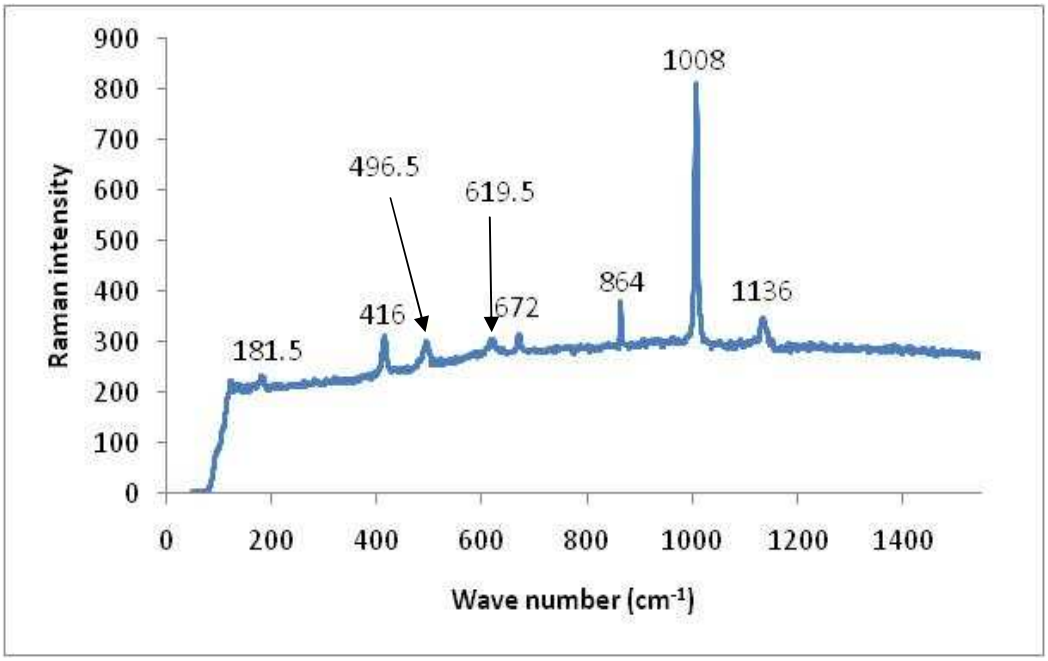

Figure 4.12. Raman spectrum of WC-27VC-11Co (wt.%) hardmetal before corrosion.

4.3 Corrosion behaviour in 1 m hydrochloric acid (HCl)

4.3.1 Open circuit potential (OCP) measurements

The open circuit potential (OCP), which is a measure of the potential of the sample at zero current, generally decreased within the first hour and then rose again slightly as shown in Figure 4.13, before stabilising. The WC-27VC-11Co (wt.%) had the most electronegative potentials of the four alloys.

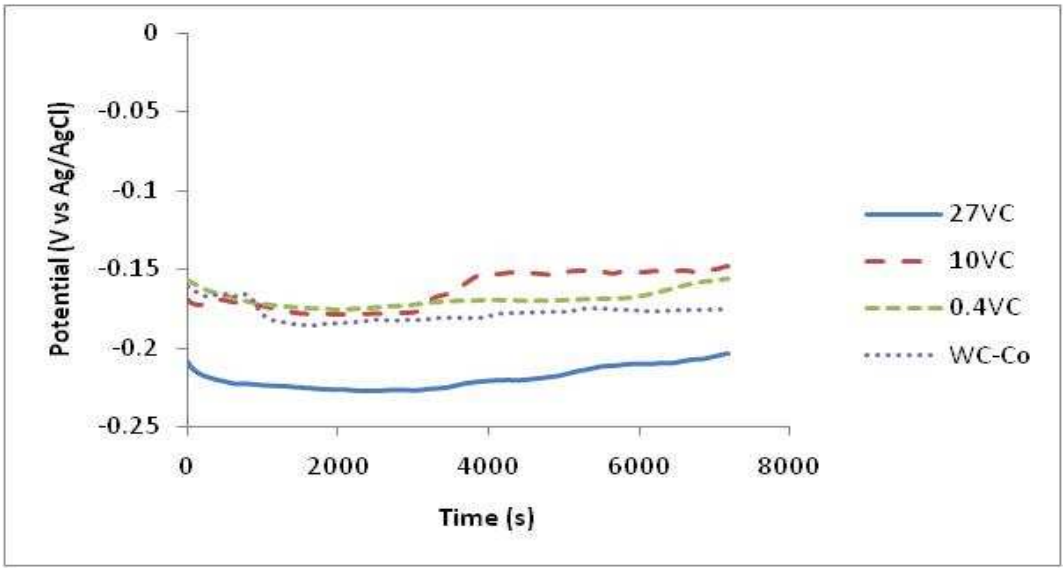

Figure 4.13. OCP curves of the various WC-VC-Co samples in 1 M HCl.

4.3.2 Potentiodynamic polarisation measurements

Except for the base alloy, the VC samples in 1 M HCl all have almost similar i_{pass} values of about 3.08E-02 A/cm^2 as reported in Figure 4.14, with the WC-27VC-11Co alloy's being the lowest. The addition of VC in the hardmetal affects the pseudopassivity thereof, by increasing the i_{pass} values between the potentials 0.8 V to 1.2 V when compared to the WC-10Co alloy. Below 0.8 V, the WC-10Co shows some difference compared with the rest of the alloys. An

active to passive transition seem to occur around 0.55 V. Sutthiruangwong & Mori (2003) reported a similar peak around 0 V. The current density of the WC-10Co alloy was found to decrease rapidly after 0.8 V. This agrees with the findings of Sutthiruangwong & Mori (2003). At above 0.8 V, WC in the WC-VC-Co hardmetals undergo oxidation and the oxidised product acted as a barrier to retard the further diffusion of Co ions into solutions out of the carbide skeleton. The pseudopassivation potential range of the straight grade was small compared to those of the WC-VC-Co hardmetals.

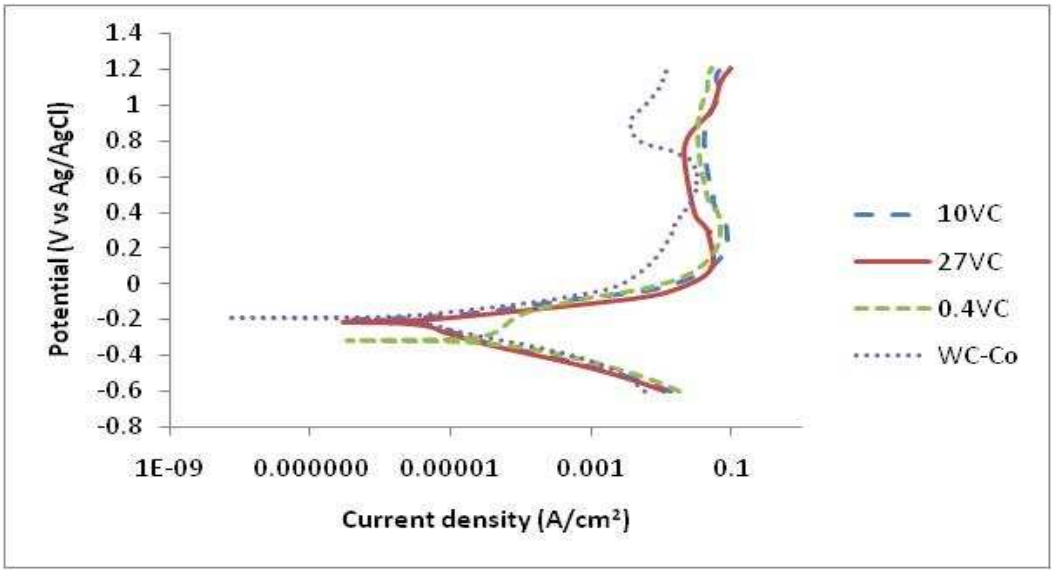

Figure 4.14. The potentiodynamic polarisation curves of the samples in 1 M HCl

4.3.3 Corrosion rate and E_{corr}

E_{corr} is a measure of the reactivity of a material while i_{corr} is proportional to corrosion rate. With the exception of WC-0.4VC-10Co (wt.%), which had the most negative E_{corr} value, the rest of the samples had similar E_{corr} values in 1 M HCl (Table 4.1). The corrosion current density remained similar for all the alloys, but decreased by one order of magnitude as the amount of VC

increased to 27wt.%VC. There was a consistent reduction of i_{corr} values as VC content increased. The WC-0.4VC-10Co (wt.%) showed the highest rate of corrosion compared to the rest of the samples.

Table 4.1**.** Electrochemical corrosion parameters of the various WC-VC-Co samples in 1 M HCl

Samples (wt.%)	E_{corr} (V)	i_{corr} (A/cm^2)	Corrosion rate (mm/year)
WC-10Co	-0.189	1.1E-06	7.6E-03
WC-0.4VC-10Co	-0.317	1.1E-05	7.3E-02
WC-10VC-12Co	-0.195	1.0E-06	8.0E-03
WC-27VC-11Co	-0.213	3.2E-07	3.1E-03

4.3.4 Chronoamperometry

Figure 4.15 shows the chronoamperometry curves of the samples in 1 M HCl. The potentials used were 0.6 V for the WC-VC-Co hardmetals, and 0.85 V for the straight WC-Co grade. All the samples showed a sharp drop in current density. It appears that an increase in VC content did not have a dramatic effect on the hardmetals as the chronoamperometry behaviour in 1 M HCl changed very little.

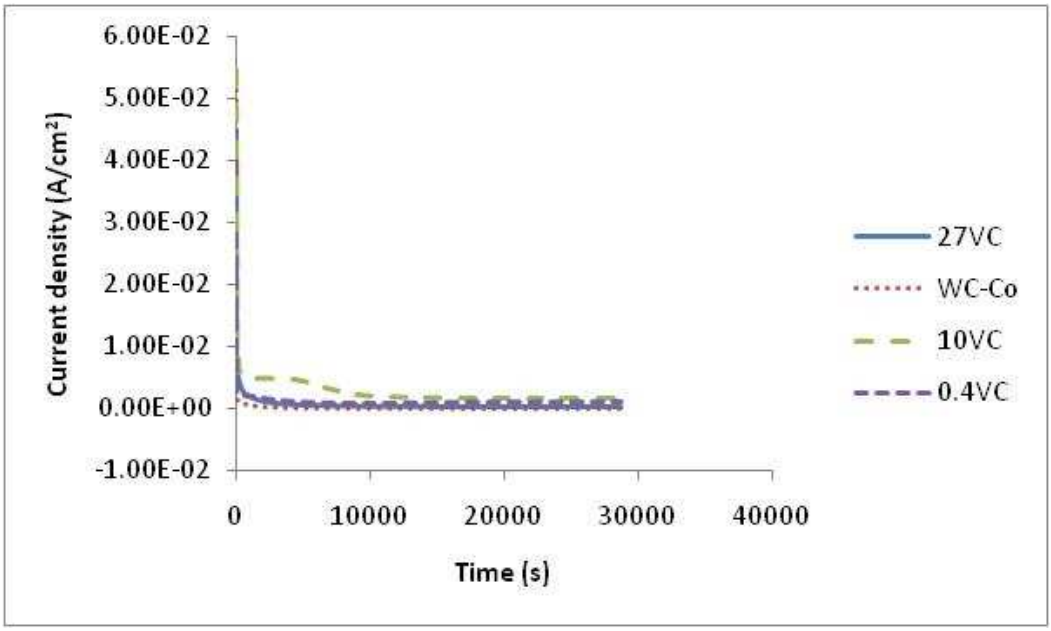

Figure 4.15. Chronoamperometry measurements of the various WC-VC-Co samples in 1 M HCl

4.3.5 Scanning electron microscopy (SEM)

Figures 4.16 to 4.19 are the SEM images of the corroded surfaces of the samples after polarisation scans, followed by eight hours of chronoamperometry measurements. The images show the formation of the various products on top of the individual samples. All the surface films were cracked, probably due to drying of the passive films.

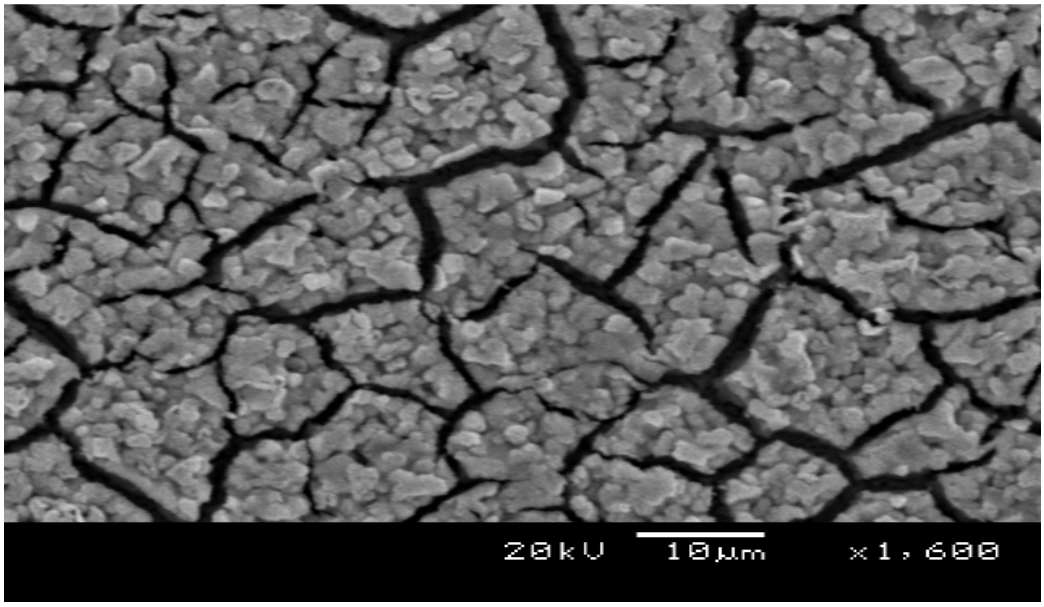

Figure 4.16 SEM image of the corroded surface of WC-10Co (wt.%) in 1 M HCl.

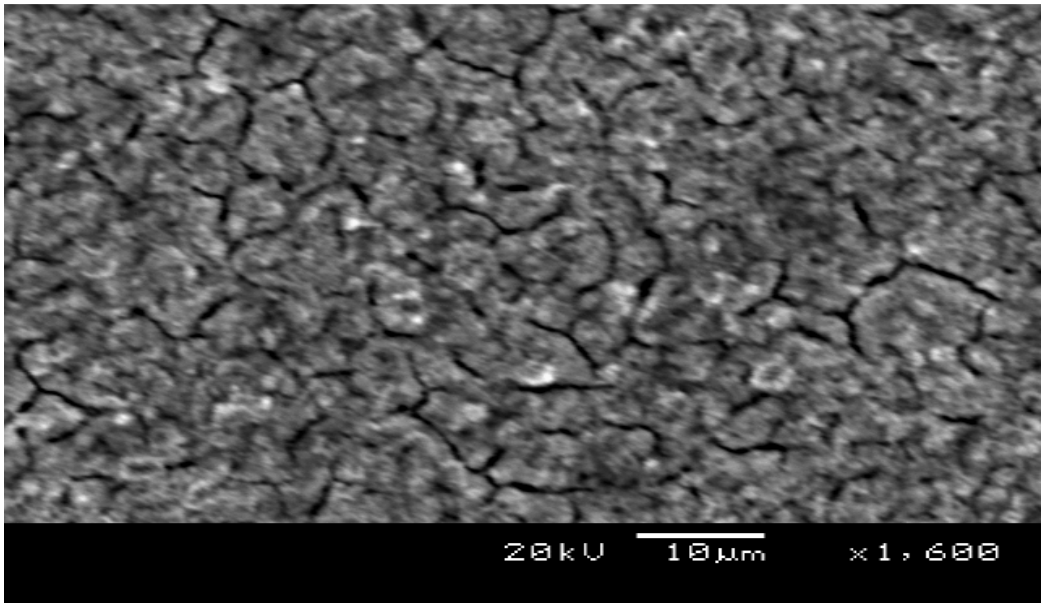

Figure 4.17 SEM image of corroded surface of WC-0.4VC-10Co (wt.%) in 1 M HCl.

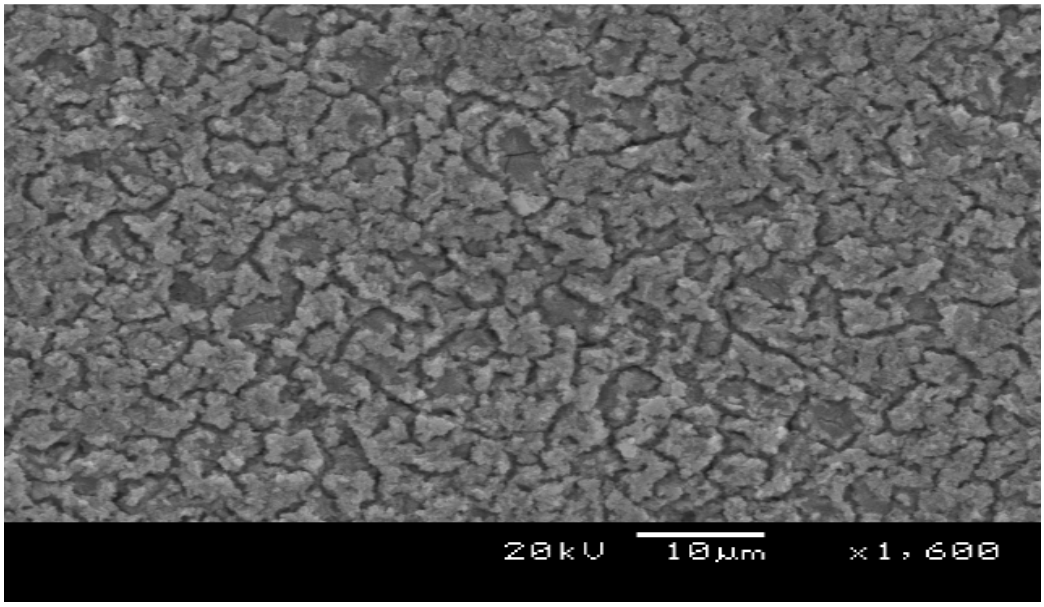

Figure 4.18 SEM image of corroded surface of WC-10VC-12Co (wt.%) in 1 M HCl.

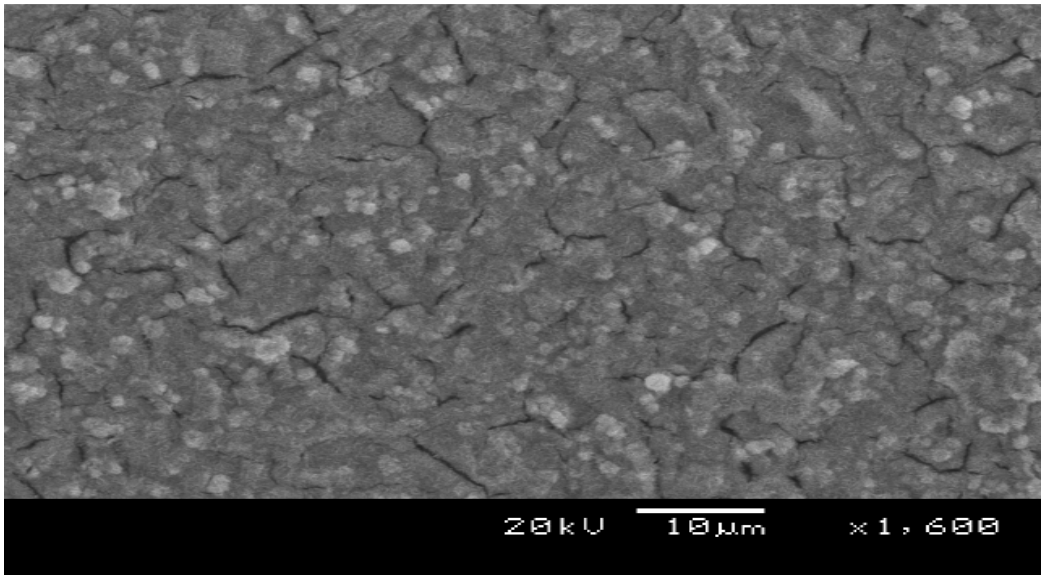

Figure 4.19 SEM image of corroded surface of WC-27VC-11Co (wt.%) in 1 M HCl.

4.3.6 X-ray diffraction (XRD)

WC-10Co (wt.%)

Figure 4.20 shows the XRD pattern of corroded surface of WC-10Co in 1 M hydrochloric acid (HCl) solution, which indicates the formation of hydrated tungsten oxide ($WO_3.H_2O$) as the corrosion product.

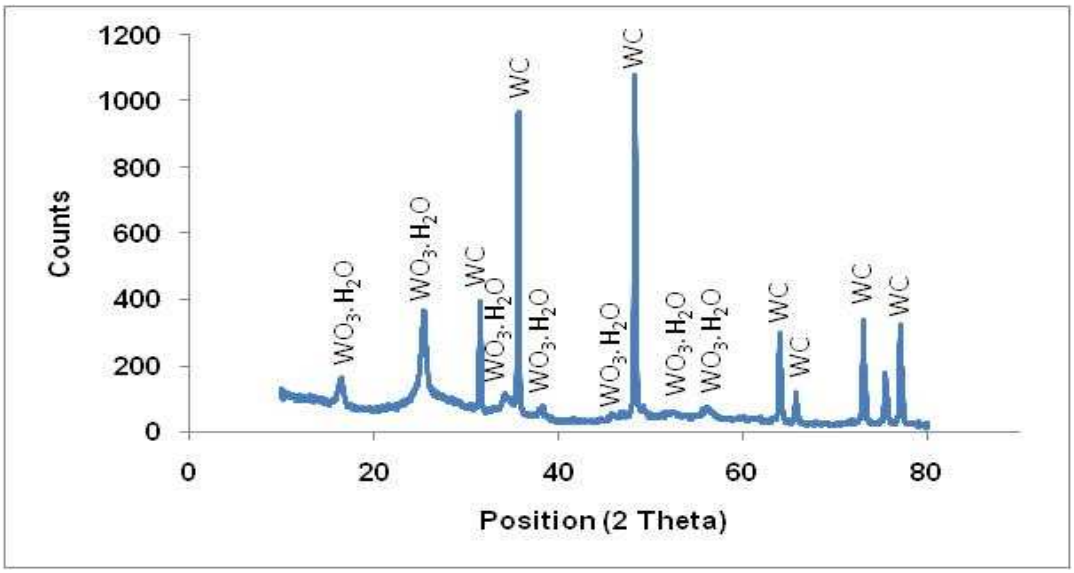

Figure 4.20 XRD pattern of the corroded surface of WC-10Co (wt.%) in 1 M HCl

WC-0.4VC-10Co (wt.%)

For WC-0.4VC-10Co, the XRD pattern showed the corrosion product as hydrated tungsten oxide ($WO_3.H_2O$), as two new peaks were found at 16.7° and 25.5°2 θ in Figure 4.21. No Co compound peaks were observed.

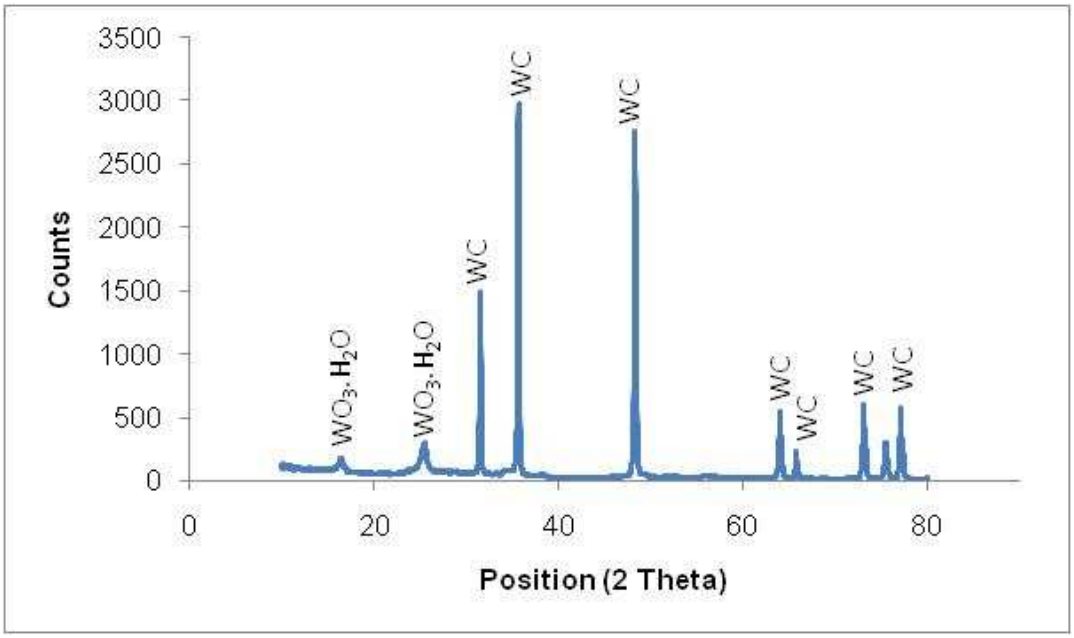

Figure 4.21 XRD pattern of corroded surface of WC-0.4VC-10Co (wt.%) in 1 M HCl

WC-10VC-12Co (wt.%)

Figure 4.22 shows that the relative peak intensity of the (W,V)C phase decreased as compared to the XRD pattern of the uncorroded sample (Figure 4.3), possibly as a result of the formation of hydrated tungsten oxide ($WO_3.H_2O$) observed as the corrosion product in HCl with the new peaks at the same positions as those found in Figure 4.21.

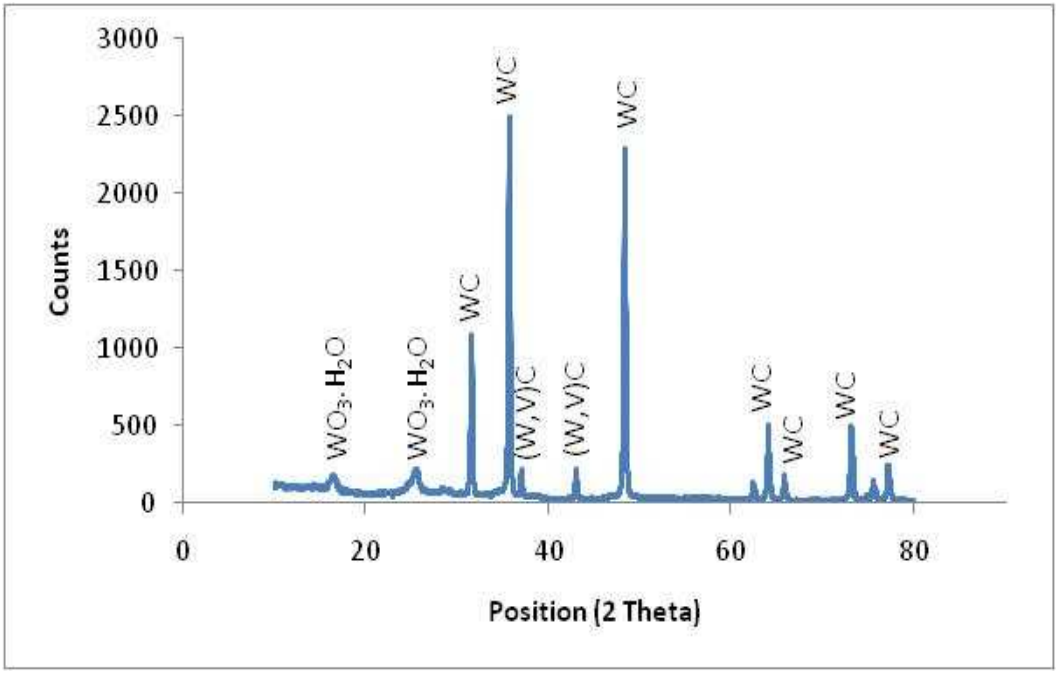

Figure 4.22 XRD pattern of corroded surface of WC-10VC-12Co (wt.%) in 1 M HCl

WC-27VC-11Co (wt.%)

Figure 4.23 shows that hydrated tungsten oxide ($WO_3.H_2O$) also formed on the WC-27VC-11Co (wt.%) in 1 M HCl solution. There was an increase in the peak intensities of the $WO_3.H_2O$ as compared to Figure 4.22 and a reduction in intensities of the (W,V)C phase as compared to the uncorroded sample, shown in Figure 4.4. Not all the peaks were matched and Co or its phases were missing.

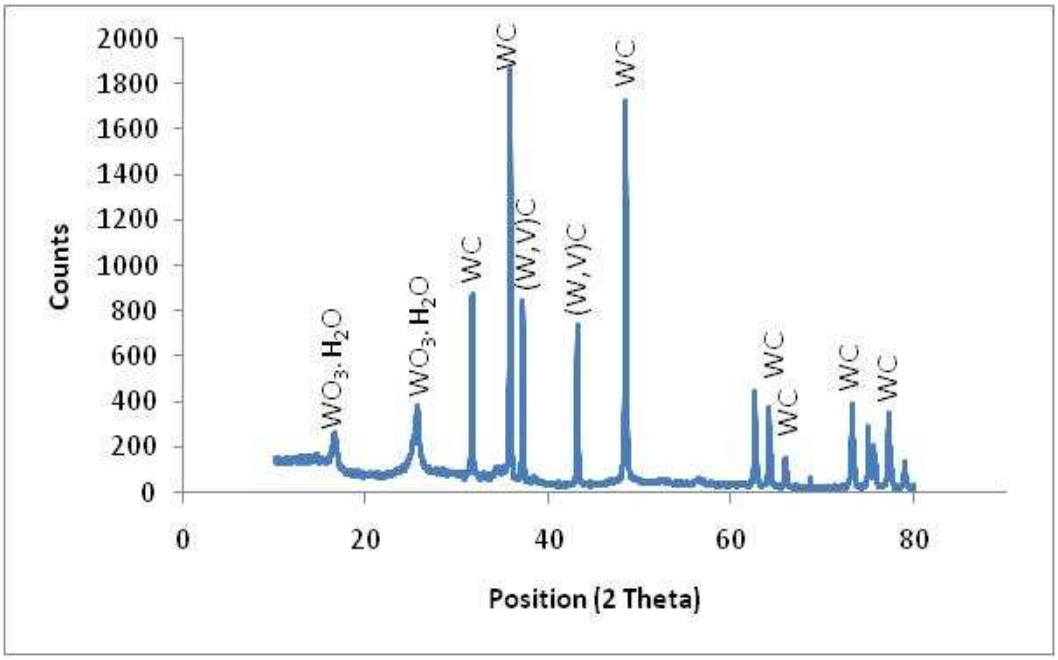

Figure 4.23 XRD pattern of corroded surface of WC-27VC-12Co (wt.%) in 1 M HCl

4.3.7 Raman Spectroscopy

The detection limit of the micro-Raman is much lower than that of the XRD technique, and it could potentially identify corrosion products formed during the process that are not detectable by XRD measurements. Figure 4.24 shows the Raman spectrum of the corrosion product on WC-10Co in 1 M HCl done within the 50 – 1550 cm^{-1} spectral range. The most prominent bands observed were 131, 263, 704, and 805 cm^{-1}, and are attributable to the monoclinic phase of WO_3 as reported by Regragui *et al.* (2000), Ingham *et al*. (2005), Wachs *et al*. (1987), Enesca *et al*. (2007), Bozzini *et al*. (2003 {a}, 2004), Daniel *et al*. (1987) and Wolcott *et al*. (2006).

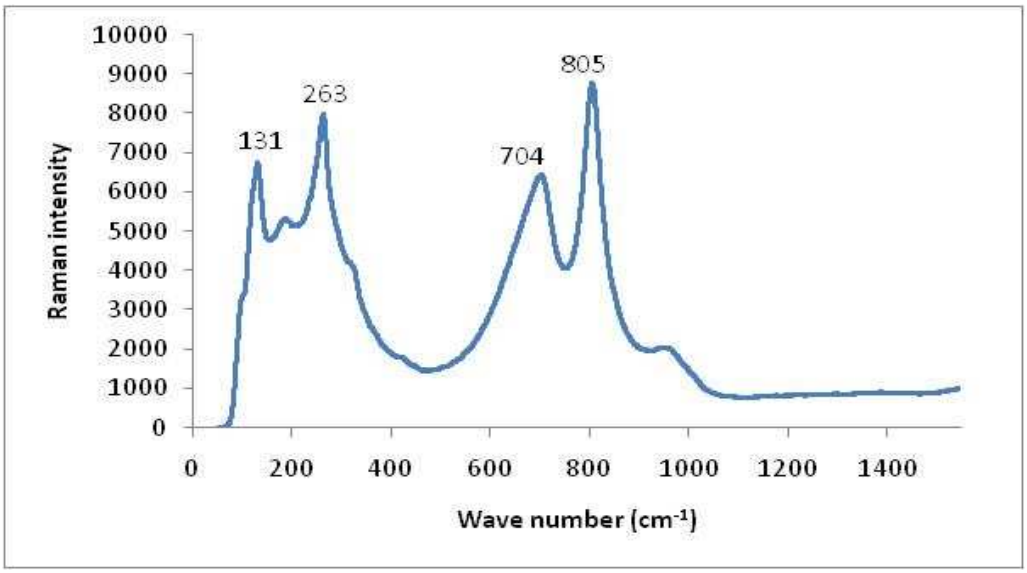

Figure 4.24. Raman spectrum of the corrosion product on WC-10Co (wt.%) in 1 M HCl

Figures 4.25 to 4.27 report the Raman spectra of WC-0.4VC-10Co (wt.%), WC-10VC-12Co (wt.%) and WC-27VC-11Co (wt.%) in 1 M HCl. Raman shifts for the corrosion products were observed at 131, 262, 705, 805, and 965 cm^{-1} for WC-0.4VC-10Co alloy. 131, 266, 705, 806 and 954.5 cm^{-1} for WC-10VC-12Co hardmetal and 131, 264, 328, 707, 804 and 883 cm^{-1} for WC-27VC-11Co. These were identified as tungsten oxide and hydrated tungsten oxide as reported already. These phases confirmed what was found on the XRD patterns.

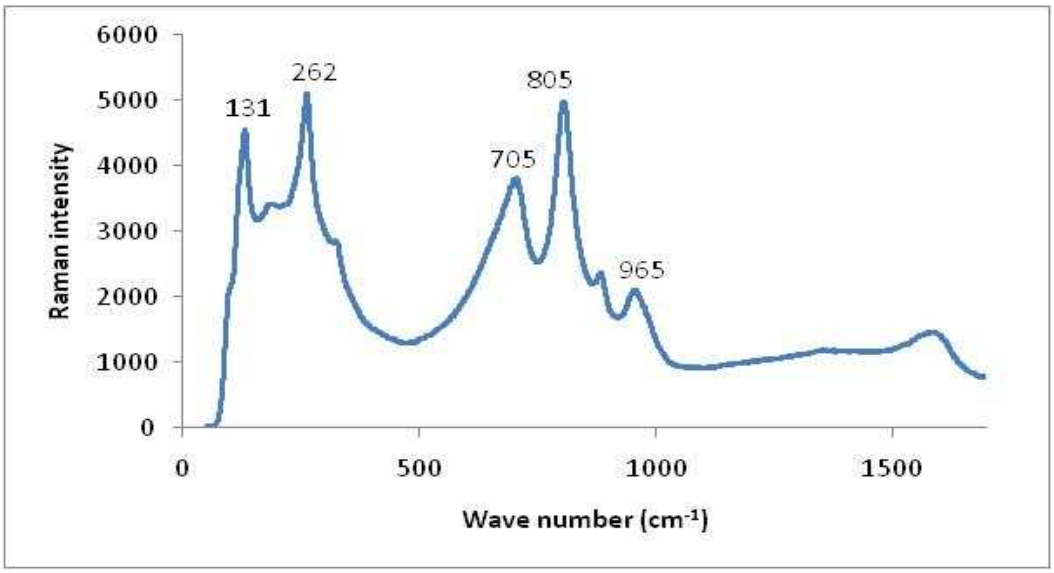

Figure 4.25. Raman spectrum of corrosion product on WC-0.4VC-10Co (wt.%) in 1 M HCl.

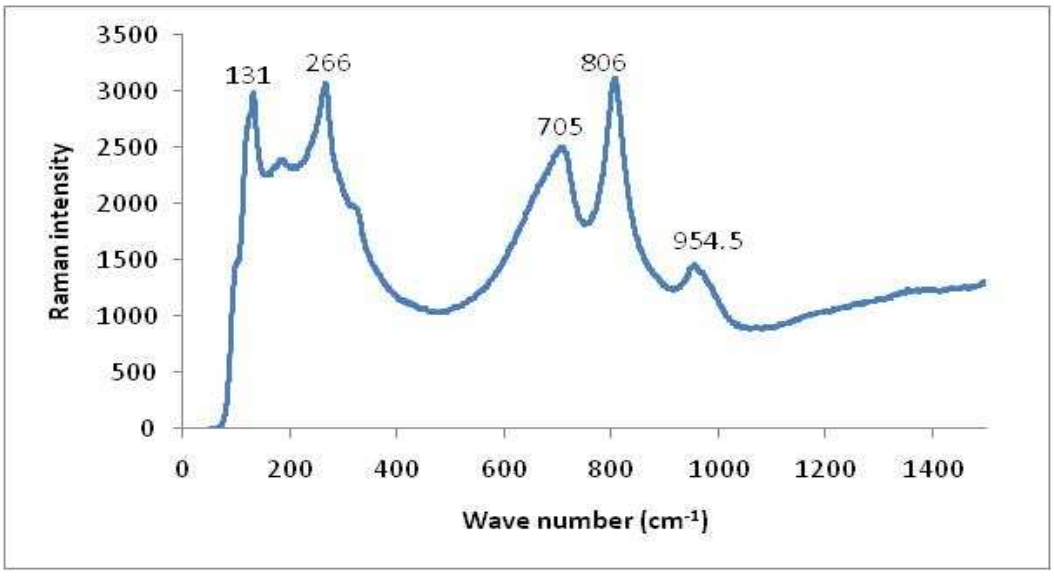

Figure 4.26. Raman spectrum of corrosion product on WC-10VC-12Co (wt.%) in 1 M HCl.

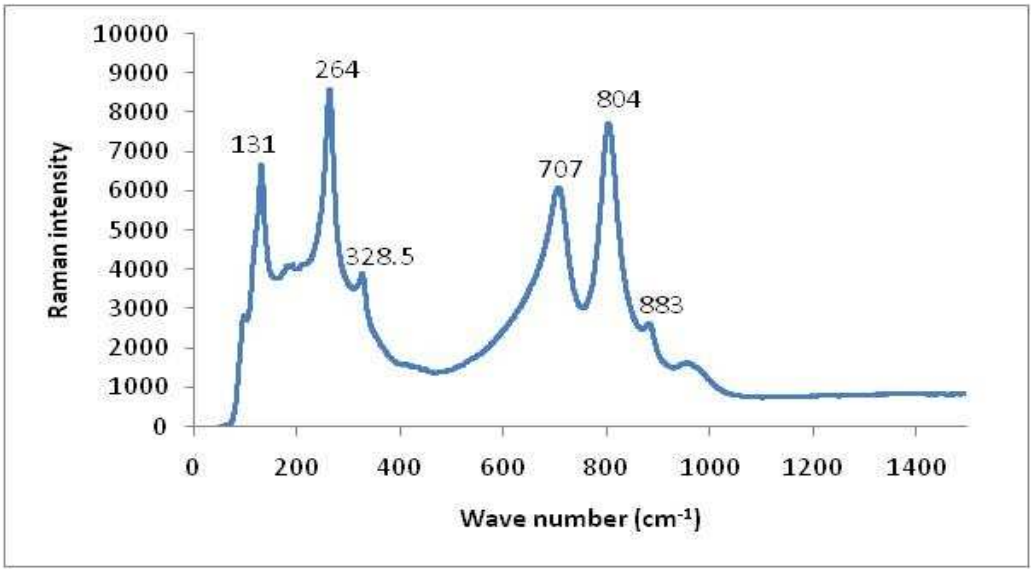

Figure 4.27. Raman spectrum of corrosion product on WC-27VC-11Co (wt.%) in 1 M HCl.

Table 4.2 summarizes the main phases detected on the surfaces of the test specimens before and after corrosion. All the test alloys lost Co after corrosion, and formed a new phase, either WO_3 or $WO_3.H_2O$, or both after corrosion.

Table 4.2 Main phases detected on alloy surfaces before and after corrosion in 1 M HCl

Alloy (wt.%)	Phases detected		
	Before corrosion (XRD analysis)	After corrosion	
		XRD	Raman
WC-10Co	WC Co	WC $WO_3.H_2O$	WO_3
WC-0.4VC-10Co	WC Co	WC $WO_3.H_2O$	WO_3 $WO_3.H_2O$
WC-10VC-12Co	WC (W,V)C Co	WC (W,V)C $WO_3.H_2O$	WO_3 $WO_3.H_2O$
WC-27VC-11Co	WC (W,V)C Co	WC (W,V)C $WO_3.H_2O$	WO_3 $WO_3.H_2O$

4.3.8 Discussion

The decrease in OCP of the WC-VC-Co hardmetal (Figure 4.13) shows that there was corrosion of the hardmetals for the first hour, as the chloride ions interacted with the hardmetal surfaces. This caused the Co ions to go into solution. High VC content in the WC-Co made the alloy slightly less noble, but there was not much difference between the OCP values for the lower VC additions.

In the anodic potentiodynamic curves (Figure 4.14), the increase of the i_{pass} values between the potentials 0.8 V to 1.2 V for the WC-VC-Co alloys when compared to the WC-10Co (wt.%) is due to the addition of the VC in the hardmetal, for with even the small amount of 0.4 wt.%, the electrochemical behaviour changed during the anodic polarisation. The i_{pass} of the WC-VC-Co alloys reduced positively between the potentials 0.8 and 1.2 V as VC increased.

The XRD revealed the formation of $WO_3.H_2O$ as the passive film formed by the WC-VC-Co hardmetals. This film accounts for the pseudopassivity observed on the polarisation curves of the specimens (Figure 4.14). No VC-based compound was obtained in the surface film. This suggests that VC did not take part in the passivation behaviour of the VC alloys. This is unlike the behaviour of Cr_2C_3 (Sutthiruangwong *et al*., 2005) and points to the fact that VC is not passivating. The small potential passive range of the base alloy might be due to the chloride ions as similar range was observed in 1 M NaCl (Figure 4.44).

The E_{corr} values, with the exception of WC-0.4VC-10Co (wt.%), were similar in the 1 M HCl media (Table 4.1). This is an indication that the effect of VC in

the hardmetal is small and E_{corr} is not affected much. The increase in VC content brought about a decrease in the corrosion rate probably as a result of the decrease in the volume fraction of the binder phase, all of which disappeared after corrosion (Table 4.2). This shows that the increasing VC content affected corrosion resistance positively.

The sharp drop of the current density during the chronoamperometry measurements (Figure 4.15), was due to the resistance of a passive film, that was shown by both XRD (Figures 4.20 – 4.23) and Raman spectroscopy (Figures 4.24 – 4.27) to be WO_3-based. An increase in VC content did not affect the variation of current, in line with earlier findings that the VC increment did not have a pronounced effect on the corrosion behaviour. The sharp drop in current densities and their stabilisation to steady state values was caused probably by the fact that the specimens were tested at potentials in their pseudopassive range (Lekatou *et al*., 2008).

The XRD and Raman measurements revealed the presence of hydrated tungsten oxide on the surfaces of all the test specimens. The formation of the oxide was due to the oxidation of WC. No VC based compound was present for the VC alloys. This shows that vanadium in the hardmetal did not take part in the formation of the passive film. The reduction in intensity of the (W,V)C phases in the XRD pattern of WC-10VC-12Co (wt.%) (Figure 4.22) might be due to it falling out of the hardmetal. Schnyder *et al*. 2004 has earlier found that the continuous dissolution of Co from a WC-Co surface can lead to the falling out of the hard carbides. The absence of Co peaks or its products on the XRD patterns of all the specimens is attributed to the galvanic coupling existing between Co and the hard carbides, thus enhancing its dissolution (Hochstrasser-Kurz *et al*., 2007, 2008).

4.4 Corrosion behaviour in 1 M sulphuric acid

Presented in this Section are the results and discussion of the corrosion behaviour of WC-VC-Co alloys exposed to 1 M sulphuric acid (H_2SO_4). The corrosion measurements i. e., the OCP, anodic polarisation and chronoamperometry scans are reported first followed by the surface analysis using SEM, XRD, and Raman spectroscopy.

4.4.1 Open circuit potential (OCP) measurements

Testing in H_2SO_4 revealed that the open circuit potential (OCP) of the samples were relatively stable throughout the two hours of exposure (Figure 4.28). The potential of the WC-0.4VC-10Co (wt.%) decreased gradually for the first twenty minutes and then stabilised afterwards. Generally, as the VC content increased, the OCP values decreased.

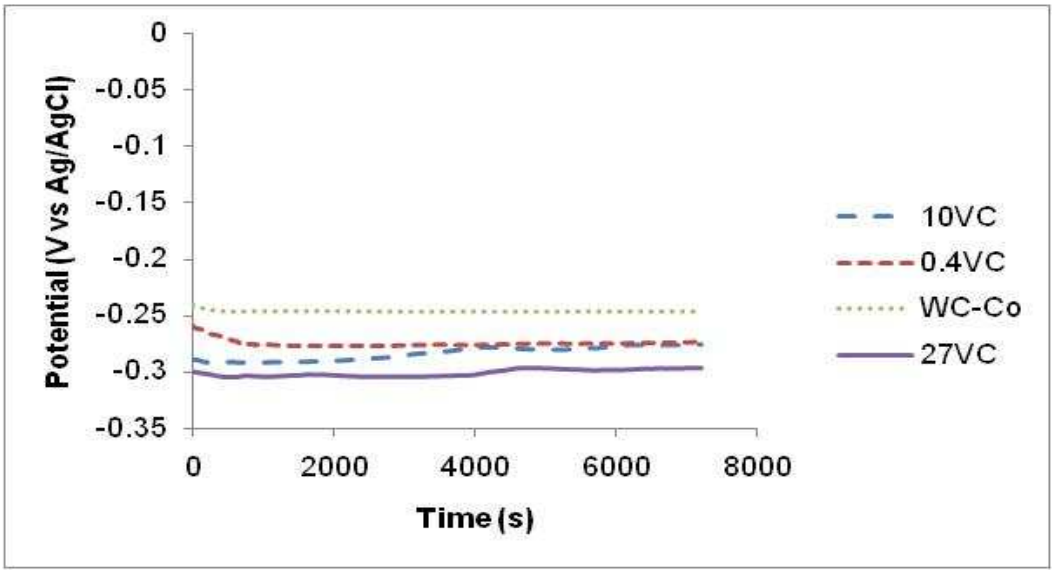

Figure 4.28 OCP curves of the various WC-VC-Co samples in 1 M H_2SO_4

4.4.2 Potentiodynamic polarisation measurements

The anodic potentiodynamic polarisation curves of the samples in 1 M H_2SO_4 are given in Figure 4.29. The base alloy and the VC containing samples all showed pseudopassivation behaviour. The pseudopassivity observed here for the base alloy is in agreement with literature (Broccardo, 2003; Sebeya, 2006; Sutthiruangwong & Mori, 2003; Human & Exner, 1997). The WC-10VC-12Co (wt.%) and WC-27VC-11Co (wt.%) seem to undergo a temporary secondary passivation after the transpassive region at 1.1 V. The secondary passivation behaviour of WC-10VC-12Co (wt.%) and WC-27VC-11Co (wt.%) is in agreement with earlier findings of Broccardo (2003). High amounts of VC in the hardmetal reduce the i_{pass} compared to small amounts.

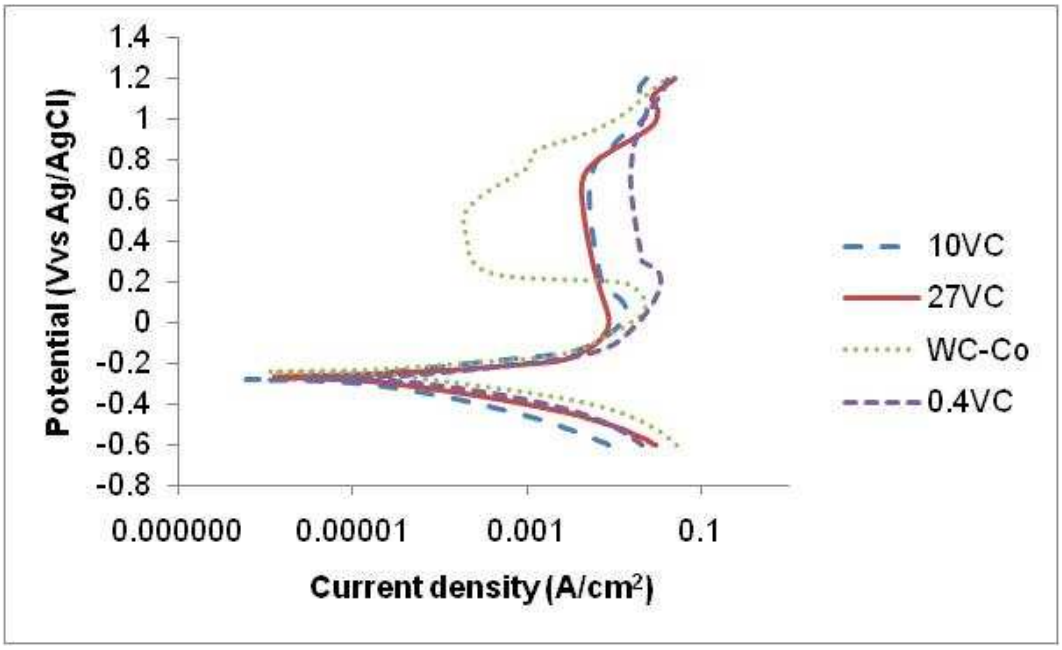

Figure 4.29 The potentiodynamic polarisation curves of the samples in 1 M H_2SO_4

4.4.3 Corrosion rate and E_{corr}

The samples all have similar E_{corr} values, as is shown in Table 4.3. The inclusion of VC did shift the E_{corr} values of the samples in H_2SO_4 to slightly more negative values. The E_{corr} value of WC-10Co (wt.%) agrees with values reported by Sebeya (2006) and Human *et al*. (1991). There was little change in corrosion current density for the various hardmetals in H_2SO_4. The corrosion rate values depicts that little change occurred with the addition of VC to the hardmetal. This corresponds to Sebeya's (2006) and Broccardo's (2003) findings that the corrosion rate between two WC-VC-Co hardmetals of low Co content could be similar.

Table 4.3 Electrochemical corrosion parameters of the various WC-VC-Co samples in 1 M H_2SO_4

Samples (wt.%)	E_{corr} (V)	i_{corr} (A/cm^2)	Corrosion rate (mm/year)
WC-10Co	-0.235	5.6E-06	3.8E-02
WC-0.4VC-10Co	-0.271	9.3E-06	6.2E-02
WC-10VC-12Co	-0.274	4.5E-06	3.5E-02
WC-27VC-11Co	-0.263	2.9E-06	2.7E-02

4.4.4 Chronoamperometry

Figure 4.30 shows the chronoamperometry curves of the investigated samples in 1 M sulphuric acid. The potentials used for the chronoamperometry measurements were 0.5 V for WC-10Co and 0.7 V for the VC containing hardmetals. The chronoamperometric curves displayed an instantaneous dramatic drop of the current density to a constant value throughout the whole period. This phenomenon is in contrast with results obtained by Sutthiruangwong *et al*. (2005). The difference might be due to the conditions used for the experiments: Sutthiruangwong *et al*. (2005) used

aerated 1N H_2SO_4 solutions while a non-aerated 1M H_2SO_4 solution has been used in the current study. The similarity of the chronoamperometric curves obtained in the current study supports earlier findings that an increasing VC content did not have a pronounced effect in acidic sulphate solutions (Sebeya, 2006; Broccardo, 2003).

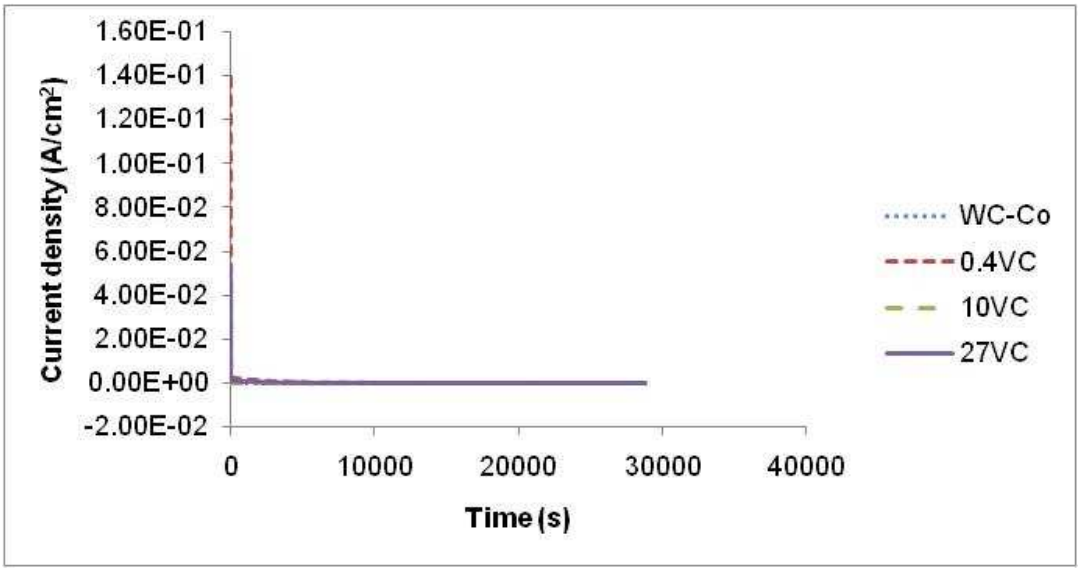

Figure 4.30. Chronoamperometry measurements of the various WC-VC-Co samples in 1 M H_2SO_4

4.4.5 Scanning electron microscopy (SEM)

Presented in Figures 4.31 to 4.34 are the SEM images of the corroded surfaces of the WC-VC-Co samples. Except for the surface of WC-10Co, those of the WC-VC-Co hardmetals were all cracked, probably because of the surfaces being dried.

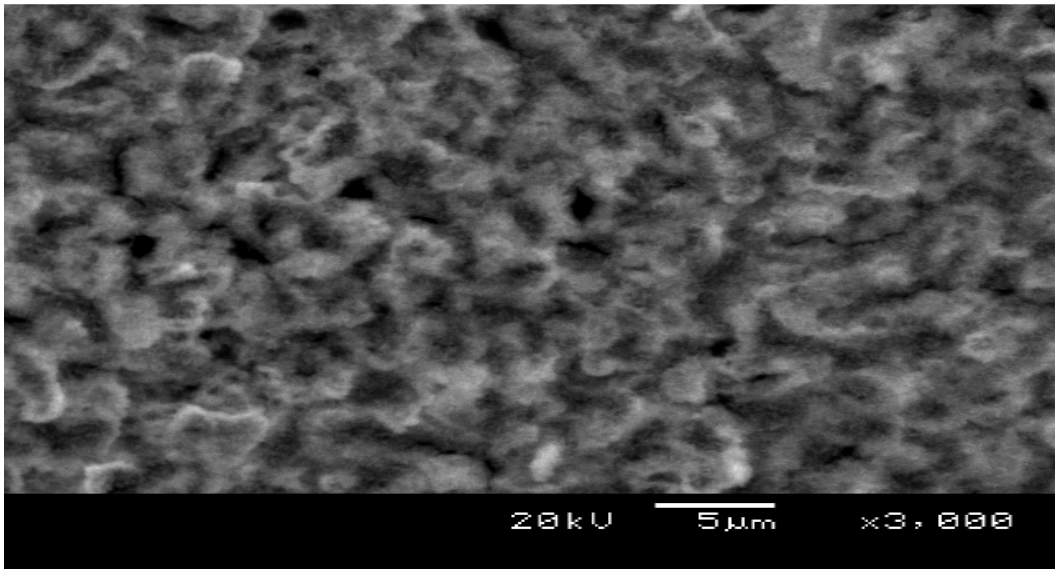

Figure 4.31. SEM image of the corroded surface of WC-10Co (wt.%) in 1 M H_2SO_4.

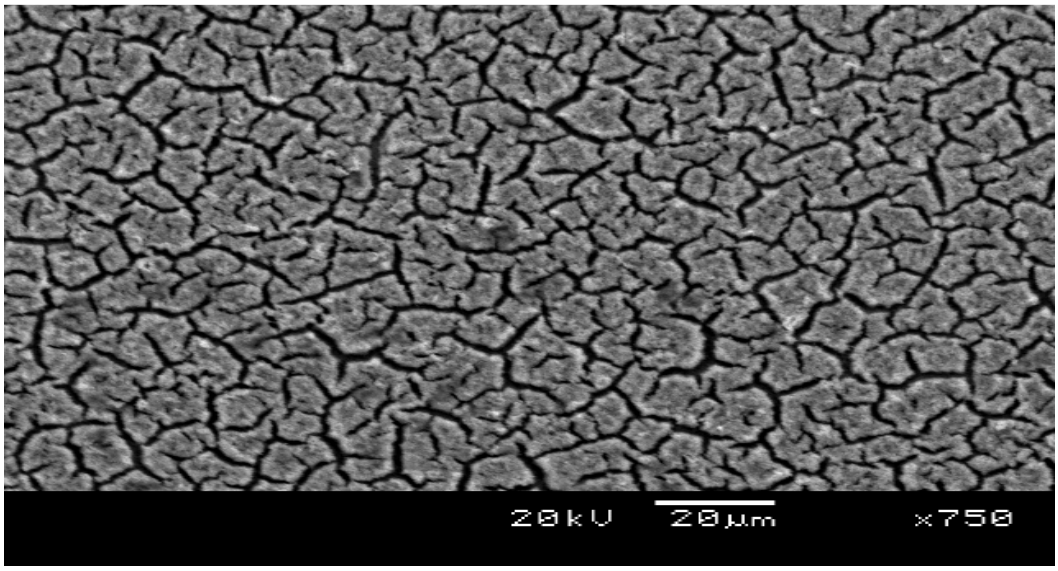

Figure 4.32. SEM image of the corroded surface of WC-0.4VC-10Co (wt.%) in 1 M H_2SO_4.

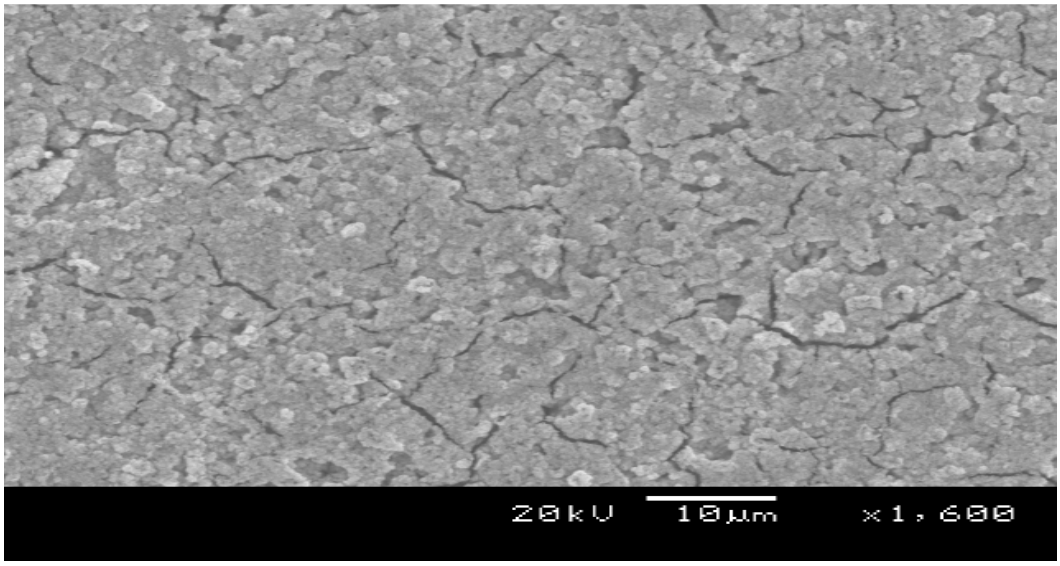

Figure 4.33. SEM image of the corroded surface of WC-10VC-12Co (wt.%) in 1 M H_2SO_4.

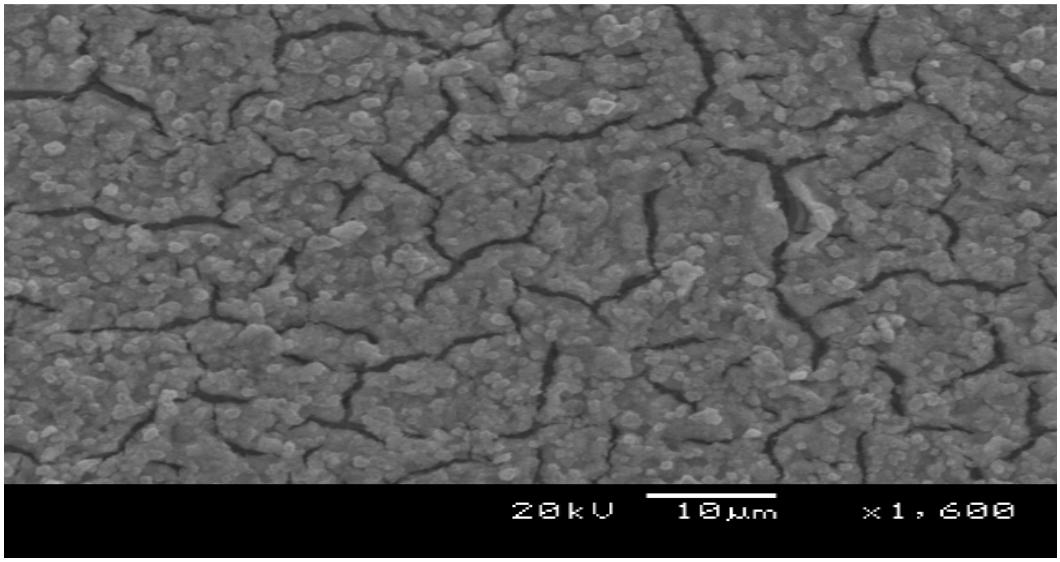

Figure 4.34 SEM image of the corroded surface of WC-27VC-11Co (wt.%) in 1 M H_2SO_4.

4.4.6 X-ray diffraction (XRD)

Figures 4.35 – 4.38 show the XRD patterns of the corroded surfaces of the test specimens in 1 M sulphuric acid (H_2SO_4) solution. Compared to the patterns before corrosion, (Figures 4.1 – 4.4), Co peaks are missing. This indicates that the Co went into solution during the polarisation measurements, thus supporting the observation that corrosion occurred in the binder phase (Hochstrasser-Kurz *et al*., 2007, 2008; Ghandehari, 1980; Schnyder *et al*., 2004). All the specimens had peaks for a hydrated form of tungsten oxide: $WO_3.2H_2O$ formed on WC-10Co (wt.%) (Figure 4.35) while $WO_3.H_2O$ formed for WC-0.4VC-10Co (wt.%), WC-10VC-12Co (wt.%), and WC-27VC-11Co (wt.%) (Figures 4.36 – 4.38). A second new phase, vanadyl sulphate ($VOSO_4.H_2O$) also formed in WC-10VC-12Co (wt.%) and WC-27VC-11Co (wt.%). No $VOSO_4.H_2O$ passive film formed for WC-0.4VC-10Co (wt.%) as reported in literature (Sutthiruangwong *et al*., 2005). For alloys WC-10VC-12Co (wt.%) and WC-27VC-11Co (wt.%) (Figures 4.37 and 4.38), the relative intensity of the peaks of the (W,V)C phase reduced as compared to the uncorroded samples, shown in Figures 4.3 and 4.4.

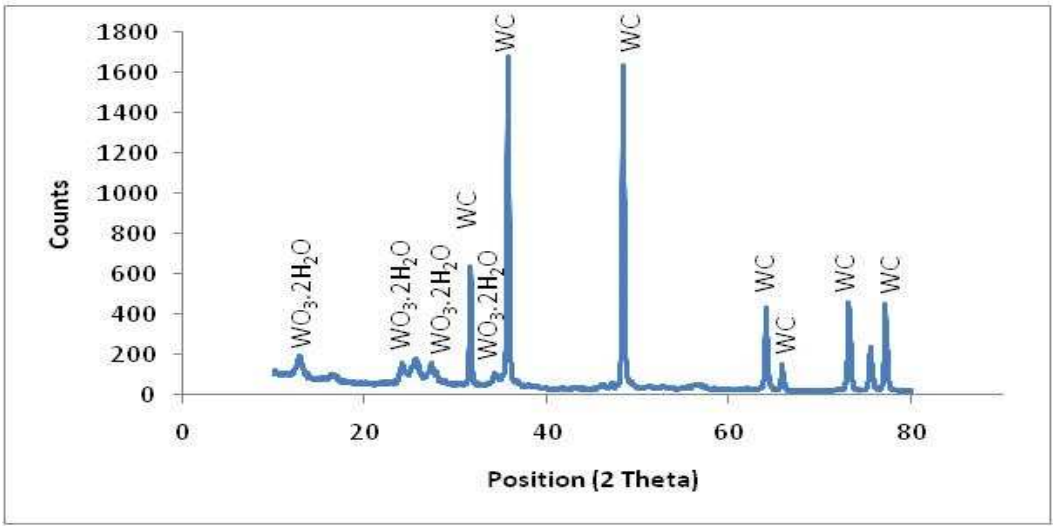

Figure 4.35. XRD pattern of the corroded surface of WC-10Co (wt.%) in 1 M H_2SO_4

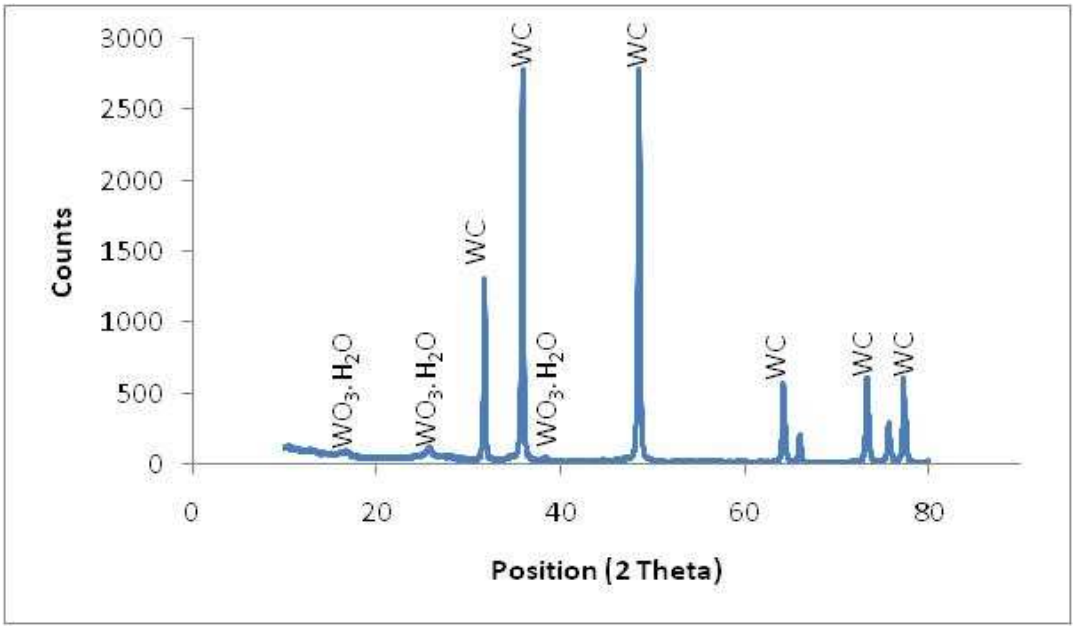

Figure 4.36. XRD pattern of the corroded surface of WC-0.4VC-10Co (wt.%) in 1 M H_2SO_4

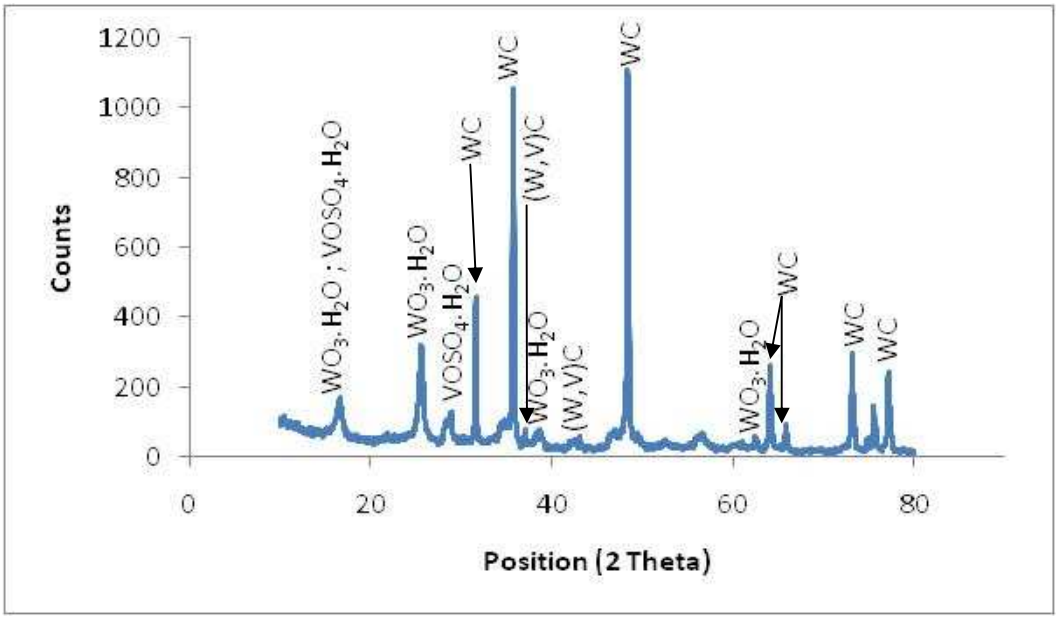

Figure 4.37. XRD pattern of the corroded surface of WC-10VC-12Co (wt.%) in 1 M H_2SO_4. Not all the peaks were matched.

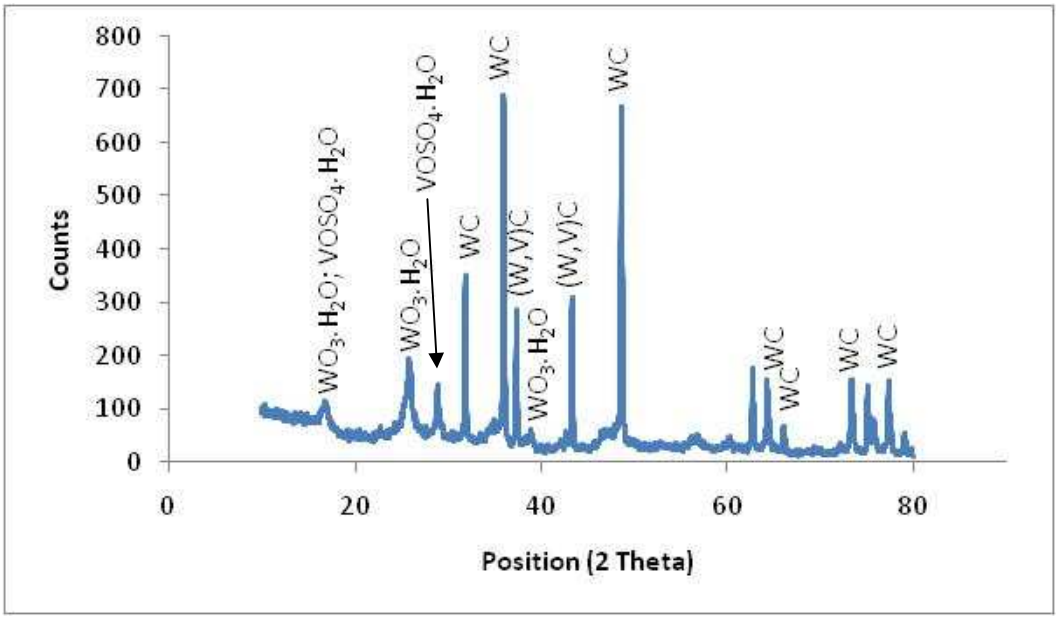

Figure 4.38. XRD pattern of the corroded surface of WC-27VC-11Co (wt.%) in 1 M H_2SO_4.

4.4.7 Raman spectroscopy

Figures 4.39 – 4.42 show the Raman spectra obtained on the surfaces of WC-VC-Co alloys after corrosion in H_2SO_4. Raman shifts for the corrosion products were observed at 131, 261, 705, 805, and 965 cm^{-1} for WC-10Co alloy; at 130, 261, 325.5, 707, 803 and 951 cm^{-1} for WC-0.4VC-10Co hardmetal; at 131, 262, 700, 800 and 950 cm^{-1} for WC-10VC-12Co; and at 194, 666 and 950 cm^{-1} for WC-27VC-11Co alloy. These wavenumbers were attributable to WO_3 and $WO_3.xH_2O$ (Regragui *et al.,* 2000; Ingham *et al*., 2005; Wachs *et al*., 1987; Enesca *et al*., 2007; Bozzini *et al*., 2003 {a}, 2004; Daniel *et al*., 1987; Wolcott *et al*., 2006; Gotic *et al*., 2000). This occurrence of WO_3 and $WO_3.xH_2O$ confirms the observations of the XRD analysis (Figures 4.35 – 4.38). No wave shifts attributable to $VOSO_4.H_2O$ were observed for alloys WC-10VC-12Co and WC-27VC-11Co.

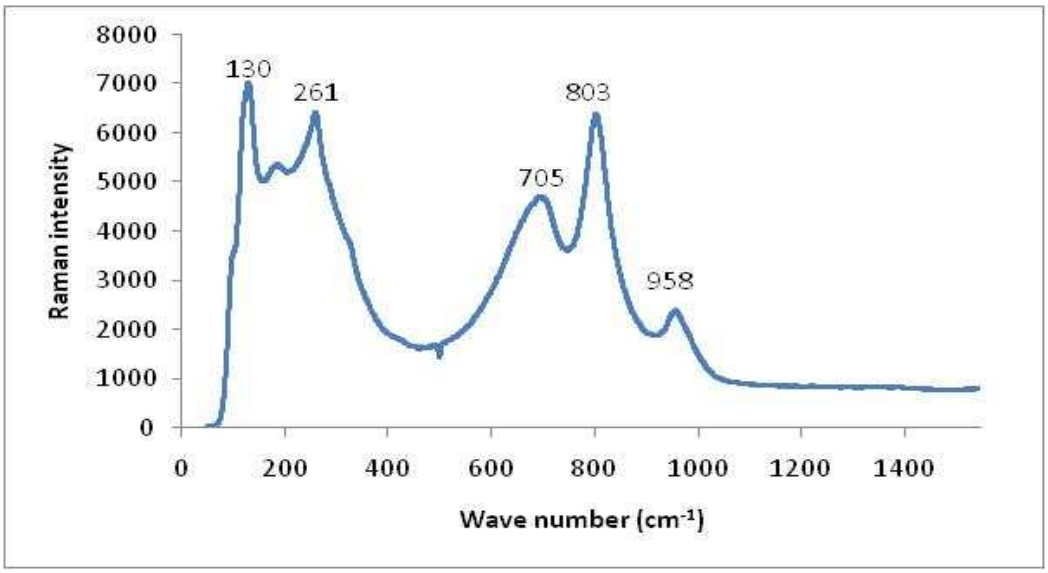

Figure 4.39. Raman spectrum of corrosion product on WC-10Co (wt.%) in 1 M H_2SO_4

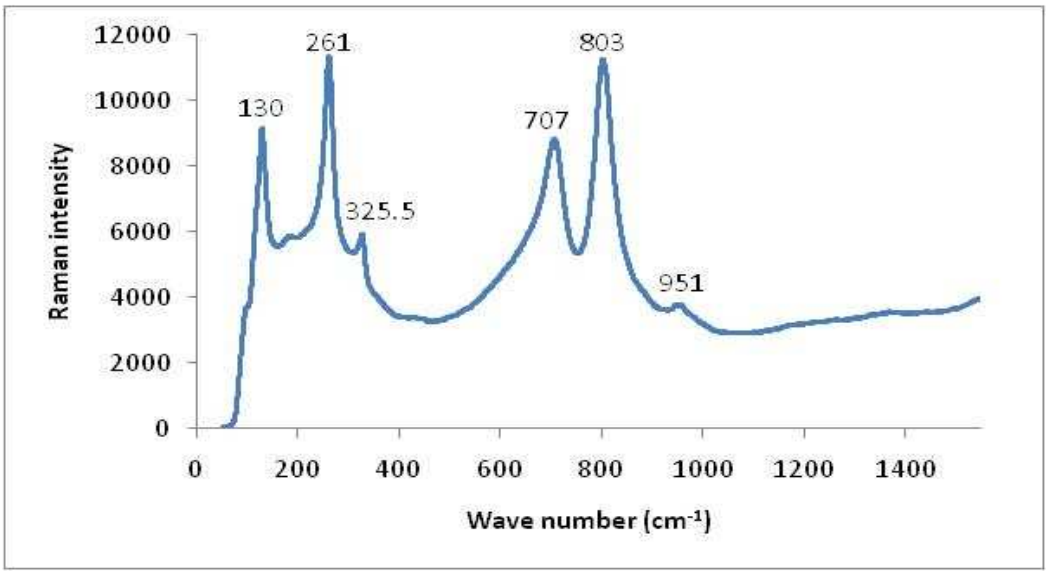

Figure 4.40. Raman spectrum of corrosion product on WC-0.4VC-10Co (wt.%) in 1 M H_2SO_4.

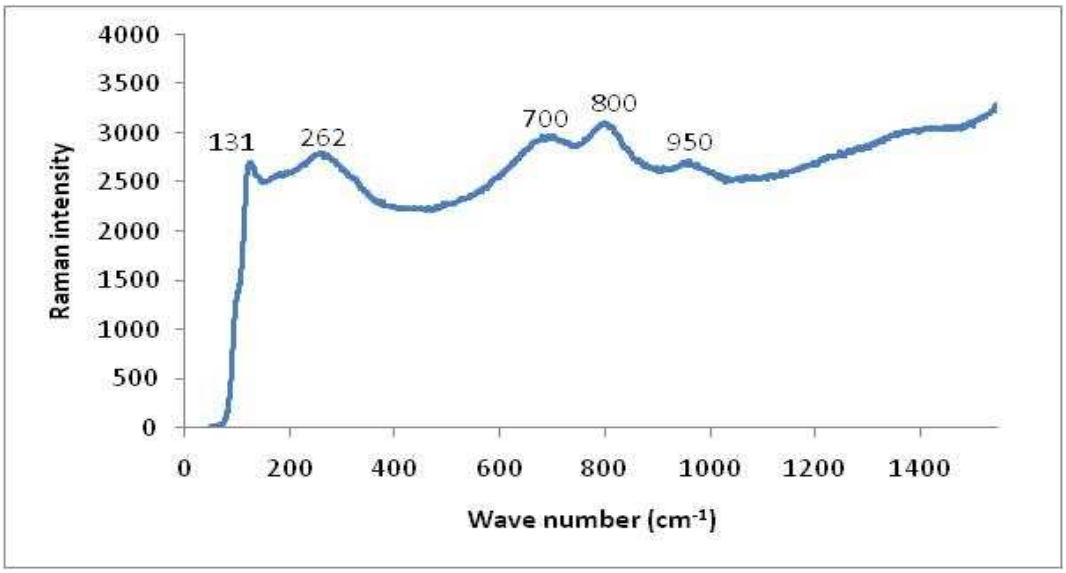

Figure 4.41. Raman spectrum of corrosion product on WC-10VC-12Co (wt.%) in 1 M H_2SO_4

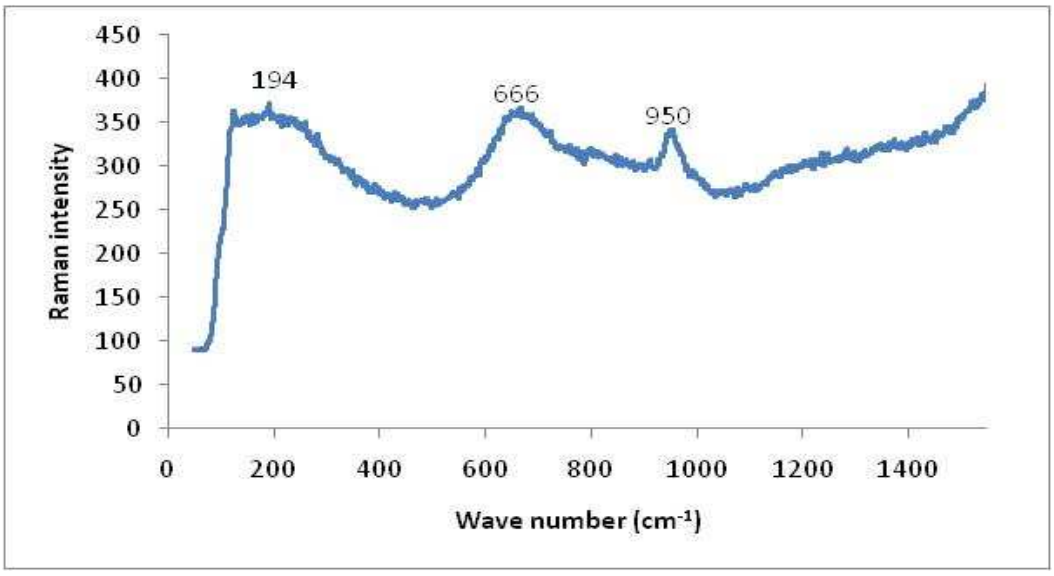

Figure 4.42. Raman spectrum of corrosion product on WC-27VC-11Co (wt.%) in 1 M H_2SO_4

Table 4.4 summarizes the main phases detected on the surfaces of the test specimens before and after corrosion. All the test alloys lost Co after

corrosion, and formed a new phase, either WO_3 or $WO_3.xH_2O$, or both after corrosion.

Table 4.4 Main phases detected on alloy surfaces before and after corrosion in 1 M H_2SO_4

Alloy (wt.%)	Phases detected		
	Before corrosion (XRD analysis)	After corrosion	
		XRD	Raman
WC-10Co	WC Co	WC $WO_3.2H_2O$	WO_3 $WO_3.xH_2O$
WC-0.4VC-10Co	WC Co	WC $WO_3.H_2O$	WO_3 $WO_3.xH_2O$
WC-10VC-12Co	WC (W,V)C Co	WC (W,V)C $VOSO_4.H_2O$ $WO_3.H_2O$	WO_3 $WO_3.xH_2O$
WC-27VC-11Co	WC (W,V)C Co	WC (W,V)C $VOSO_4.H_2O$ $WO_3.H_2O$	WO_3 $WO_3.xH_2O$

4.4.8 Discussion

The OCP of the WC-10Co alloy was very stable, probably because a passive film formed (Figure 4.28). The OCP of the WC-0.4VC-10Co (wt.%) suggests that it corroded during the first twenty minutes and then a passive film formed on the surface that stabilised it. For the WC-VC-Co alloys, the OCPs were more electronegative than the base alloy and this implies that in acidic sulphate solutions, increasing VC contents make the alloys less noble.

The anodic polarisation behaviour of the WC-10Co (wt.%) hardmetal, which was due to the formation of a hydrate form of WO_3, is in agreement with literature (Bozzini *et al*., 2003 {a}, 2004), where these researchers reported the formation of a passive film as an oxidation product of the WC phase (Figure 4.29). XRD (Figures 4.35 – 4.38) and Raman spectroscopy (Figures

4.39 – 4.42) results of both the base alloy and the WC-VC-Co hardmetals confirmed this WC oxidation: the common surface film that formed for all alloys investigated was $WO_3.H_2O$ while $VOSO_4.H_2O$ also formed for the high VC content alloys. The pseudopassive bahaviour of the base alloy is that the current density decreased only minimally. True passivity occurs when the i_{pass} is less than 10 $\mu A/cm^2$ (Human & Exner, 1997). It is also likely that the presence of VC might have made the surface films that formed more permeable leading to higher i_{pass} currents. The almost similar i_{pass} values of the WC-10VC12Co (wt.%) and WC-27VC-11Co (wt.%) could be attributed to the fact that they had similar passive films.

The introduction of VC shifted the E_{corr} to slightly negative values, and the corrosion resistance appeared to increase with VC content (Table 4.3) due the attendant decrease of the volume fraction of the Co binder.

Chronoamperometric curves (Figure 4.30) had an L shape and the dramatic drop of the current density is an indication that a passive film formed very quickly. The constant current density shows that a non-porous film formed which limited further diffusion of ions through the film.

The formation of tungsten oxide and its hydrate for the base alloy found in the XRD measurements correlate well with work by Bozzini *et al*. (2003 {a}, 2004) who found a two-phase structure of WO_3 and hydrated WO_3, i.e. $WO_3.xH_2O$ (with x = ½, 1, 2). The formation of vanadyl sulphate for the WC-VC-Co alloys, except WC-0.4VC-10Co (wt.%), might be due to the vanadium in the hardmetal selectively reacting with oxygen and with sulphate ions in solution (Figures 4.37 – 4.38).

Raman spectroscopy determined the corrosion products as WO_3 and its hydrate on the WC-VC-Co alloys (Figures 4.40 – 4.42) and confirmed XRD

findings (Figures 4.36 – 4.38). The Raman analysis however was not able to confirm the formation of $VOSO_4.H_2O$ on the surfaces of WC-10VC-12Co (wt.%) and WC-27VC-11Co (wt.%). It is probable that may be $VOSO_4.H_2O$ is not Raman active in which case, no peaks attributable to it would appear on a Raman spectrum.

4.5 Corrosion behaviour in 1 M sodium chloride

This Section reports the results and discussion of the various corrosion measurements and the surface analysis for the corrosion of the various hardmetal alloys in 1 M sodium chloride (NaCl). The ICP-OES analysis for solutions in which corrosion in SMW and NaCl took place, is also presented.

4.5.1 Open circuit potential (OCP) measurements

Figure 4.43 reports the open circuit potential (OCP) of the samples in 1 M NaCl over a period of two hours. The variation of potential for all specimens was rather minimal, indicating that pitting (localized corrosion), if any, was limited. The effect of VC additions appeared to depend on the amount introduced. With a small addition of VC, the OCP increased gradually on immersion and then stabilised around the initial value. The potential for WC-10VC-12Co (wt.%) alloy gradually decreased with immersion time. The OCP of WC-27VC-11Co (wt.%), on the other hand, increased throughout the whole immersion period, which could be an indication of continuous film formation. In general, the OCP values did not show a consistent increase or decrease with the addition of VC. All alloys with VC additions had more noble stable OCP values than the base alloy, WC-10%Co (wt.%).

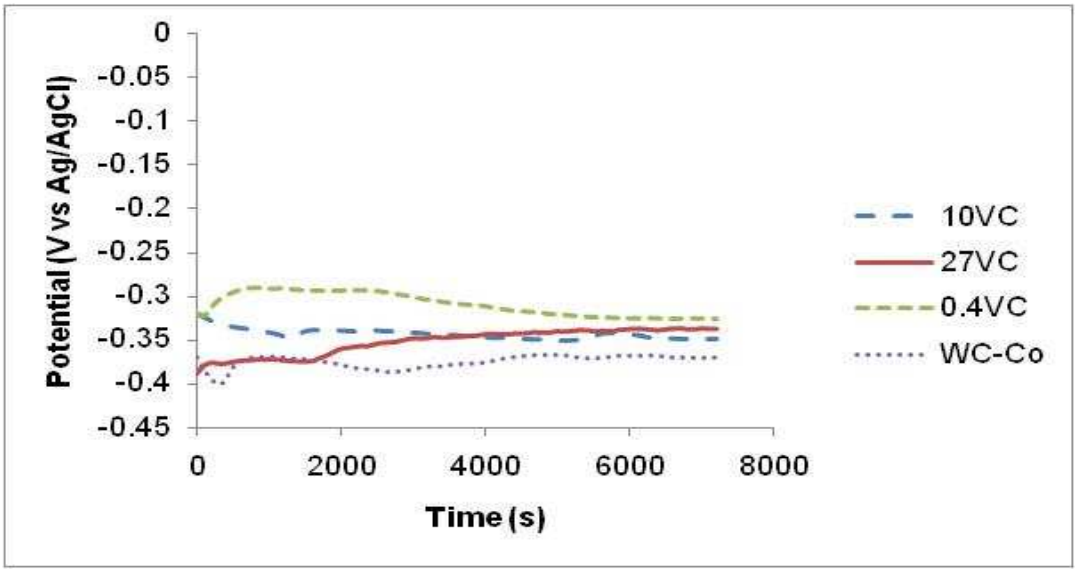

Figure 4.43. OCP curves of the various WC-VC-Co samples in 1 M NaCl

4.5.2 Potentiodynamic polarisation measurements

Figure 4.44 shows the anodic polarisation curves of the WC-VC-Co samples in 1 M NaCl electrolyte. There is a slight decrease of corrosion current in the anodic part of polarisation for all the specimens, a behaviour commonly referred to as pseudopassivation (Human and Exner, 1996, Sutthiruangwong *et al*., 2005). The pseudopassive behaviour observed for WC-10Co (wt.%) hardmetal here is in contrast with other literature where it was found that WC-Co exhibits continuous anodic corrosion in neutral chloride solutions (Schnyder *et al*., 2004; Hochstrasser-Kurz *et al*., 2007). The decrease in passivation current density (i_{pass}) was more pronounced for WC-10Co (wt.%), even though the pseudopassivity extended over a larger potential range for the specimens with VC.

Pseudopassive behaviour is thought to be due to the formation of a porous film on the surface of the corroding specimens (Human and Exner, 1996). For WC-Co grades in solutions of pH 7, this film is speculated to be tungsten oxide (WO_3) (Engqvist *et al*., 2000). For the VC specimens, the small addition

of VC into the base alloy shifted the i_{pass} from approximately 3.7 mA/cm^2 to a value of 40 mA/cm^2, an order of magnitude larger. With subsequent increase of VC, the pseudopassive behaviour was slightly more pronounced in the WC-27VC-11Co (wt.%) compared to the other two VC additions, as there was not much difference between the WC-10VC-12Co (wt.%) and WC-0.4VC-10Co (wt.%) alloys.

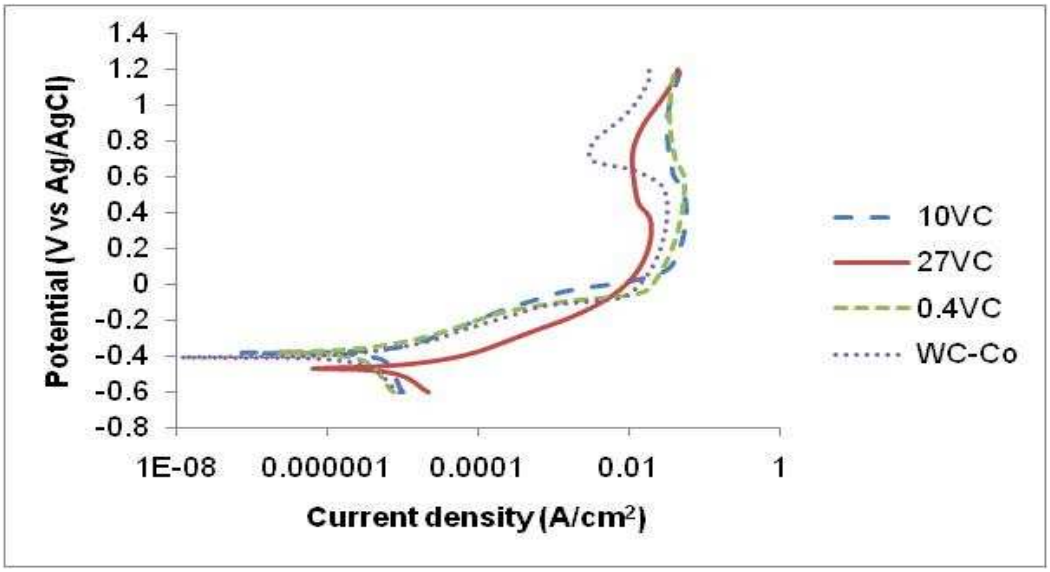

Figure 4.44. The anodic polarisation curves of the various WC-VC-Co samples in 1 M NaCl

4.5.3 Corrosion rate and E_{corr}

Table 4.5 shows the electrochemical corrosion parameters of the samples exposed to 1 M NaCl. The E_{corr} of the base alloy is in agreement with literature where it has been reported to be -0.397 V (Schnyder *et al*., 2004). The introduction of VC did not significantly change the E_{corr} values compared to the base alloy, i. e. that the addition of VC only affected the corrosion potential marginally. The corrosion current density of the base alloy was an order of magnitude less than that of the WC-VC-Co samples, suggesting that VC enhanced the corrosion reactions. Since i_{corr} is proportional to corrosion

rate, the specimens with VC had higher corrosion rate values compared to the base alloy.

Table 4.5 Electrochemical corrosion parameters of the various WC-VC-Co samples in 1 M NaCl

Samples (wt.%)	E_{corr} (V)	i_{corr} (A/cm^2)	Corrosion rate (mm/year)
WC-10Co	-0.399	3.0E-08	2.0E-04
WC-0.4VC-10Co	-0.469	2.0E-07	1.3E-03
WC-10VC-12Co	-0.370	3.6E-07	2.8E-03
WC-27VC-11Co	-0.361	2.8E-07	2.6E-03

4.5.4 Chronoamperometry

The pseudopassive potentials that were used for the chronoamperometry measurements were 0.8 V for WC-10Co (wt.%) and 0.7 V for the WC-VC-Co (wt.%) hardmetals. Figure 4.45 shows the current density variation as a function of holding time. The current density of WC-Co (wt.%) remained relatively constant at steady-state value over time. This indicates that the specimen was immediately passivated on immersion.

The variation of currents for the specimens containing VC depended on the amount thereof. The current density of the WC-0.4VC-10Co (wt.%) alloy decreased gradually, before attaining a steady state value punctuated by small spikes, probably indicating some pitting or that the oxide film was porous. On the other hand, the current densities for WC-10VC-12Co (wt.%) and WC-27VC-11Co (wt.%) decreased only very gradually and never attained a steady state value in the initial two hours of monitoring of current. It was therefore decided that the holding time should be increased to 12 hours. The current density of WC-10VC-12Co (wt.%) then decreased to a near zero

steady state value, unlike that of WC-27VC-11Co (wt.%) whose current density slightly increased and then appeared stabilized (Figure 4.46). The initial decrease of current density for these specimens points to a build-up of corrosion products on the surfaces (Bozzini *et al*., 2003{a}).

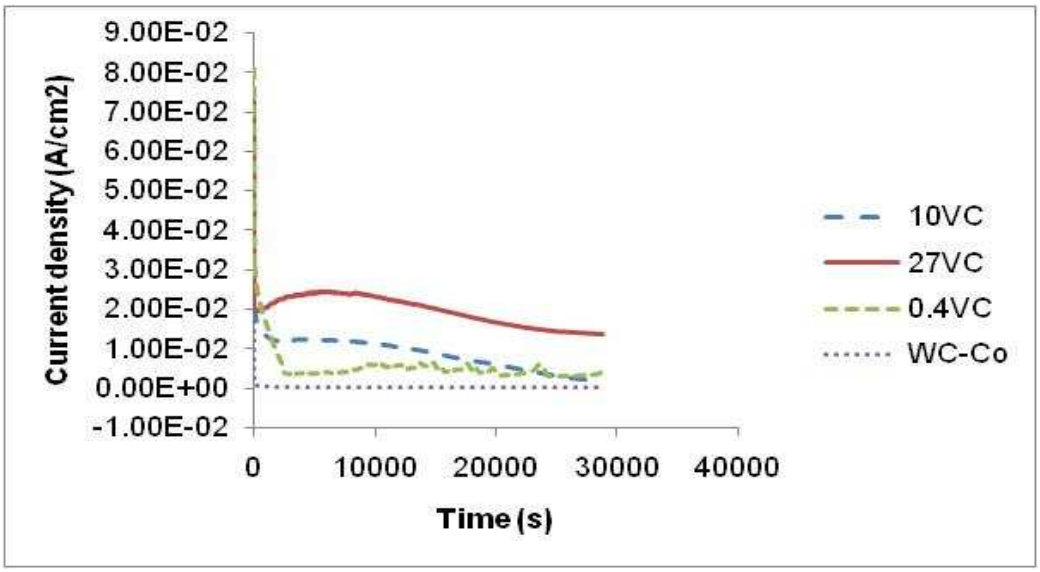

Figure 4.45 Chronoamperometry measurements of the various WC-VC-Co samples in 1 M NaCl.

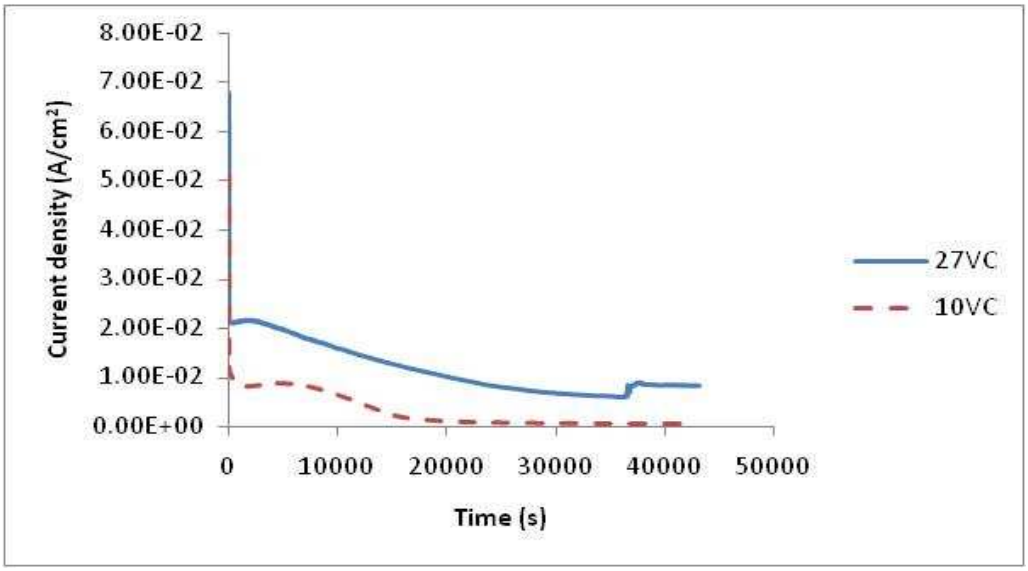

Figure 4.46 Chronoamperometry measurements on WC-10VC-12Co (wt.%) and WC-27VC-11Co (wt.%) for 12 hours.

4.5.5 Scanning electron microscopy (SEM)

Figures 4.47 to 4.50 present the SEM images of the various corrosion surfaces of the samples. The corrosion surfaces of samples WC-10Co (wt.%) and WC-0.4VC-10Co (wt.%) (Figures 4.47 and 4.48) are extensively cracked, and the surface appearances are akin to dried up mud. It is expected that the surfaces cracked as the specimens dried. In contrast, the surfaces of samples WC-10VC-12Co (wt.%) and WC-127VC-11Co (wt.%) are not cracked (Figures 4.49 and 4.50). Instead, the surfaces appear to show selective dissolution of phases.

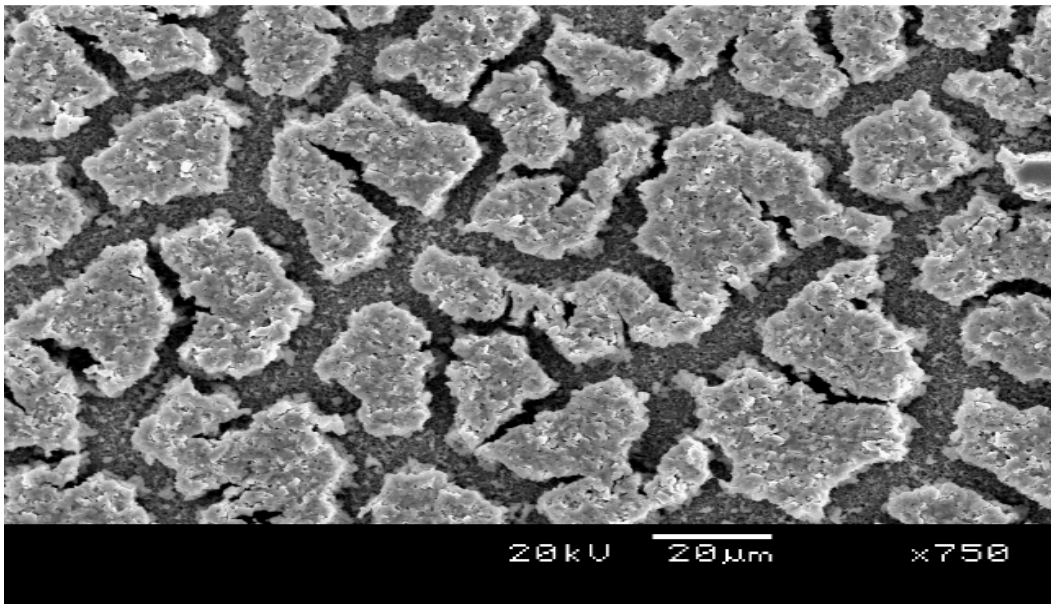

Figure 4.47. SEM image of the corroded surface of WC-10Co (wt.%) in 1 M NaCl.

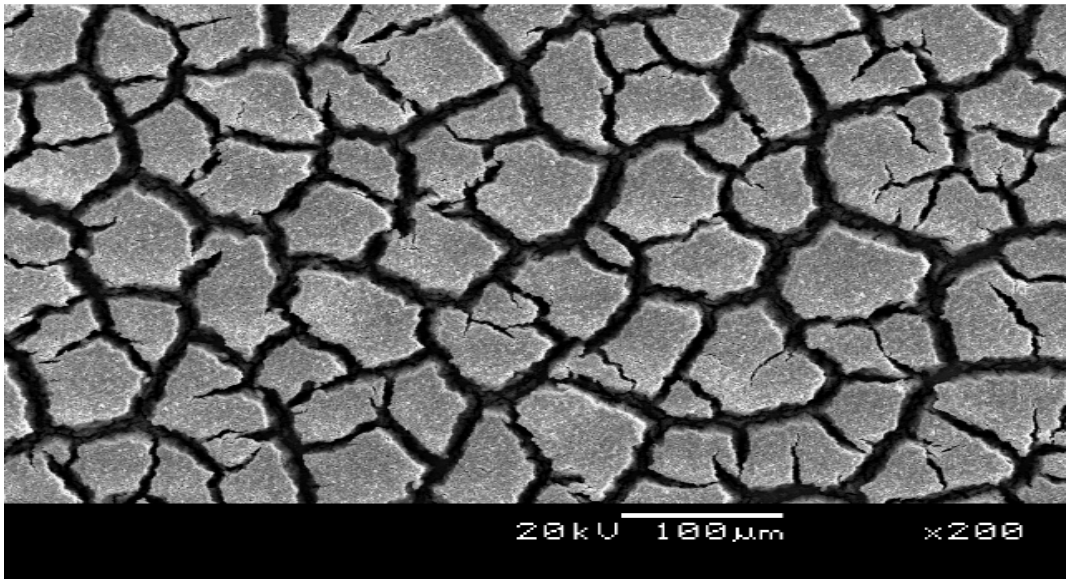

Figure 4.48. SEM image of the corroded surface of WC-0.4VC-10Co (wt.%) in 1 M NaCl.

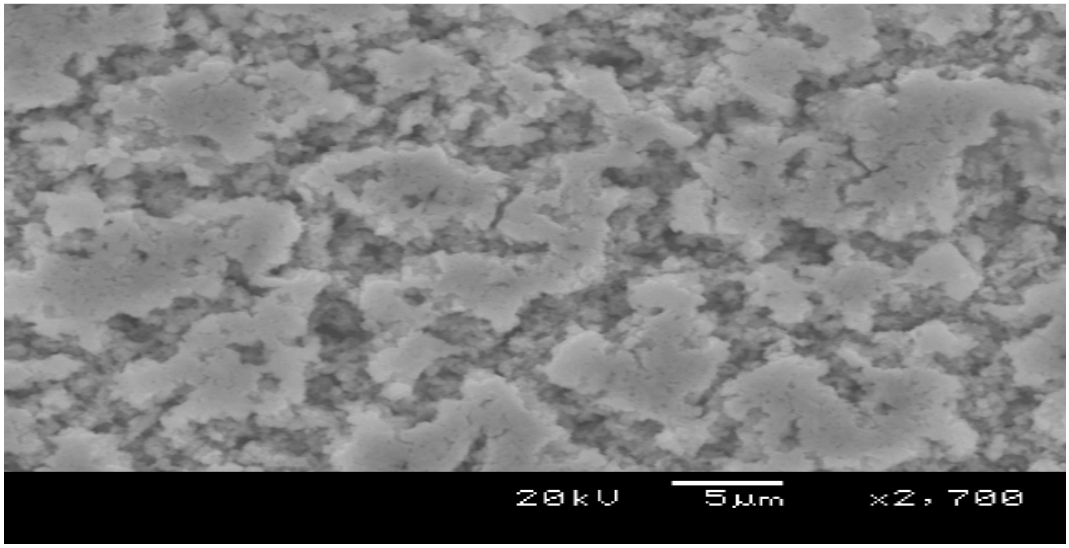

Figure 4.49. SEM image of the corroded surface of WC-10VC-12Co (wt.%) in 1 M NaCl.

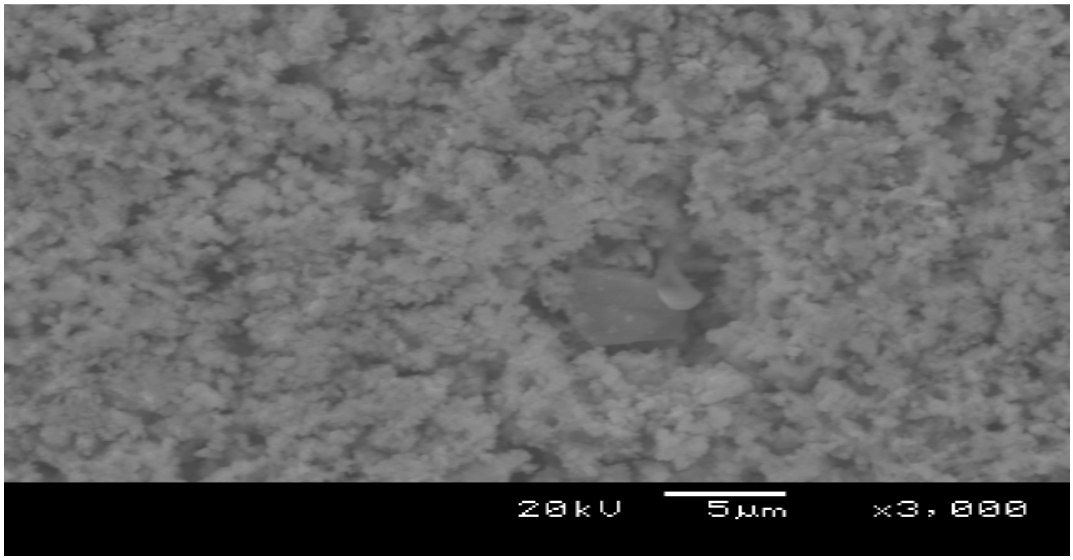

Figure 4.50 SEM image of the corroded surface of WC-27VC-11Co (wt.%) in 1 M NaCl.

4.5.6 X-ray diffraction (XRD)

WC-10Co (wt.%)

Figure 4.51 is the XRD pattern of the surface of the base alloy after corrosion. The main peaks belong to WC. Unlike the as-received specimen, peaks for Co are missing, indicating that Co might have dissolved. New peak positions at 28.5°, 38.2°, and 46.7°2 θ were formed, and were identified as belonging to a tungsten oxide (W_3O_8).

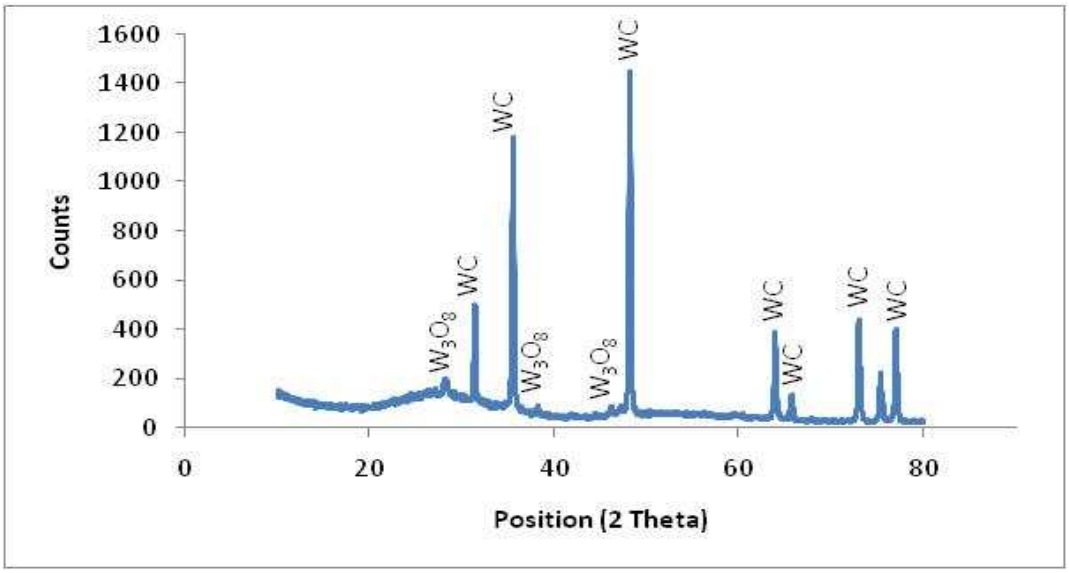

Figure 4.51 XRD pattern of the corroded surface of WC-10Co (wt.%) in 1 M NaCl

WC-0.4VC-10Co (wt.%)

Figure 4.52 shows the XRD pattern of the corroded surface of WC-0.4VC-10Co (wt.%) after the chronoamperometry measurements. The main phase on the XRD pattern is WC. New peaks 28.1, 38.2, 42, 46.3°2 θ were identified as belonging to WO_3 and its anion, disodium ditungstate ($Na_2W_2O_7$).

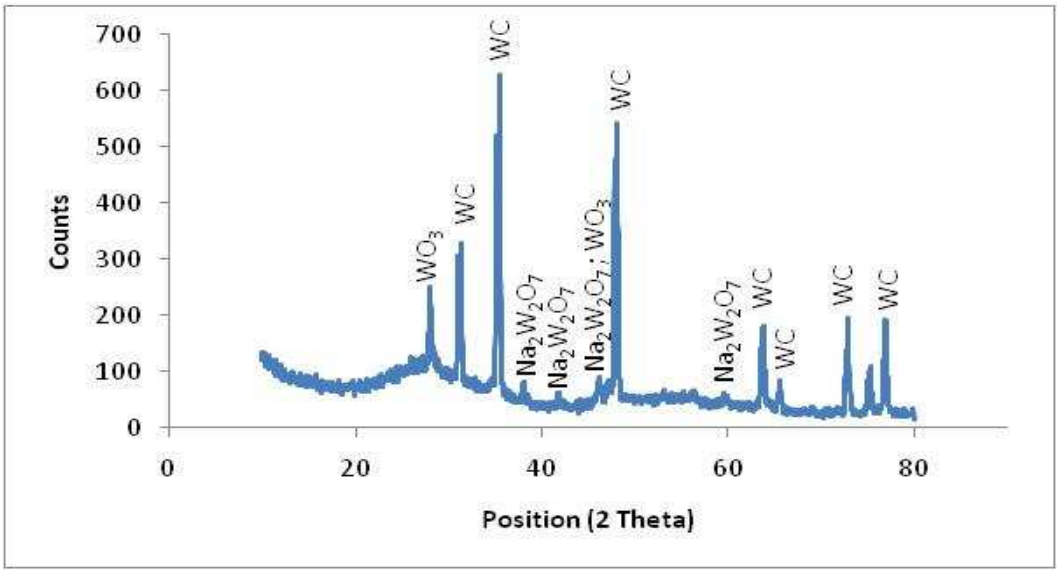

Figure 4.52 XRD pattern of the corroded surface of WC-0.4VC-10Co (wt.%) in 1 M NaCl.

WC-10VC-12Co (wt.%)

The XRD pattern (Figure 4.53) revealed that (W,V)C vanished completely as did the Co peaks, indicating that these phases might have dissolved from the surface. New peaks formed at 2θ positions of 28.8°, 39° and 42.5° and were identified as belonging to tungsten oxide (WO_3).

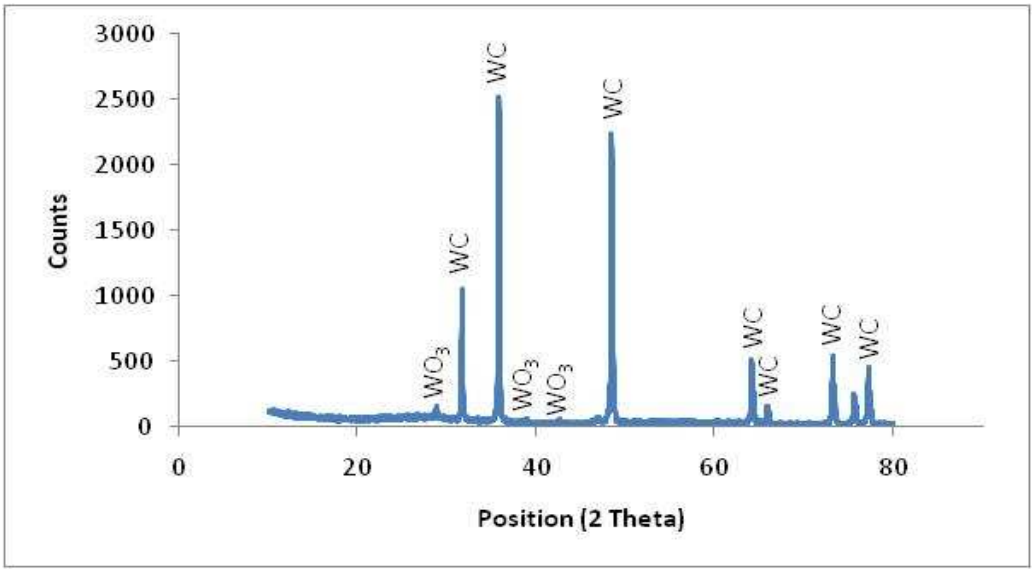

Figure 4.53. XRD pattern of corrosion product on WC-10VC-12Co (wt.%) in 1 M NaCl

WC-27VC-11Co (wt.%)

The XRD pattern of the corroded surface of (Figure 4.54) showed only peaks for WC. Peaks for (W,V)C and Co were missing, indicating that these two phases might have dissolved from the surface, which could explain the roughening observed on the SEM micrographs of the corroded sample (Figure 4.50).

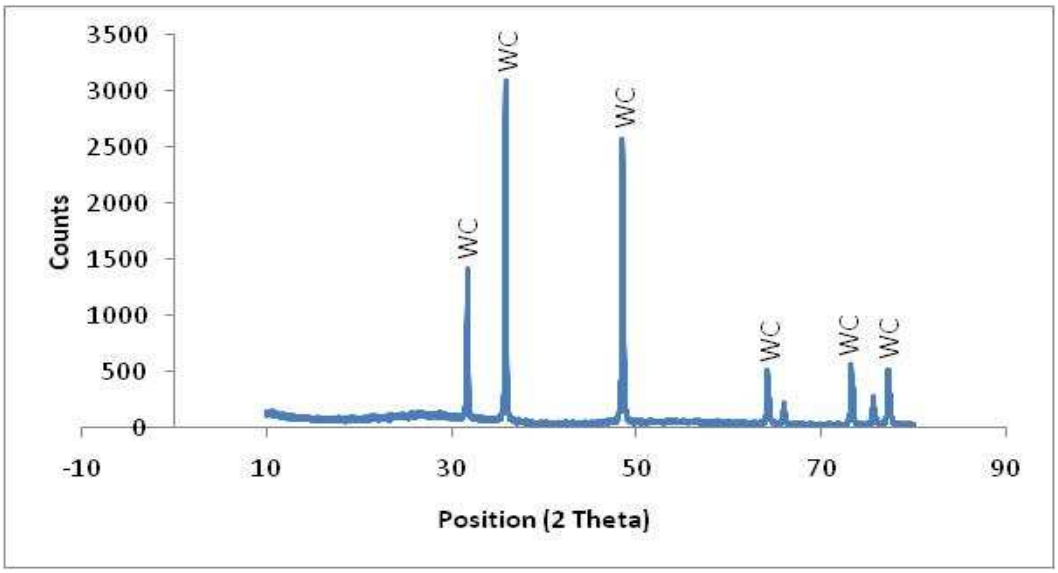

Figure 4.54 XRD pattern of the corroded surface of WC-27VC-11Co (wt.%) in 1 M NaCl.

4.5.7 Raman spectroscopy

WC-10Co (wt.%)

Figure 4.55 shows the Raman spectrum of the surface of WC-10Co (wt.%) in 1 M NaCl after the chronoamperometry measurements. The Raman shifts observed are 133, 249, 697, 814.5 and 958.5 cm^{-1} for tungsten oxide (WO_3) and its hydrate (Regragui *et al.*, 2000; Ingham *et al.*, 2005; Wachs *et al.*, 1987; Enesca *et al.*, 2007; Bozzini *et al.*, 2003, 2004; Wolcott *et al.*, 2006; Daniel *et al.*, 1987).

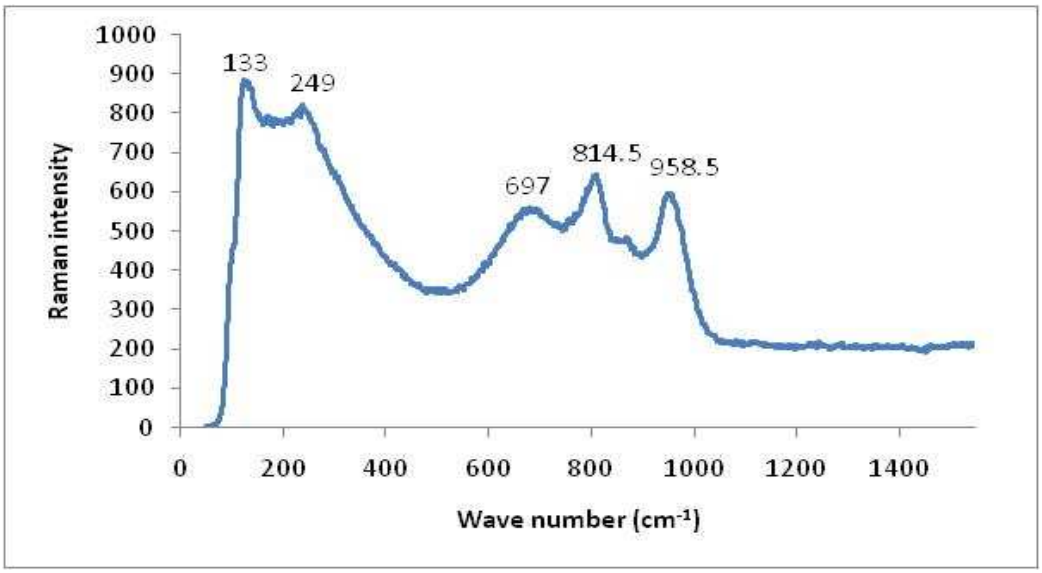

Figure 4.55 Raman spectrum of corrosion product on WC-10Co (wt.%) in 1 M NaCl

WC-0.4VC-10Co (wt.%)

Figure 4.56 is the Raman spectrum of the surface of WC-0.4VC-10Co (wt.%) hardmetal after the chronoamperometry measurements. The wavenumbers were 131, 697, and 813.5 cm^{-1} for the tungsten oxide (WO_3) (Regragui *et al.*, 2000; Ingham *et al*., 2005; Wachs *et al*., 1987; Enesca *et al*., 2007; Bozzini *et al*., 2003, 2004; Wolcott *et al*., 2006; Daniel *et al*., 1987), while 881.5 and 968.5 cm^{-1} could be assigned to the tungsten oxide anion $W_2O_7^{2-}$ (Wachs *et al*., 1987). These phases confirm what was found from the XRD measurements.

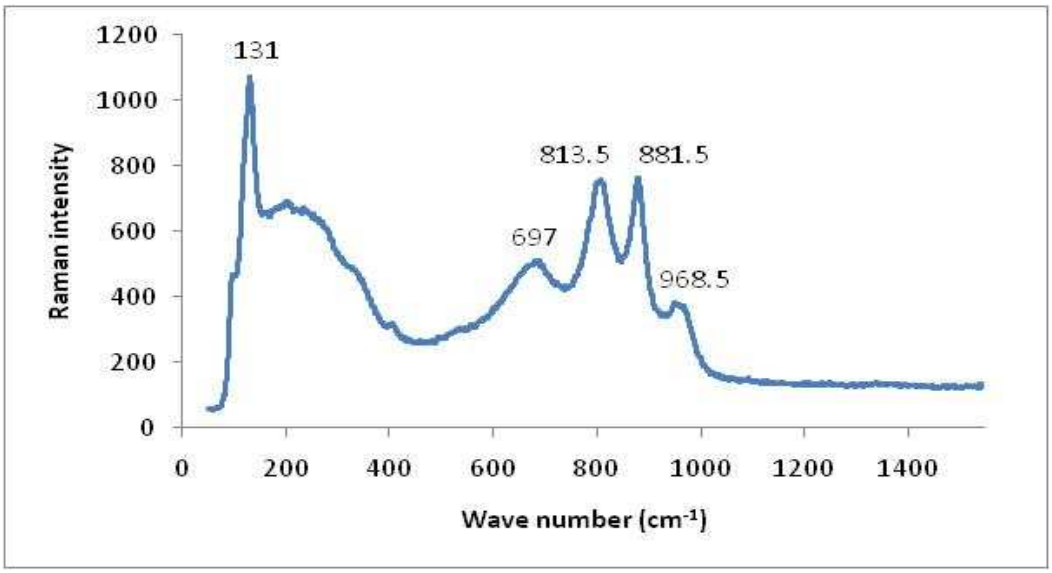

Figure 4.56 Raman spectrum of corrosion product on WC-0.4VC-10Co (wt.%) in 1 M NaCl

WC-10VC-12Co (wt.%)

The Raman spectrum for the surface of WC-10VC-12Co (wt.%) after chronoamperometry measurements in 1 M NaCl is shown in Figure 4.57. The Raman shifts observed were at 131, 261, 803 and 962 $cm^{-1}$and these can be assigned to tungsten oxide and its hydrate, as has been found in literature before. This appears to suggest that the new peaks that formed on the XRD pattern for this specimen after polarisation were for these phases.

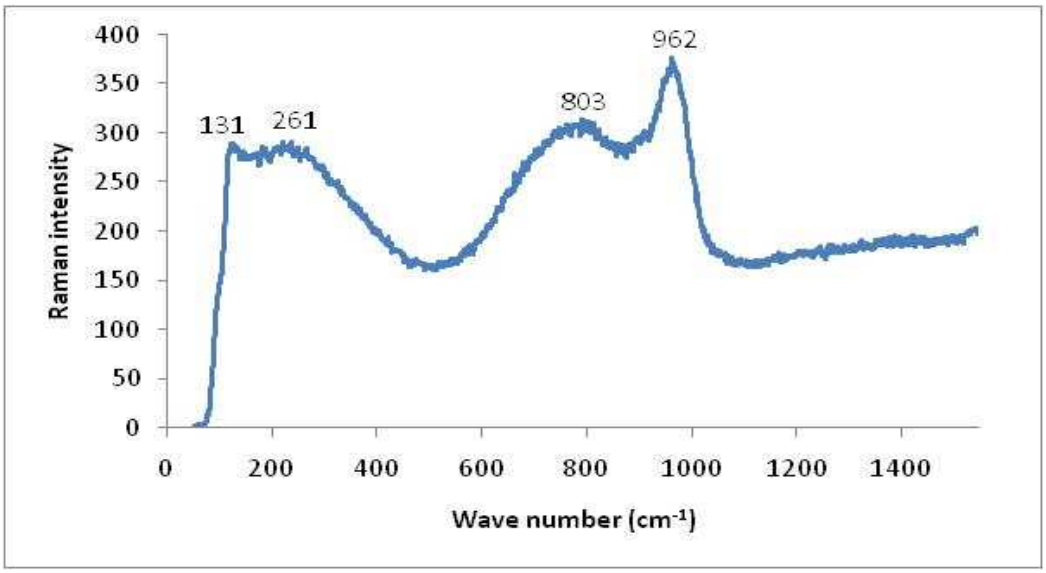

Figure 4.57. Raman spectrum of corrosion product on WC-12VC-12Co (wt.%) in 1 M NaCl

WC-27VC-11Co (wt.%)

Figure 4.58 is the Raman spectrum of the surface of WC-27VC-11Co (wt.%) in 1 M NaCl. The Raman wave numbers obtained were 132.5, 261.5, 700 and 805.5 cm^{-1}. These can be attributed to tungsten oxide as previously explained.

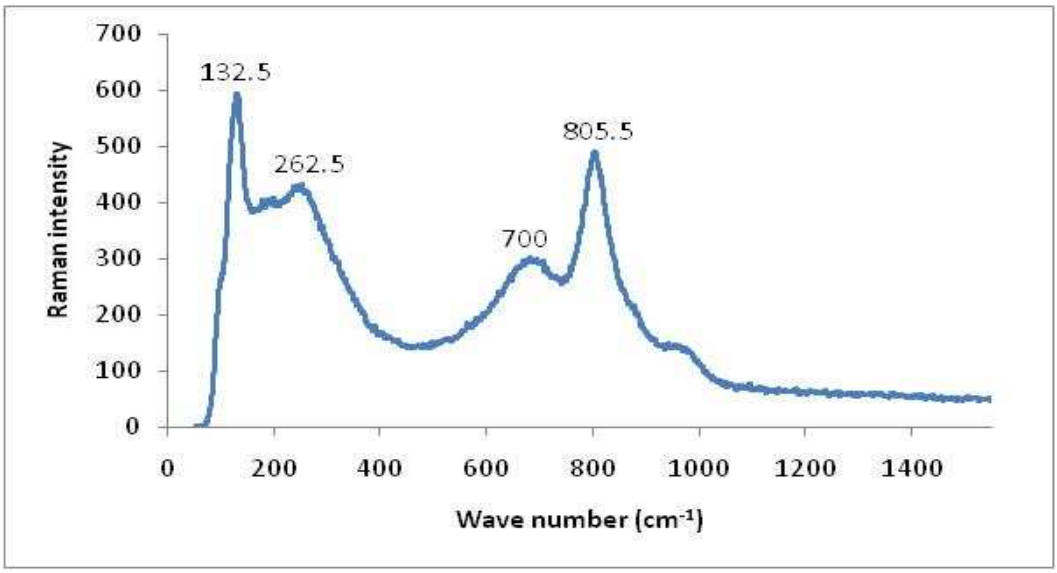

Figure 4.58. Raman spectrum of corrosion product on WC-27VC-11Co (wt.%) in 1 M NaCl

Table 4.6 summarizes the main phases detected on the surfaces of the test specimens before and after corrosion. All the test specimens lost Co after corrosion, and formed one or more new phases: alloy WC-10Co (wt.%) formed WO_3, W_3O_8 and $WO_3.H_2O$; alloy WC-0.4VC-10Co (wt.%) formed WO_3 and $W_2O_7^{2-}$; alloy WC-10VC-12Co (wt.%) formed WO_3; and alloy WC-27VC-11Co (wt.%) formed WO_3 and $WO_3.H_2O$ and $WO_3.xH_2O$. In addition, alloys WC-10VC-12Co (wt.%) and WC-27VC-11Co (wt.%) also lost (W,V)C.

Table 4.6 Main phases detected on alloy surfaces before and after corrosion in 1 M NaCl

Alloy (wt.%)	Phases detected		
	Before corrosion (XRD analysis)	After corrosion	
		XRD	Raman
WC-10Co	WC Co	WC W_3O_8	WO_3 $WO_3.H_2O$
WC-0.4VC-10Co	WC Co	WC WO_3 $Na_2W_2O_7$	WO_3 $W_2O_7^{2-}$
WC-10VC-12Co	WC (W,V)C Co	WC WO_3	WO_3 $WO_3.xH_2O$
WC-27VC-11Co	WC (W,V)C Co	WC	WO_3

4.5.8 Discussion

The OCP curves of the specimens in the NaCl test solution (Fig 4.43) are generally devoid of fluctuations, implying that all the test specimens were equally resistant to pitting attack during the test, irrespective of the VC content. Pitting, especially of passivated surfaces as of stainless steels, causes OCP values to fluctuate (Sherif *et al*., 2009).

The OCP of the 0.4wt.%VC specimen was the most noble, i.e. the most positive throughout the test, implying that this specimen would possess a greater driving force not to corrode. The binder of this specimen probably had the highest concentration of dissolved W and therefore a greater corrosion resistance, as shown by Hochstrasser-Kurz *et al*. (2007) and Sutthiruangwong *et al*. (2005). However, it should be emphasized here that the OCP, being a potential, can only show the tendency of the specimens towards corrosion.

Higher amounts of VC only affect the OCP values marginally compared to the base alloy (WC-Co). This improvement by VC additions could have been caused by the reduction in the volume fraction of the binder phase. It is known that even in neutral solutions, the corrosion of WC-based hardmetals is controlled by that of the binder (Hochstrasser-Kurz *et al*., 2007, 2008; Ghandehari, 1980; Schnyder *et al*., 2004). Between the VC specimens, 10VC had a more positive OCP value than the 27wt.%VC specimen at the start of the experiment but the order changed after continued exposure. The very minimal effect appears to imply that the best performance of VC in high amounts appears to be equal to that of the base alloy.

All the test specimens exhibited pseudopassive behaviour during anodic polarisation (Fig. 4.44). The behaviour of the WC-Co was contradictory to previous literature reports (Hochstrasser-Kurz *et al*., 2007; Schnyder *et al*., 2004) where continuous anodic dissolution has been observed. The difference between the results here and literature could have been caused by the difference in the concentration of electrolytes used: the higher concentration used in the current study could have encouraged the formation of some surface salt film, and/or hindered some corrosion reaction, as has been suggested before (Hochstrasser-Kurz *et al*., 2007). It can be seen that the inclusion of VC rather increased the i_{pass} values compared to the base alloy. The failure of VC to influence the electrochemical behaviour implies that it does not possess passivating behaviour, as e.g. Cr_3C_2 (Tomlinson & Ayerst, 1989).

The corrosion current, which is the critical factor during corrosion, increased with VC content (Table 4.5), implying that VC caused a decrease in the corrosion resistance. It would appear that the VC also corroded, alongside the binder phase. This is supported by the results of the analysis of the test

solution after chronoamperometric tests (Table 4.7), which show that the VC took part in the corrosion process, and formed V^{2+} detected in the solution.

The variation of current density during chronoamperometric tests (Fig 4.45 and 4.46), implied an absence of pitting. The absence of pitting observed here is in agreement with the earlier observation made from the variation of OCP (Fig. 4.43). The effect of VC was to delay the passivation or to altogether prevent it (passivation) from occurring (Figure 4.46). The observed detrimental effect of VC suggests, again, that it does not possess passivation characteristics. It also implies that VC, in large additions, affects the formation of passive oxide films.

The pseudopassive behaviour observed during potentiodynamic polarisation and for some specimens during chronoamperometric tests was due to the formation of oxides of W, as seen by XRD (Fig. 4.51 – 4.54) and Raman spectroscopy (Fig. 4.55 – 4.48). The formation of W based oxides has been known to cause pseudopassive behaviour in acidic test media (Bozzini *et al*., 2002, 2004; Sutthiruangwong & Mori, 2003). It is also seen that addition of VC changed the various tungsten oxides as revealed by XRD and Raman measurements. For instance, the small VC changed the oxide from W_3O_8 to WO_3 and $Na_2W_2O_7$. No V based salts or oxides were found on the surfaces of the VC containing specimens, again suggesting that VC did not take part in the formation of surface films.

4.5.9 ICP-OES analysis of corrosion solutions

During the chronoamperometry measurements of the WC-VC-Co hardmetals, i.e. WC-0.4VC-10Co (wt.%), WC-10VC-12Co (wt.%) and WC-27VC-11Co (wt.%), in NaCl and synthetic mine water (SMW) solutions, the formation of light green solids was observed. Gaseous bubbles due to oxygen reduction

were also seen (Sutthiruangwong & Mori, 2003). Table 4.7 shows the ionic concentrations of the test solutions after testing, obtained by inductively coupled plasma optical emission spectroscopy (ICP-OES). The ionic concentrations show that the light green colour was due to the presence of a vanadium cation probably V(II). It has been observed before that VO and VCl_2 are both light green solids (Gupta & Krishnamurthy, 1992).

Table 4.7 ICP-OES results of WC-27VC-11Co (wt.%), WC-10VC-11Co (wt.%), and WC-0.4VC-10Co (wt.%) corrosion product solutions after dissolution in NaCl and SMW

(wt.%)	Rsd	Vanadium
		ppm
WC-27VC in SMW	3.1	58.4
WC-10VC in SMW	3.7	15.1
WC-0.4VC in SMW	1.3	46.7
WC-27VC in NaCl	0.3	2.0
WC-10VC in NaCl	2.7	24.9
WC-0.4VC in NaCl	3.5	83.1

Rsd = relative standard deviation

4.6 Corrosion behaviour in synthetic mine water (SMW)

This Section reports the results obtained after exposing test hardmetal samples to synthetic mine water (SMW). Also included is a comparison of the effect of the various corrosive electrolytes used to evaluate the corrosion behaviour of the hardmetals.

4.6.1 Open circuit potential (OCP) measurements

The variation of open circuit potential (OCP) with time of the various samples in synthetic mine water (SMW) is shown in Figure 4.59. In terms of the potential, the addition of VC did not have a consistent effect, as the base alloy and the WC-27VC-11Co (wt.%) had almost the same value. The other two additions shifted the potential towards less negative values.

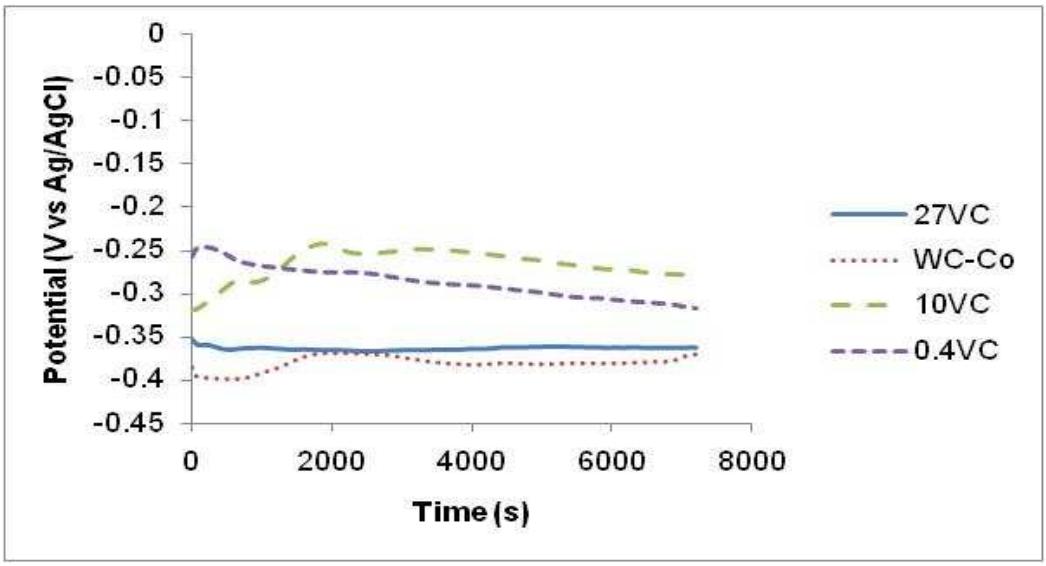

Figure 4.59. OCP curves of the various WC-VC-Co samples in SMW .

4.6.2 Potentiodynamic polarisation measurements

There were no substantial differences between the anodic polarisation behaviour of the different samples in synthetic mine water (SMW) (Figure 4.60): all the samples underwent increasing anodic dissolution with increasing potential, and none exhibited pseudopassivity. This shows that the electrochemical behaviour of the WC-VC-Co hardmetal does not change with increasing VC content. The anodic potentiodynamic curve of WC-10Co (wt.%) confirms what was found by Human and Exner (1996).

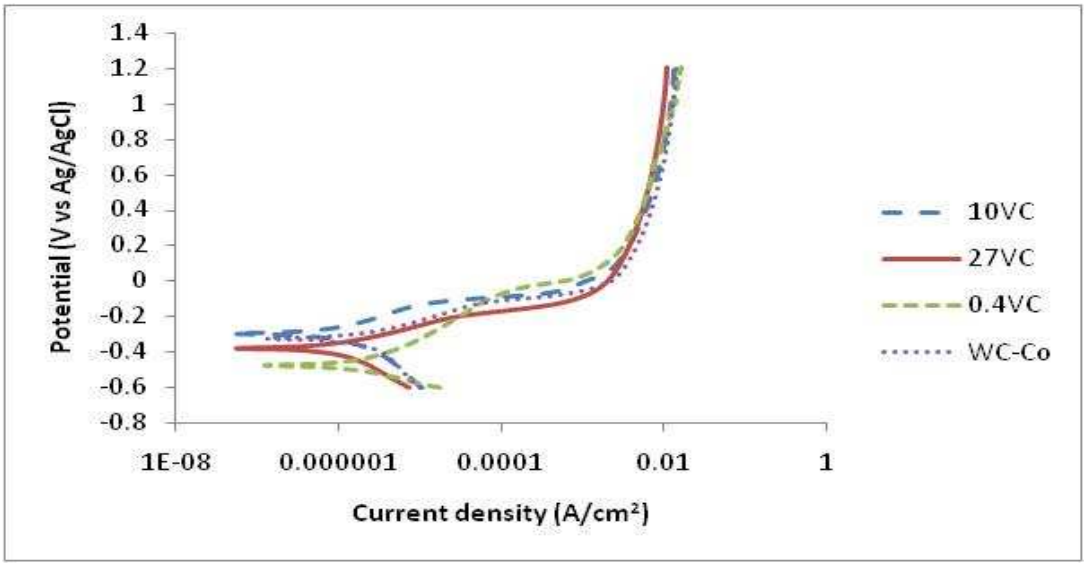

Figure 4.60. The anodic polarisation curves of the WC-VC-Co samples in SMW.

4.6.3 Corrosion rate and E_{corr}

Table 4.8 shows the E_{corr} values of the different WC-VC-Co alloys in synthetic mine water (SMW) solution during polarisation. The E_{corr} values seem to be generally more negative compared with the base alloy. Generally, the corrosion current density decreased with increasing VC content, and the current was an order of magnitude less at the highest VC addition.

Table 4.8 Electrochemical corrosion parameters of the various WC-VC-Co samples in SMW

Samples (wt.%)	E_{corr} (V)	i_{corr} (A/cm^2)	Corrosion rate (mm/year)
WC-10Co	-0.313	1.8E-07	1.2E-03
WC-0.4VC-10Co	-0.474	2.1E-07	1.4E-03
WC-10VC-12C0	-0.296	1.5E-07	1.1E-03
WC-27VC-11Co	-0.379	0. 8E-07	0. 8E-03

4.6.4 Chronoamperometry

Due to the continuous dissolution of the samples when polarised, a potential of 1.1 V was chosen for all the chronoamperometry measurements in SMW. Figure 4.61 shws the variation of current density with time. There was no sudden drop in current density when specimens were introduced to the electrolyte. The current densities decreased with time but never became zero. The current densities of the alloys containing VC stabilised at higher values than that of the base alloy, suggesting, again that VC additions to WC-Co does not provide substantial corrosion resistance benefits. The decrease in current density was probably caused by salts precipitating on the corroding surfaces.

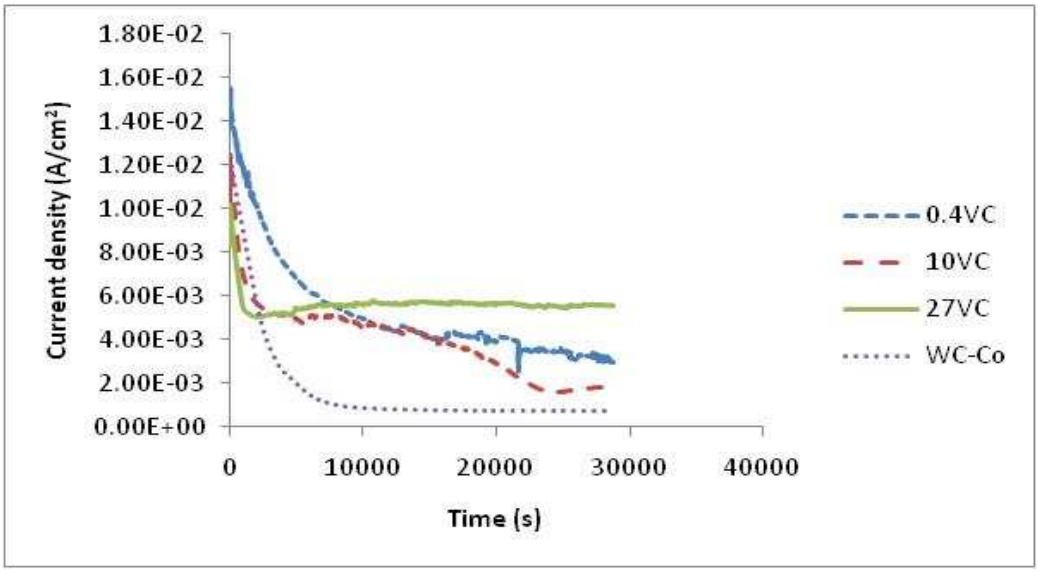

Figure 4.61. Chronoamperometry responses of the various WC-VC-Co samples with time in SMW

4.6.5 Scanning electron microscope (SEM)

Figures 4.62 to 4.65 are the scanning electron microscope (SEM) images of the corroded surfaces of the various WC-VC-Co samples in SMW. Except for alloy WC-27VC-11Co (wt.%) (Figure 4.65), all the other alloys had cracked corroded surfaces.

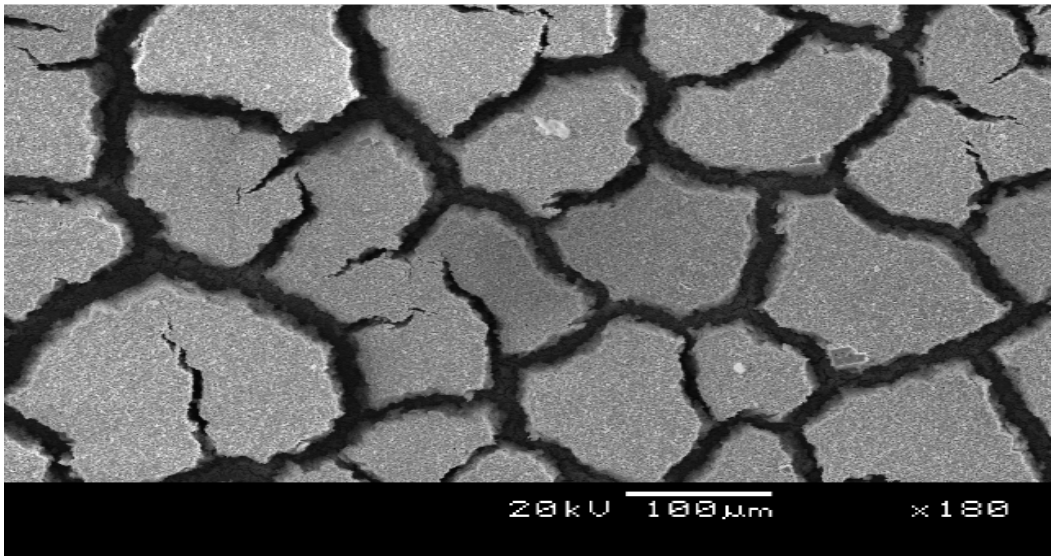

Figure 4.62 SEM image of corroded surface of WC-10Co (wt.%) in SMW.

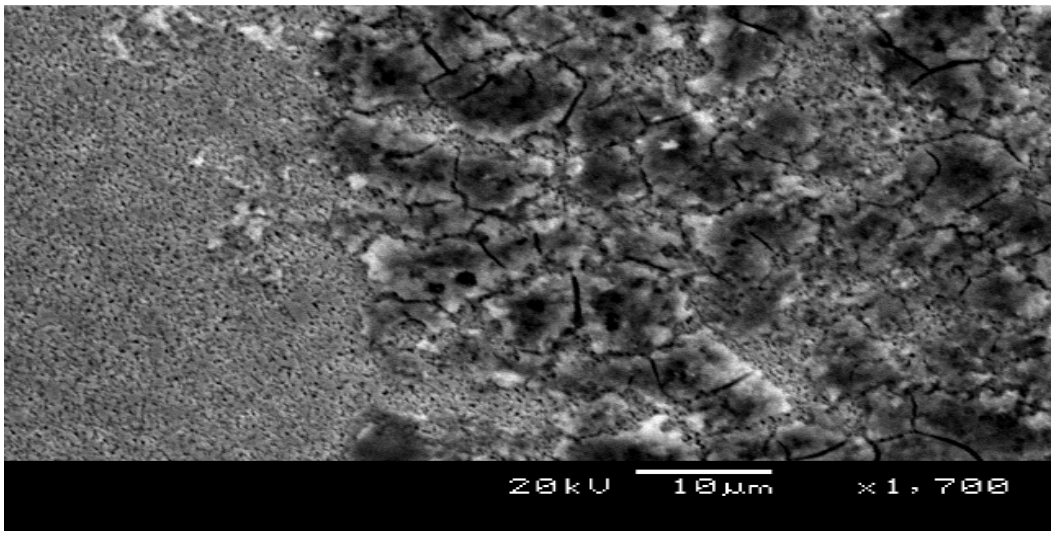

Figure 4.63. SEM image of corroded surface of WC-0.4VC-10Co (wt.%) in SMW.

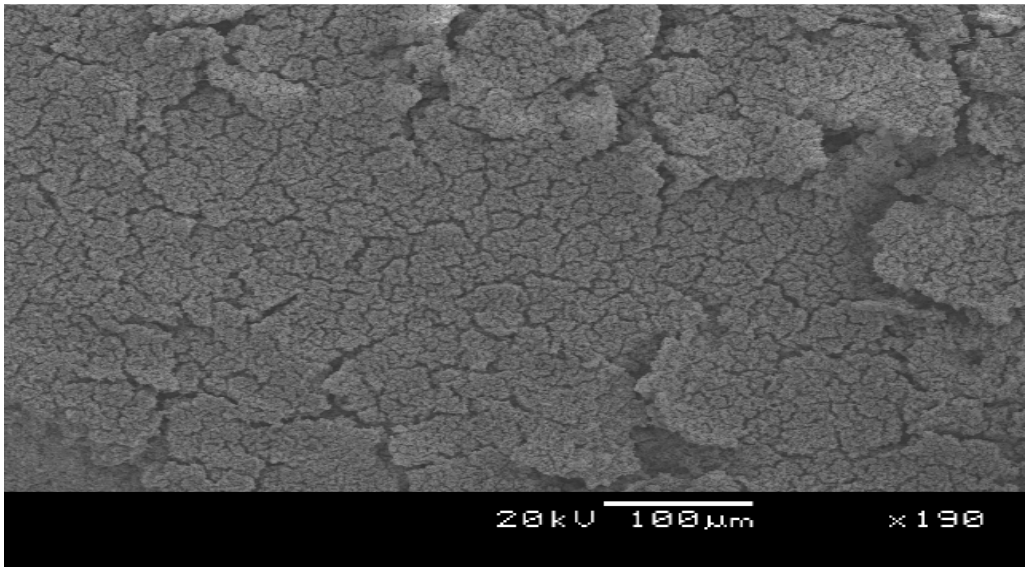

Figure 4.64. SEM image of corroded surface of WC-10VC-12Co (wt.%) in SMW.

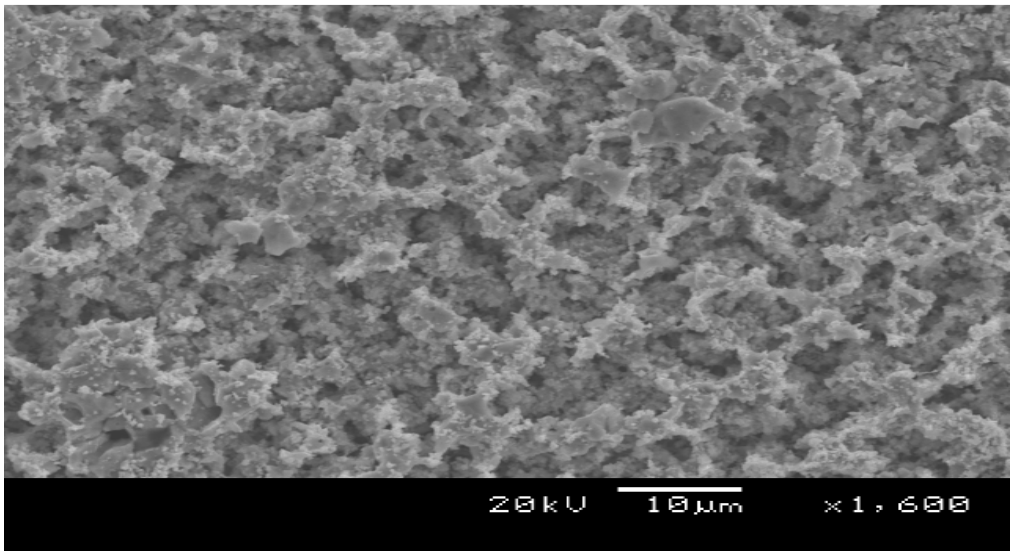

Figure 4.65. SEM image of corroded surface of WC-27VC-11Co (wt.%) in SMW.

4.6.6 X-ray diffraction (XRD)

The XRD spectra of the corroded surfaces of the various WC-VC-Co alloys in SMW are shown in Figures 4.66 to 4.69. New peaks were observed on the surfaces of WC-10Co (wt.%) (Figure 4.66), WC-10VC-12Co (wt.%) (Figure 4.68) and WC-27VC-11Co (wt.%) (Figure 4.69) but they could not be matched with any of the known compounds of the constituents of the WC-VC-Co alloys. So no corrosion product formation was detected, and only the WC and (W,V)C peaks of the original alloy composition were found.

WC-10Co (wt.%)

There were no new peaks on the XRD spectrum shown in Figure 4.66.

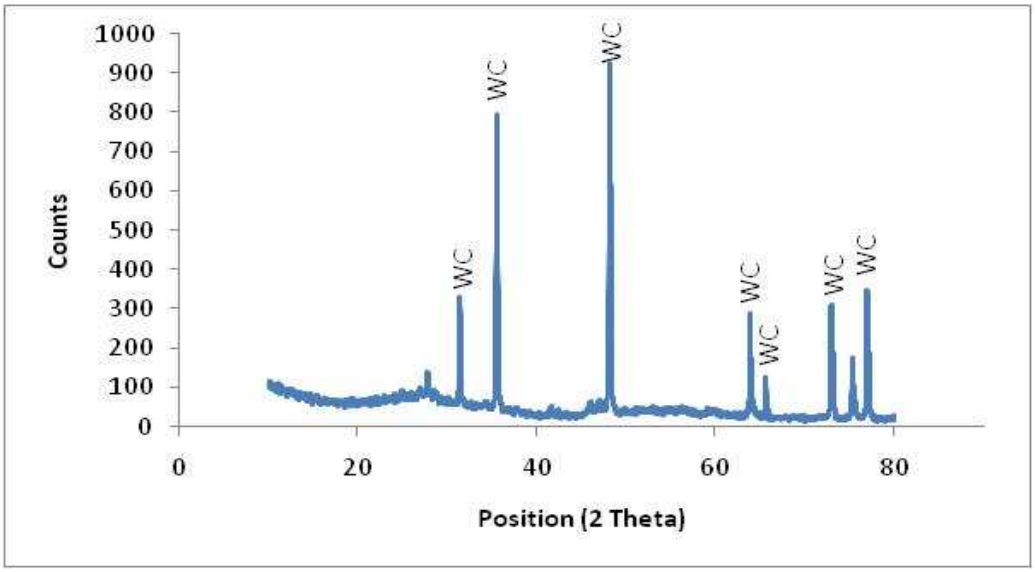

Figure 4.66. XRD pattern of corroded surface of WC-10Co (wt.%) in SMW

WC-0.4VC-10Co (wt.%)

There were no new peaks on the XRD spectrum shown in Figure 4.67 as compared to that of the base alloy.

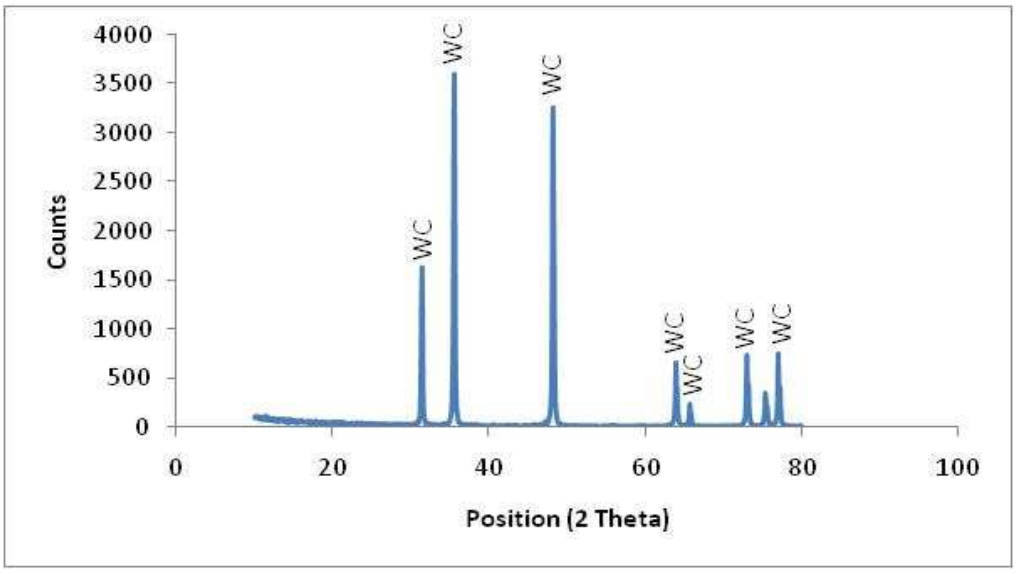

Figure 4.67. XRD pattern of corroded surface of WC-0.4VC-10Co (wt.%) in SMW

WC-10VC-12Co (wt.%)

The XRD pattern of WC-10VC-12Co (wt.%) after corrosion in SMW is shown in Figure 4.68.

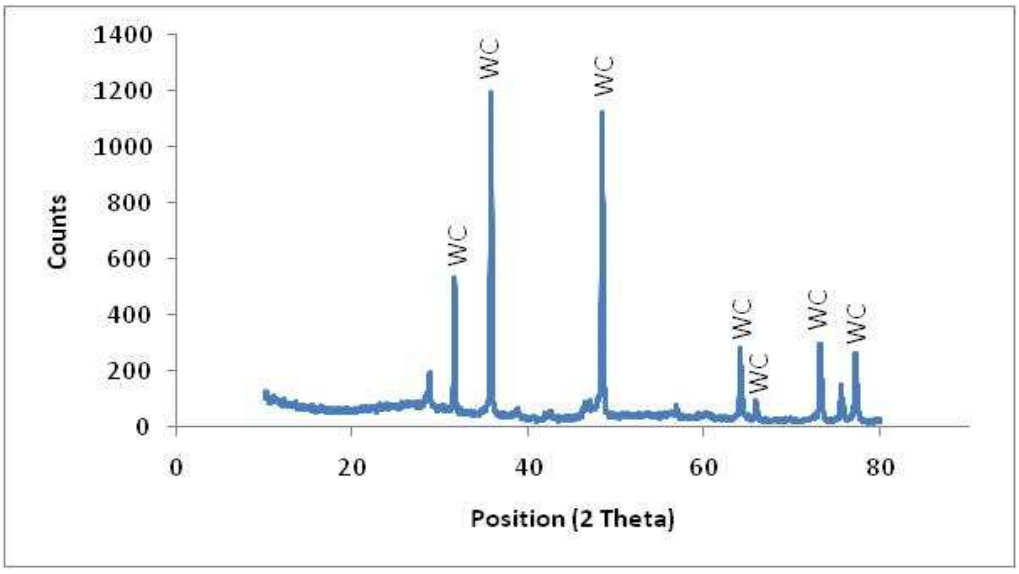

Figure 4.68. XRD pattern of corroded surface of WC-10VC-12Co (wt.%) in SMW

WC-27VC-11Co (wt.%)

Figure 4.69 shows the corrosion product of WC-27VC-11Co (wt.%) in SMW.

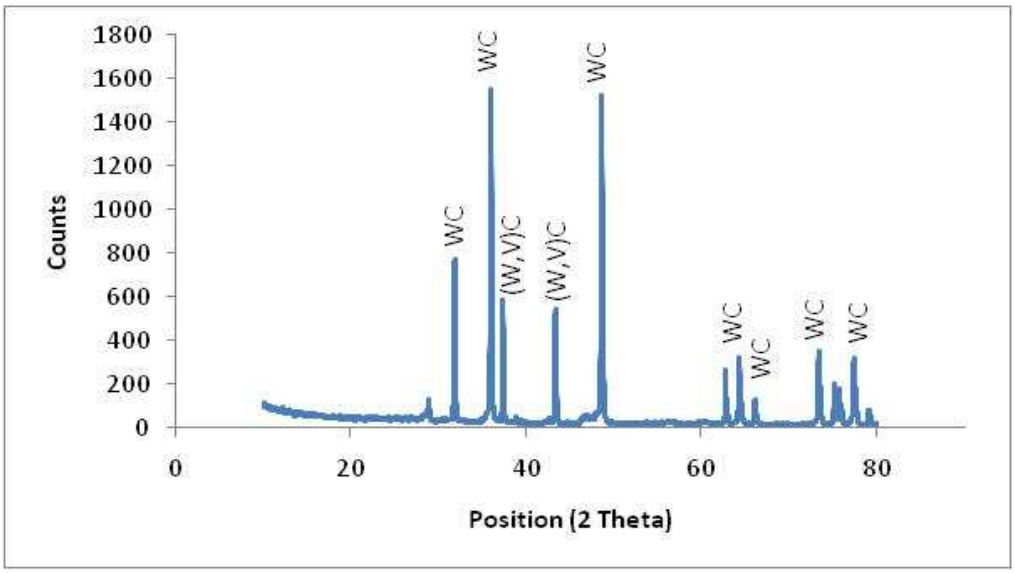

Figure 4.69. XRD pattern of corroded surface of WC-27VC-11Co (wt.%) in SMW

4.6.7 Raman spectroscopy

The Raman spectra of the corroded surfaces are shown in Figures 4. 70 – 4. 73. The shift positions in the different spectra, although sometimes shifted slightly in comparison with one another, indicate the presence of WO_3 and the hydrate of tungsten oxide. This corresponds to observations from other researchers reported in literature. (Regragui *et al.*, 2000; Ingham *et al*., 2005; Wachs *et al*., 1987; Enesca *et al*., 2007; Bozzini *et al*., 2003{a}, 2004; Wolcott *et al*., 2006; Daniel *et al*., 1987).

WC-10Co (wt.%)

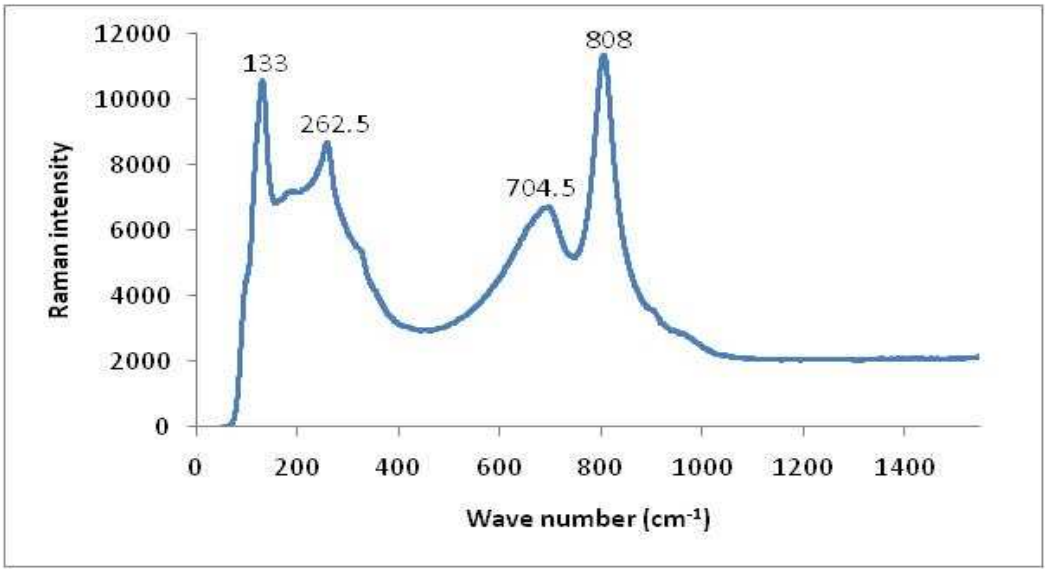

Figure 4.70. Raman spectrum of corrosion product on WC-10Co (wt.%) in SMW

WC-0.4VC-10Co (wt.%)

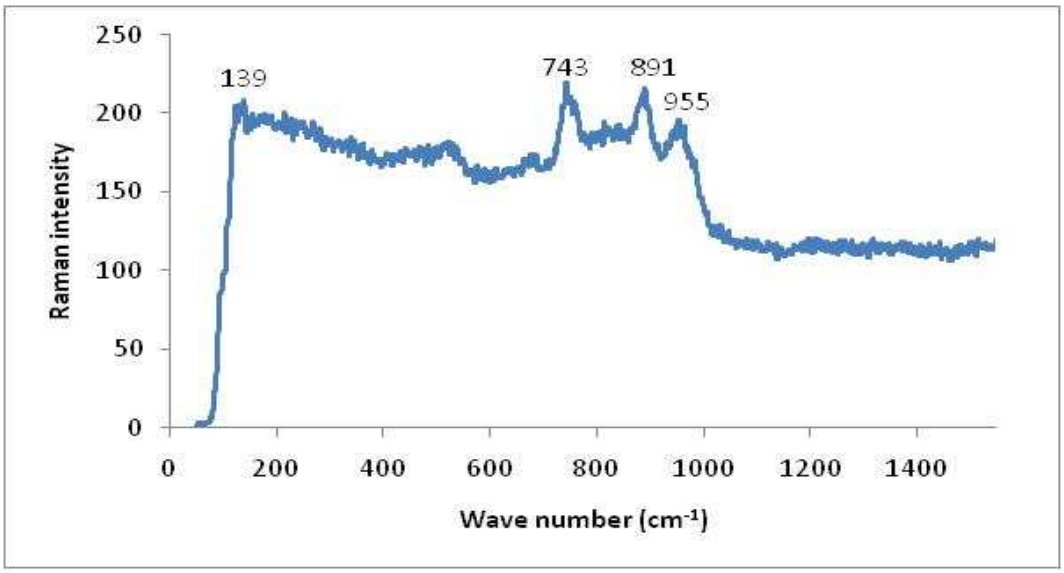

Figure 4.71. Raman spectrum of corrosion product on WC-0.4VC-10Co (wt.%) in SMW

WC-10VC-12Co (wt.%)

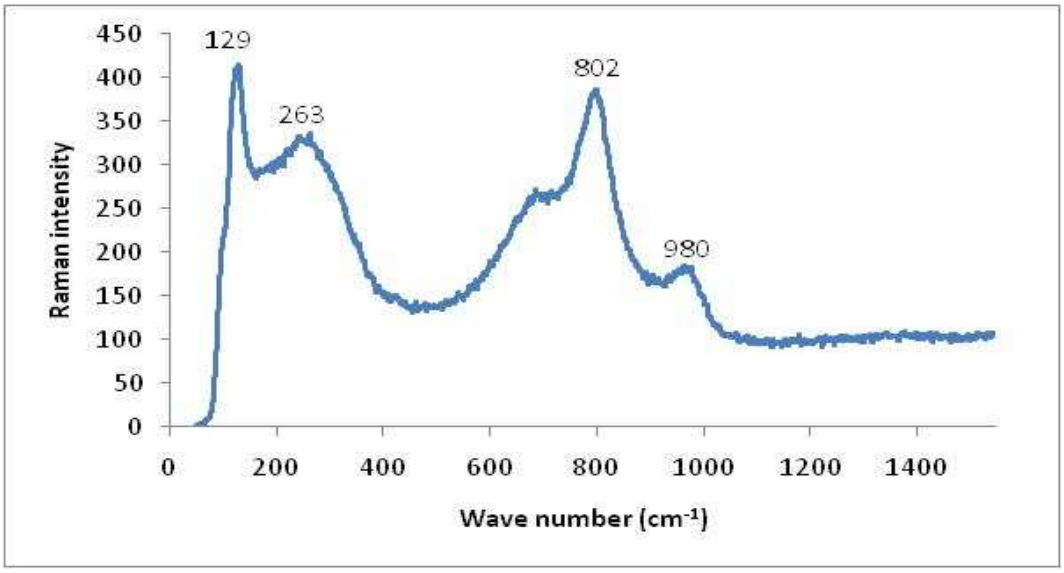

Figure 4.72. Raman spectrum of corrosion product on WC-10VC-11Co (wt.%) in SMW

WC-27VC-11Co (wt.%)

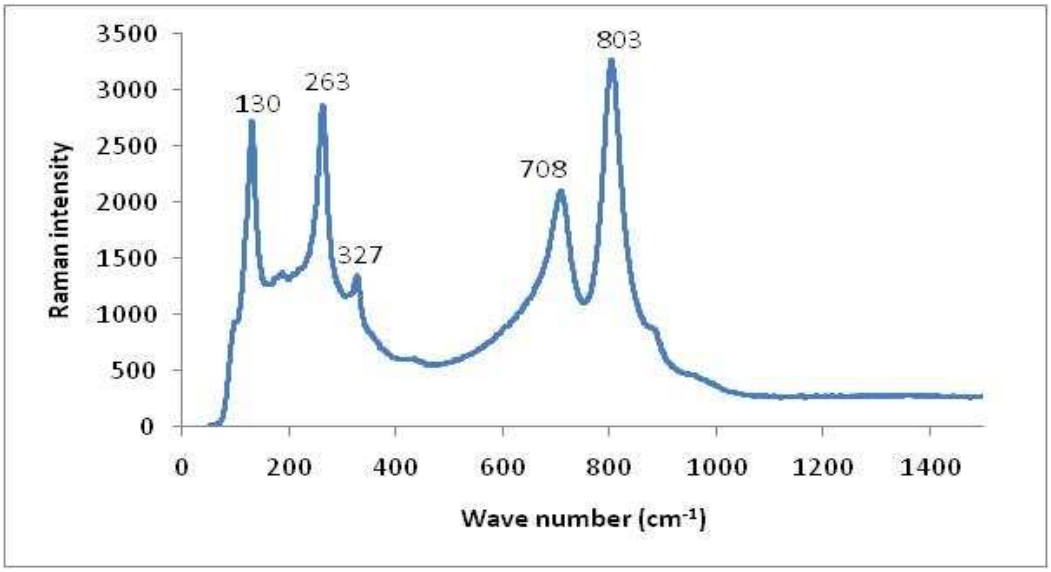

Figure 4.73. Raman spectrum of corrosion product on WC-27VC-11Co (wt.%) in SMW

Table 4.9 summarizes the main phases detected on the surfaces of the test specimens before and after corrosion. All the test specimens lost Co after corrosion, and formed new phases WO_3, and $WO_3.H_2O$. In addition, alloy WC-10VC-12Co (wt.%) also lost (W,V)C.

Table 4.9 Main phases detected on alloy surfaces before and after corrosion in SMW

Alloy (wt.%)	Phases detected		
	Before corrosion (XRD analysis)	After corrosion	
		XRD	Raman
WC-10Co	WC Co	WC Un-identifiable phase	WO_3 $WO_3.H_2O$
WC-0.4VC-10Co	WC Co	WC	WO_3 $WO_3.H_2O$
WC-10VC-12Co	WC (W,V)C Co	WC Un-identifiable phase	WO_3 $WO_3.H_2O$
WC-27VC-11Co	WC (W,V)C Co	WC (W,V)C Un-identifiable phase	WO_3 $WO_3.H_2O$

4.6.8 Discussion

The OCP values of all the test specimens (Figure 4.59) were generally devoid of fluctuations, implying that no specimen was susceptible to pitting. The WC-27VC-11Co (wt.%) potential seemed to have a rather constant value implying the possibility of a stable passive film. Of the OCP of the WC-VC-Co hardmetals, that of the 27wt.%VC had the most negative value.

The continuous anodic dissolution behaviour occurring in the synthetic mine water (SMW) reveals that Co continuously dissolves, which could lead to loss of WC particles, which can fall out and cause failure of hardmetal (Schnyder *et al*., 2004). This could be one of the reasons why SMW is detrimental to

WC-Co hardmetals. Low concentration solutions have been shown previously to result in continuous anodic dissolution (Ringas *et al*., 1990; Schnyder *et al*., 2004). The inclusion of VC into the hardmetal did not influence passivity as the same anodic dissolution behaviour was observed and there was no difference in the curves. At higher applied potentials, the curves of all the specimens developed plateaus, indicating the anodic current nearly became independent of the potential. The development of the plateaus was probably caused by ohmic resistance, due to the formation of a corrosion film on all the surfaces, as was shown by microscopy (Figures 4.62 – 4.65).

The introduction of VC into WC-Co did not change the electrochemical behaviour in SMW. This could have been due to the lack of passivating properties of the VC. The introduction of elements with passivating properties leads to a change in the electrochemical behaviour in SMW (Human & Exner, 1997) and in other solutions (Tomlinson & Ayerst, 1989). Howewer, the i_{corr} and corrosion rate values decreased with increasing VC additions, in tandem with decreasing volume fraction of the binder phase.

The chronoamperometry results showed that the current density of base alloy reduced for about two hours to acquire stable non-zero value for the rest of the test period. This could be attributed to the stabilizing of ohmic resistance. Overall, the current of the alloys containing VC stabilised at a higher value than that of the base alloy. For the VC alloys, the current passing increased with VC addition (Figure 4.61). This observation again points to the lack of passivity of VC.

The XRD patterns of the surfaces after chronoamperometric studies revealed WC as the major phase. No Co peaks were observed for any alloy, indicating that Co could have dissolved. The dissolution of Co has been reported also for neutral chloride solutions by several authors (Hochstrasser-Kurz *et al*.,

2007, 2008; Ghandehari, 1980; Schnyder *et al*., 2004) and acidic solutions (Bozzini *et al*., 2002, 2003 {a}; Hochstrasser-Kurz *et al*., 2007, 2008; Ghandehari, 1980). Alloy WC-10VC-12Co was also found to be missing (W,V)C, probably as a result of the grains falling off the surface after the Co binder was lost. The surface analysis of the WC-VC-Co alloys by Raman spectroscopy revealed tungsten oxide and the hydrate as the corrosion product.

4.7 Effect of electrolytes

From Table 4.10, it can be seen that the corrosion potential of the base alloy was the most noble in HCl. Moreover, there is a clear difference in the E_{corr} values in the neutral chloride containing solutions. The E_{corr} of the hardmetal was shifted to a less negative value in H_2SO_4 compared to SMW and this agrees with what was found by Human and Exner (1996). For i_{corr}, there was no change in the order of magnitude of the acids whilst in the neutral solutions, it decreased by one order from the NaCl with respect to SMW. This might be due to the amount of solutes or the additional sulphate ions present in each solution. The NaCl was found to cause the lowest corrosion rate value, whilst the H_2SO_4 caused the highest. This shows that WC-10Co will perform better in the neutral salts than in the acids.

Table 4.10 Electrochemical parameters of WC-10Co (wt.%) in the various electrolytes

Electrolyte	E_{corr} (V)	i_{corr} (A/cm^2)	Corrosion rate (mm/year)
HCl	-0.189	1.1E-06	7.6E-03
H_2SO_4	-0.235	5.6E-06	3.8E-02
NaCl	-0.399	3.0E-08	2.0E-04
SMW	-0.313	1.8E-07	1.2E-03

The introduction of small VC in the hardmetal yielded the most noble E_{corr} electrolyte in H_2SO_4 (Table 4.11). The i_{corr} values revealed a difference of one order of magnitude between the acids and the neutral solutions.

Table 4.11 Electrochemical parameters of WC-0.4VC-10Co (wt.%) in the various electrolytes

Electrolyte	E_{corr} (V)	i_{corr} (A/cm^2)	Corrosion rate (mm/year)
HCl	-0.317	1.1E-05	7.3E-02
H_2SO_4	-0.271	9.3E-06	6.2E-02
NaCl	-0.469	2.0E-07	1.3E-03
SMW	-0.474	2.1E-07	1.4E-03

With the addition of 10VC, the E_{corr} values moved to slightly more positive (noble) values. There was an order of magnitude difference between the acids and the neutral salts in terms of i_{corr} values. The corrosion rate values showed that the H_2SO_4 electrolyte was the most aggressive as it had the biggest value.

Table 4.12 Electrochemical parameters of WC-10VC-12Co (wt.%) in the various electrolytes

Electrolyte	E_{corr} (V)	i_{corr} (A/cm^2)	Corrosion rate (mm/year)
HCl	-0.195	1.0E-06	8.0E-03
H_2SO_4	-0.274	4.5E-06	3.5E-02
NaCl	-0.370	3.6E-07	2.8E-03
SMW	-0.296	1.5E-07	1.1E-03

With the introduction of 27wt.%VC in the hardmetal, all the electrolytes had the same order of magnitude for the corrosion rate values, except H_2SO_4

(Table 4.13). The increased VC in the hardmetal WC-10Co (wt.%) seem to be particularly detrimental to the corrosion resistance in H_2SO_4. In most other solutions it had almost no or only a marginal effect on the corrosion resistance and rate.

Table 4.13 Electrochemical parameters of WC-27VC-11Co (wt.%) in the various electrolytes

Electrolyte	E_{corr} (V)	i_{corr} (A/cm^2)	Corrosion rate (mm/year)
HCl	-0.213	3.2E-07	3.1E-03
H_2SO_4	-0.263	2.9E-06	2.7E-02
NaCl	-0.361	2.8E-07	2.6E-03
SMW	-0.379	0. 8E-07	0. 8E-03

CHAPTER FIVE

5 CONCLUSIONS AND RECOMMENDATIONS

5.1 Conclusions

The corrosion behaviour and the surface films of WC-VC-Co hardmetals with increasing VC concentrations were investigated in four solutions. The hypothesis made was that increasing VC content will increase the corrosion resistance of the hardmetal. The electrochemical methods used were open circuit potential, potentiodynamic anodic polarisation, and chronoamperometry. The solutions in which the corrosion resistance was evaluated, were hydrochloric acid (HCl), sulphuric acid (H_2SO_4), sodium chloride (NaCl), and synthetic mine water (SMW).

The aim, which was to investigate the corrosion behaviour and the passive films formed in these solutions, was achieved. The hypothesis of the investigations proved false in all the media except HCl where corrosion resistance increased with increasing VC. According to measured corrosion rates, H_2SO_4 was the most aggressive of all the electrolytes, whilst NaCl was the least corrosive for the base alloy. With 0.4wt.%VC and 10wc.%VC, the neutral chlorides were less aggressive when compared to the acids. High VC in the hardmetal in most of the solutions had almost no or only a marginal effect on the corrosion resistance and rate. Therefore the hypothesis of the investigation was proved to be false.

Raman and XRD investigations showed that the corrosion products formed in the neutral and acidic solutions were mostly tungsten oxides (WO_3, W_3O_8 and $W_2O_7^{2-}$) and hydrated tungsten oxide ($WO_3.xH_2O$, with x = 1,2). Vanadium was absent in all the corrosion products, except in H_2SO_4, where $VOSO_4.H_2O$

formed and was detected by the XRD analysis. This shows that VC in the hardmetal does not contribute to the passivation film formation in the media studied.

5.2 Recommendations

- The effect of higher VC levels have to be evaluated at constant Co concentrations with a maximum VC content of around 50% because of embrittlement occurring above a 50% VC level.
- Another characterisation of the passive film(s) in synthetic mine water should be carried out using XPS and/or Auger electrons to ascertain the composition of corrosion products more accurately.
- The effect of increasing Co levels together with increasing VC contents in WC-VC-Co hardmetals should be further evaluated, as increased Co has proved to increase corrosion resistance in H_2SO_4.
- *In-situ* Raman work on the corrosion behaviour of hardmetals should be carried out to investigate the reactions taking place during the corrosion process.

REFERENCES

Adorjan, A., Schubert, W.D., Schon, A., Bock, A. & Zeiler, B. 2006, WC grain growth during the early stages of sintering, *International Journal of Refractory Metals and Hard Materials,* vol. 24, no. 5, pp. 365-373.

ASTM G3 – 89: Standard reference test method for making potentiodynamic anodic polarization measurements, ASTM book of standards, 1999.

Bozzini, B., De Gaudenzi, G.P., Fanigliulo, A. & Mele, C. 2003 (a), Anodic behaviour of WC-Co type hardmetal, *Materials and Corrosion,* vol. 54, no. 5, pp. 295-303.

Bozzini, B., De Gaudenzi, G.P. & Mele, C. 2003 (b), An in-situ FT-IR investigation of the anodic behaviour of WC-Co hardmetal, *Materials and Corrosion,* vol. 54, no. 9, pp. 694-696.

Bozzini, B., De Gaudenzi, G.P., Serra, M., Fanigliulo, A. & Bogani, F. 2002, Corrosion behaviour of WC-Co based hardmetal in neutral chloride and acid sulphate media, *Materials and Corrosion,* vol. 53, no. 5, pp. 328-334.

Bozzini, B., Gaudenzi, P.D., Fanigliulo, A. & Mele, C. 2004, Electrochemical oxidation of WC in acidic sulphate solution, *Corrosion Science,* vol. 46, no. 2, pp. 453-469.

Broccardo, S.P. 2003, *An investigation into the corrosion resistance of WC-VC-Co hardmetals*, M.Sc dissertation, University of the Witwatersrand, Johannesburg.

Colthup, N.B., Daly, L.H. & Wiberly, S.E. (eds) 1975, *Introduction to Infrared and Raman Spectroscopy*, 2nd edn, Academic Press Incoporated, New York.

da Silva, A.G.P., Schubert, W.D. & Lux, B. 2001, The Role of the Binder Phase in the WC-Co Sintering, *Materials Research,* vol. 4, no. 2, pp. 59-62.

Daniel, M.F., Desbat, B., Lassegues, J.C., Gerand, B. & Figlarz, M. 1987, Infrared and Raman Study of WO_3 Tungsten Trioxides and $WO_3.xH_2O$ Tungsten Trioxides Hydrates, *Journal of Solid State Chemistry,* vol. 67, no. 2, pp. 235-247.

Denny, A.J. 1996, *Principles and Prevention of Corrosion,* 2nd Edition edn, Prentice Hall, Upper Saddle River, NJ, USA.

Enesca, A., Duta, A., Isac, L., Manolache, S. & Schoonman, J. 2007, The influence of the annealing process on the properties of WO_3 photoelectrode used in a photoeletrochemical cell (PECC), *Journal of Physics*, pp. 472-476.

Engqvist, H., Beste, U. & Axén, N. 2000, The influence of pH on sliding wear of WC-based materials, *International Journal of Refractory Metals and Hard Materials,* vol. 18, no. 2-3, pp. 103-109.

Exner, H.E. 1979, Physical and chemical nature of cemented carbides, *International Metals Reviews,* vol. 24, no. 4, pp. 149-173.

Fang, Z., Maheshwari, P., Wang, X., Sohn, H.Y., Griffo, A. & Riley, R. 2005, An experimental study of the sintering of nanocrystalline WC–Co powders, *International Journal of Refractory Metals and Hard Materials,* vol. 23, no. 4-6, pp. 249-257.

Fernandes, P. J. L., Luyckx, S.B., Human, A.M. & Robinson, F. P. A. 1992, Does the Cobalt Free Path Affect the Corrosion Behaviour of WC-Co?, *Journal of Hard Materials,* vol. 3, no. ICSHMA-PAPER 61, pp. 727-736.

Fontana, G.M. & Greene, D.N. 1982, *Corrosion Engineering,* 2nd Edition edn, Mcgraw-Hill International Book Company, Tokyo.

Ghandehari, M.H. 1980, Anodic Behaviour of Cemented WC-6% Co Alloy in Phosphoric Acid Solutions, *Journal of the Electrochemical Society,* vol. 127, no. 10, pp. 2144-2147.

Gotic, M., Ivanda, M., Popovic, S. & Music, S. 2000, Synthesis of tungsten trioxide hydrates and their structural properties, *Materials Science and Engineering B,* vol. B77, pp. 193-201.

Gupta, C.K. & Krishnamurthy, N. 1992, *Extractive Metallurgy of Vanadium,* 1st edn, Elsevier Science Publishers B. V., Amsterdam, The Netherlands.

Hashe, N.G., Norgren, S., Andrén, H.-O., Neethling, J.H. & Berndt, P.R. 2008 Reduction of carbide grain growth in WC–VC–Co by sintering in a nitrogen atmosphere, *International Journal of Refractory Metals and Hard Materials,* vol. In Press, Corrected Proof.

Hochstrasser-Kurz, S., Mueller, Y., Latkoczy, C., Virtanen, S. & Schmutz, P. 2007, Analytical characterization of the corrosion mechanisms of WC–Co by electrochemical methods and inductively coupled plasma mass spectroscopy, *Corrosion Science,* vol. 49, no. 4, pp. 2002-2020.

Hochstrasser-Kurz, S., Reiss, D., Suter, T., Latkoczy, C., Gunther, D., Virtanen, S., Uggowitzer, P.J. & Schmutz, P. 2008, ICP-MS, SKPFM, XPS, and microcapillary investigation of the local corrosion mechanisms of WC-Co hardmetal, *Journal of the Electrochemical Society,* vol. 155, no. 8, pp. 415-426.

Huang, S.G., Vanmeensel, K., Van der Biest, O. & Vleugels, J. 2007 Binderless WC and WC-VC materials obtained by pulsed electric current sintering, *International Journal of Refractory Metals and Hard Materials,* vol. 26, no. 1, pp. 41-47.

Human, A.M. & Exner, H.E. 1996, Electrochemical behaviour of tungsten-carbide hardmetals, *Materials Science & Engineering A: Structural Materials: Properties, Microstructure and Processing,* vol. A209, no. 1, pp. 180-191.

Human, A.M. & Exner, H.E. 1997, Relationship between electrochemical behaviour and in-service corrosion of WC based cemented carbides, *International Journal of Refractory Metals and Hard Materials,* vol. 15, no. 1, pp. 65-71.

Human, M.A., Northdrop, T.I., Luyckx, B.S. & James, N.M. 1991, A comparison between cemented carbides containing cobalt- and nickel-based binders, *Journal of Hard Materials,* vol. 2, no. 3-4, pp. 247-257.

Ingham, B., Chong, S.V. & Tallon, J.L. 2005, Layered tungsten oxide-based organic/inorganic hybrid materials I: Infrared and Raman study, *Journal of Physical Chemistry B.,* vol. 109, no. 11, pp. 4936-4940.

Lay, S., Hamar-Thibault, S. & Lackner, A. 2002, Location of VC in VC, Cr_3C_2 codoped WC–Co cermets by HREM and EELS, *International Journal of Refractory Metals and Hard Materials,* vol. 20, no. 1, pp. 61-69.

Lekatou, A., Regoutas, E. & Karantzalis, A.E. 2008, Corrosion behaviour of cermet-based coatings with a bond coat in 0.5 M H_2SO_4, *Corrosion Science,* vol. 50, no. 12, pp. 3389-3400.

Luyckx S. 1994 (a), *Processing Powder Metallurgy 1994 World Congress*, Paris, France, June 1994, Vol. 1, Edition de Physique, pp 169.

Luyckx S. 1994 (b), *Vanadium Carbide in Hardmetals*, XVth CMMI Congress, Johannesburg, South Africa, SAIMM, vol. 2, pp 11-13

Luyckx, B.S., Osborne, C., Cornish, L.A.. & Whitefield, D. 1996, Fine Grained WC-VC-Co Hardmetal, *Powder Metallurgy,* vol. 39, no. 3, pp. 210-212.

Machio, C.N. 2005, *Preparation, Characterisation and testing of WC-VC-Co HP/HVOF Thermal Spray Coatings*, Ph.D thesis, University of the Witwatersrand, Johannesburg.

Makhele, Z.L. 2001, *The relationship between the hardness, grain size and mean free path in WC-Co*, M. Sc dissertation, University of the Witwatersrand, Johannesburg.

Mori, G., Zitter, H., Lackner, A. & Schretter, M. 2001, Influencing the corrosion resistance of cemented carbides by addition of Cr_3C_2, TiC and TaC, *15th International Plansee Seminar,* vol. 2, pp. 222-236.

Ogundipe, A., Greenberg, B., Braida, W., Christodoulatos, C. & Dermatas, D. 2006, Morphological characterisation and spectroscopic studies of the corrosion behaviour of tungsten heavy alloys, *Corrosion Science,* vol. 48, no. 10, pp. 3281-3297.

Regragui, M., Addou, M., Outzourhit, A., Bernéde, J.C., El Idrissi, E., Benseddik, E. & Kachouane, A. 2000, Preparation and characterization of pyrolytic spray deposited electrochromic tungsten trioxide films, *Thin Solid Films,* vol. 358, no. 1-2, pp. 40-45.

Ringas, C., Robinson, F.P.A., Luyckx, S.B. & Sellschop, J.P.F. 1990, Corrosion Behaviour of Ion Implanted WC-Co and WC-Ni alloys in Acid and Chloride Containing Media, *Surface Engineering,* vol. 6, no. 3, pp. 194-198.

Schnyder, B., Stössel-Sittig, C., Kötz, R., Hochstrasser-Kurz, S., Virtanen, S., Jaeggi, C., Eichenberger, N. & Siegenthaler, H. 2004, Investigation of the electrochemical behaviour of WC–Co hardmetal with electrochemical and surface analytical methods, *Surface Science,* vol. 566-568, no. Part 2, pp. 1240-1245.

Scholl, H., Hofman, B. & Rauscher, A. 1992, Anodic polarization of cemented carbides of the type [(WC,M); M = Fe, Ni or Co] in sulphuric acid solution, *Electrochimica Acta,* vol. 37, no. 3, pp. 447- 452.

Sebeya, T.T. 2006, *An Investigation into the Cause of the Difference in the Corrosion Behaviour of WC-Co and WC-VC-Co Hardmetals*, Unpublished M.Sc results, University of The Witwatersrand.

Sherif, E.M., Potgieter, J.H., Commins, J.D., Cornish, M., Olubambi, P.A. & Machio, C.N. 2009, The beneficial effect of ruthenium additions on the passivation of duplex stainless steel corrosion in sodium chloride solutions, *Corrosion Science,* vol. 51, no. 6, pp. 1364-1371.

Sutthiruangwong, S. & Mori, G. 2003, Corrosion properties of Co-based cemented carbides in acidic solutions, *International Journal of Refractory Metals and Hard Materials,* vol. 21, no. 3-4, pp. 135-145.

Sutthiruangwong, S., Mori, G. & Kosters, R. 2005, Passivity and pseudopassivity of cemented carbides, *International Journal of Refractory Metals and Hard Materials,* vol. 23, no. 2, pp. 129-136.

Terada, O. & Suzuki, H. 1997, Properties of Coarse Grained Tungsten Carbide-Cobalt With Added Vanadium Carbide, *Journal Japan Society Powder Metallurgy,* vol. 44, no. 1, pp. 102-105.

Tomlinson, W.J. & Ayerst, N.J. 1989, Anodic polarization and corrosion of WC-Co hardmetals containing small amounts of Cr_3C_2 and/or VC, *Journal of Materials Science,* vol. 24, no. 7, pp. 2348-2352.

Tomlinson, W.J. & Linzell, C.R. 1988, Anodic polarization and corrosion of cemented carbides with cobalt and nickel binders, *Journal of Materials Science,* vol. 23, no. 3, pp. 914-918.

Wachs, I., Brown, J., Via, G. Horsley, J. A. & Hardcastle, F. 1987, Structure of surface tungsten-oxide species in the WO_3/Al_2O_3 supported oxide system from X-ray absorption near-edge spectroscopy and Raman-spectroscopy, *The Journal of Physical Chemistry,* vol. 91, no. 15, pp. 4014-4020.

Wang, J. (ed) 2006, *Analytical Electrochemistry*, 3rd edn, John Wiley & Sons Incoporated, New Jersey.

Wentzel, E.J. & Allen, C. 1995, Erosion-corrosion resistance of tungsten carbide hard metals with different binder compositions, *Wear,* vol. 181-183, no. 1, pp. 63-69.

Wolcott, A., Kuykendall, T.R., Chen, W., Chen, S. & Zhang, J.N. 2006, Synthesis and Characterization of Ultrathin WO_3 Nanodisks Utilizing Long-Chain Poly(ethylene glycol), *The Journal of Physical Chemistry B,* vol. 110, no. 50, pp. 25288-25296.

Yih, S.W.H. & Wang, C.T. 1979, T*ungsten: Sources, Metallurgy, Properties, and Applications,* 1st edn, Plenum Publishing Corporation, New York.

APPENDICES

Appendix A

Masses of salts used to prepare synthetic mine water (SMW)

The determination of the masses of salts used to constitute synthetic mine water was to first calculate the number of moles of the respective ions, and to work out the masses of salts required to provide this number of moles. A mole of a chemical substance is the ratio of a given mass of the substance divided by its relative molecular or atomic mass.

Table A.0.1 Concentration and moles of ions in synthetic mine water

Ions	Concentration (mg/l)	Moles/l
SO_4^{2-}	980	0.01020174
Ca^{2+}	375	0.00935675
Cl^-	1500	0.04230954
Mg^{2+}	40	0.00164575
Na^+	943	0.04101783

Table A. 0.2 Relative atomic masses

Element	Atomic mass (g)
S	32.066
O	15.999
Ca	40.078
Cl	35.453
Mg	24.305
Na	22.990

Procedure for amounts of salts

E.g. 1 Number of moles of sulphate ions, SO_4^{2-}, in a litre of solution

$$\frac{\text{mass of sulphate ions}}{\text{molecular mass of sulphate}} \approx \frac{0.98}{96.062} \approx 0.01020174 \qquad \text{A.1}$$

Molecular mass of sulphate ions = 32.066 + (4 × 15.999) = 96.062

E.g. 2 Calculations of amounts of $MgSO_4$ and Na_2SO_4 needed to provide the number of sulphate ions in Table A.1 above.

Ratio of Mg^{2+} and SO_4^{2-} in $MgSO_4$ is 1:1 and so 0.00164575 moles of Mg^{2+} require 0.00164575 moles of SO_4^{2-}.

Hence mass of $MgSO_4$ = No. of moles × molar mass of $MgSO_4$

= 0.001645752 × 120.367 = 0.19809 g = 198.09 mg

The moles of SO_4^{2-} ions to be provided by Na_2SO_4 is the difference between the moles of SO_4^{2-} and moles obtained from $MgSO_4$

= 0.010201745 – 0.001645752 = 0.0085559993 moles

Hence mass of Na_2SO_4 = No. of moles × molecular mass of Na_2SO_4

= 0.0085559993 × 142.042 = 1.21531 g

The other atomic masses were obtained following the procedure in e. g. 2

Table A.0.3 Synthetic mine water composition

Compound	Concentration (mg/l)
Na_2SO_4	1237
$CaCl_2$	1038
$MgSO_4$	199
NaCl	1380

(Machio, 2005).

Appendix B

Raman Spectra of the as received powders.

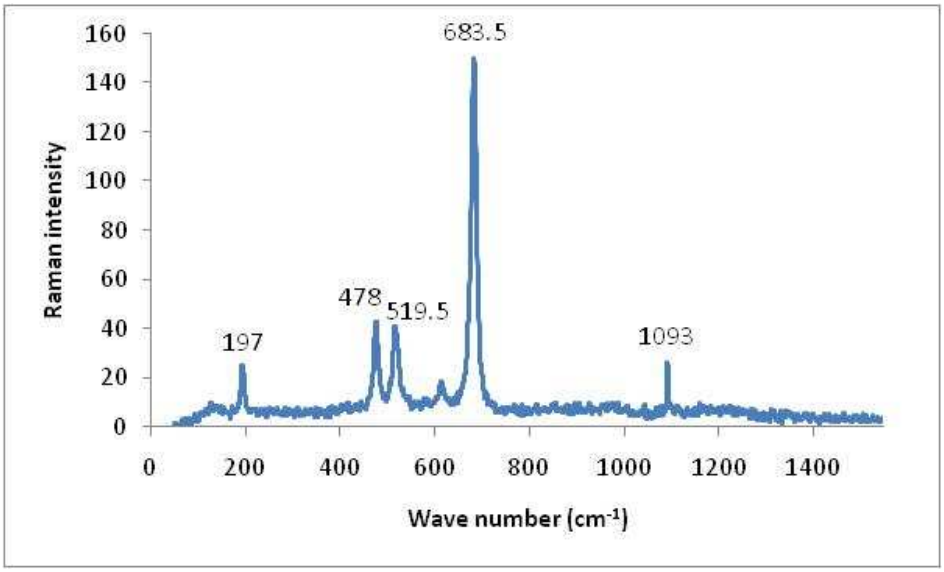

Figure B.1 Raman spectrum of cobalt powder

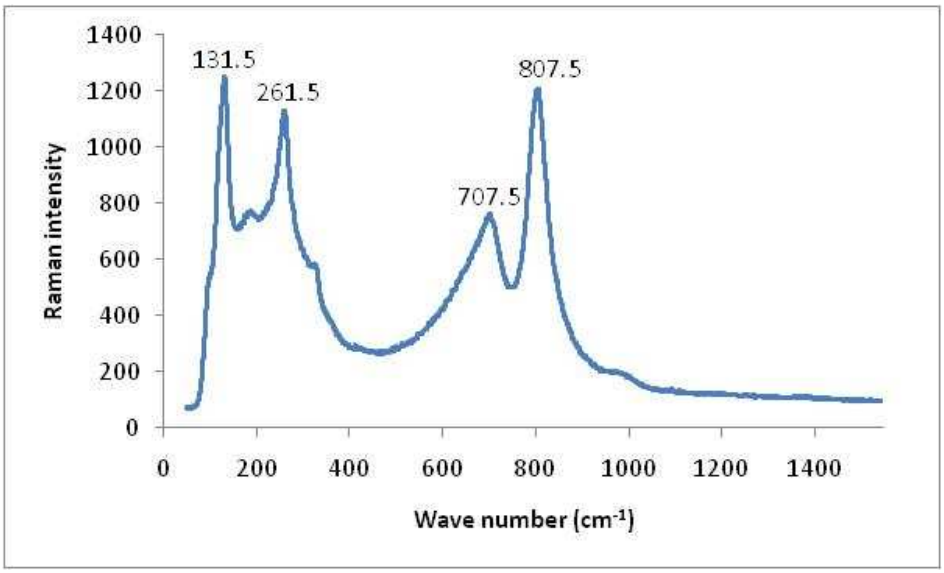

Figure B.2. Raman spectrum of tungsten carbide powder

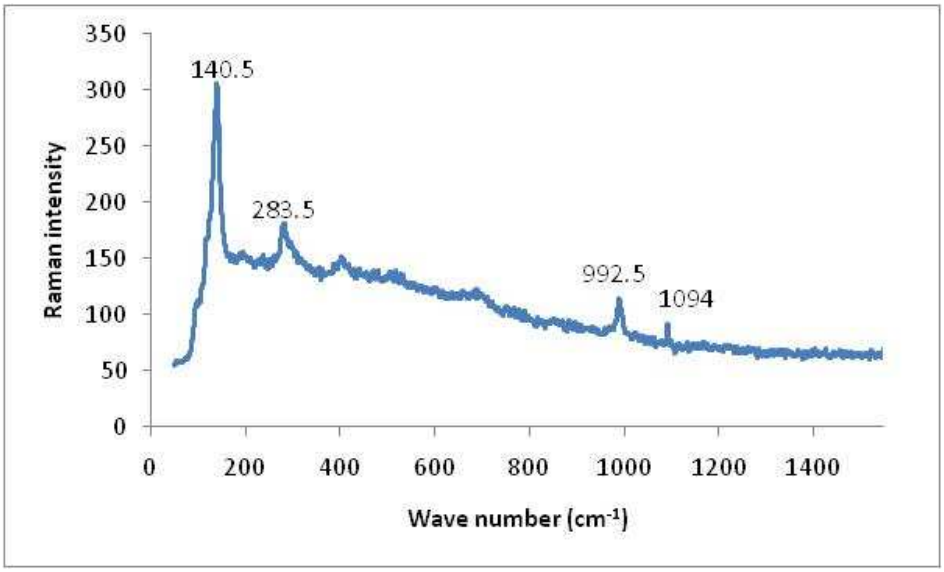

Figure B.3. Raman spectrum of vanadium carbide powder

Appendix C

Table C.0.1 Reference codes of XRD compounds

No	Reference code	compound	No	Reference code	compound
1	01-089-4307	Co	7	00-030-1432	$VOSO_4.H_2O$
2	01-089-2727	WC	8	01-081-2262	W_3O_8
3	01-089-1096	(W,V)C	9	01-073-1546	$Na_2W_2O_7$
4	00-018-1418	$WO_3.H_2O$	10	01-089-4478	WO_3
5	01-084-0886	$WO_3.H_2O$	11	00-033-1387	WO_3
6	00-018-1419	$WO_3.2H_2O$	12		

Appendix D: Article submitted for publication

Konadu, D.S., Potgieter, J.H., Vermaak-Potgieter, S., Machio, C.N. & Van der Merwe, J. The Corrosion behaviour of WC-VC-Co hardmetals in Acidic Media, *Corrosion Science*. (Submitted for publication)